NATIONAL TECHNICAL UNIVERSITY OF ATHENS

POSTGRADUATE STUDIES PROGRAM
"COMPUTATIONAL MECHANICS"

MASTER'S THESIS

Multilayer particle resuspension in a turbulent flow

Athanasios VITSAS

Supervisors:

Prof. Andreas G. BOUDOUVIS

School of Chemical Engineering, NTUA, Greece

Dr. Grégory LECRIVAIN

Institute of Fluid Dynamics, HZDR, Germany

JULY 2013

Dedicated to my parents

Acknowledgements

I would like to thank Professor Andreas Boudouvis for his trust on me and motivation during all this time. I am grateful for all the questions he raised, and for all the valuable suggestions and corrections he provided to me, enabling me to clear up obscure points and improve this work. Last but not least, I would like to thank him as Director of this Master course for all his efforts, making internships in the framework of the master's thesis, like mine, more feasible.

I am sincerely grateful to my internship supervisor Dr. Grégory Lecrivain for not only giving me the opportunity to gain such a valuable experience and knowledge in a international research center, but also being a great mentor. I would like to thank him for his constant help having always a solution to the difficulties I faced, for his scientific advice and for the many insightful recommendations making a substantial contribution to this work.

Furthermore, I would like to thank all my beloved friends and relatives for always being there when in need and of course for their patience that they showed when I had to be physically absent.

Finally, I am deeply grateful to my family for their endless support and encouragement through all these years.

This work was financially supported by the European Commission under the Grant 249337 of the THINS project.

Abstract

The work presented in this Master's thesis deals with particle re-entrainment from a multilayer particle bed exposed to a turbulent gas flow. Background motivation is the remobilization of radioactive graphite particles in the primary circuit of a gas-cooled high temperature reactor. In this particular case, the work focuses on resuspension of graphite particles with a size ranging from 1 to 20 μm.

A novel force balance model is introduced to numerically investigate particle resuspension in an obstructed channel flow. Detachment of particle clusters off the multilayer particle bed is assumed when the aerodynamic force overcomes the adhesive force. The numerical results are compared to experimental data performed at the Helmholtz-Zentrum Dresden-Rossendorf.

An algorithm is developed to reconstruct the structure of a multilayer deposit. Following the recreation of a multilayer particle bed, resembling that of the experiments, is a cluster identification procedure. It is considered that in multilayer deposits, aggregates (particle clusters) re-enter the flow. Resuspension of individual particles is unlikely.

Each cluster is assigned a resuspension probability. This probability relates with the resultant of the distribution of the wall shear stresses along the deposit (derived from a force balance model) and the time evolution of the phenomenon (conjecture of inverse time law). The wall shear stress was computed by two methods, first by the fully unsteady Large Eddy Simulation (LES) and secondly by the time-averaged solution of the LES. When solving the flow equations, the particle bed was considered as impermeable. The granular interface was thus considered a bounding geometry.

The gas flow was increased gradually to trigger sudden resuspension. Whenever a cluster resuspended, the thickness layer was determined. The numerical results showed satisfactory agreement with experimental data, especially for unsteady LES. This confirmed the assumption that wall shear stress is the main resuspension mechanism.

Περίληψη

"Επαναιώρηση σωματιδίων εντός τυρβώδους ροής"

Αυτή η μεταπτυχιακή εργασία πραγματεύεται την επαναιώρηση σωματιδίων που έχουν προσκολληθεί σε επιφάνειες, όταν υπόκεινται σε τυρβώδη ροή. Κίνητρο της εργασίας αποτέλεσε η επαναιώρηση ραδιενεργών σωματιδίων γραφίτη μέσα στους αγωγούς μίας ειδικής κατηγορίας πυρηνικών αντιδραστήρων. Για τη συγκεκριμένη αυτή εφαρμογή, η εργασία ασχολείται με επαναιώρηση σωματιδίων σκόνης γραφίτη με διάμετρο από 1 έως 20 μm.

Ένα καινοτόμο μοντέλο ισοζυγίου δυνάμεων εισάγεται ώστε να μελετήσει αριθμητικά την επαναιώρηση σωματιδίων μέσα σε έναν αγωγό, στον οποίο έχουν τοποθετηθεί περιοδικά εμπόδια κατά το μήκος του. Τα σωματίδια θεωρείται ότι αποκολλώνται από τις επιφάνειες όταν οι αεροδυναμικές δυνάμεις που τους ασκούνται ξεπεράσουν τις δυνάμεις πρόσφυσης που αναπτύσσονται μεταξύ τους ή μεταξύ των σωματιδίων και του τοιχώματος. Τα αποτελέσματα από την αριθμητική προσομοίωση συγκρίνονται με πειραματικά δεδομένα που ελήφθησαν στα εργαστήρια του ερευνητικού κέντρου HZDR.

Κατασκευάστηκε ένας αλγόριθμος ικανός να αναπαράγει ορισμένα πολυ-επίπεδα ιζήματα σωματιδίων. Μετά την ανακατασκευή κλίνης σωματιδίων, που προσομοιάζει τα πειραματικά δεδομένα, ενεργοποιείται μία διαδικασία αναγνώρισης "συστάδων" σωματιδίων. Θεωρείται ότι σε πολυ-επίπεδα ιζήματα, τα σωματίδια τείνουν να επαν-εισέρχονται στη ροή ως συστάδες σωματιδίων, παρά ως ανεξάρτητα.

Κάθε μία συστάδα σωματιδίων λαμβάνει μία πιθανότητα επαναιώρησης. Η πιθανότητα αυτή προκύπτει από την κατανομή των διατμητικών τάσεων στο τοίχωμα (απόρροια του ισοζυγίου δυνάμεων) και της χρονικής εξέλιξης του φαινομένου (εικασία ότι η επαναιώρηση φθίνει με την πάροδο του χρόνου). Οι διατμητικές τάσεις υπολογίζονται με δύο τρόπους, από τις χρονικά μεταβαλλόμενες λύσεις της Προσομοίωσης Μεγάλων Δινών (LES) και από τη χρονικά μέση τιμή των λύσεων αυτών. Κατά την επίλυση των εξισώσεων ροής, η διεπιφάνεια μεταξύ του ρευστού και της κλίνης σωματιδίων θεωρείται ως σύνορο του πεδίου επίλυσης, καθώς το ίζημα θεωρείται αδιαπέραστο από το ρευστό.

Η ταχύτητα του ρευστού αυξάνεται σταδιακά, προκαλώντας την αποκόλληση ολοένα και περισσότερων σωματιδίων από τις επιφάνειες. Όταν μία συστάδα σωματιδίων επαναιωρείται, το πάχος του ιζήματος καταγράφεται. Τα αποτελέσματα της αριθμητικής επίλυσης δείχνουν ικανοποιητική συμφωνία με τις πειραματικές μετρήσεις σε ότι αφορά τις χρονικά μεταβαλλόμενες λύσεις του μοντέλου τύρβης LES. Αυτό οδηγεί στο συμπέρασμα ότι η διατμητική τάση στο τοίχωμα λειτουργεί ως ο κύριος μηχανισμός επαναιώρησης.

Contents

List of Figures

Chapter 1

Introduction

1.1 Motivation

The present project is part of the European Commission's funded project THINS (Thermal-Hydraulics of Innovative Nuclear Systems), which aims at predicting and preventing nuclear accidents.

In the framework of THINS project, this master's thesis aims at proposing and implementing a new model for the simulation of the particle resuspension process in a turbulent flow.

Particle resuspension (or particle reentrainment) is the process where deposited particles, detach from a surface and reenter in the turbulent gas phase.

How resuspension is linked to nuclear safety?

During operation of a graphite moderated High Temperature Reactor (HTR) the friction between the graphite components within the core together with oxidation initiate the production of carbonaceous dust. The graphite dust is then conveyed by the coolant gas and eventually deposits in the primary circuit over the course of years. The multilayer deposit becomes a major source term (Moorman, 2008), (Kissane et al., 2012). In the unlikely event of a nuclear accident such as depressurization in the primary circuit contaminated particles may be remobilized and escape system boundaries.

In the next sections of this chapter some general cases are presented that are of particular interest for the phenomenon and the physics of resuspension. Then, some facts are given on graphite dust and a new type of nuclear reactors, as these relate to the case study for the simulation of resuspension in this work. In the last section, there is a short description of the research institute "Helmholtz Zentrum Dresden Rossendorf" (HZDR), since it is the place where this work was conducted.

1.2 Resuspension cases

In the context of resuspension of aerosol particles previously deposited on a surface one can distinguish two limiting cases of deposit geometry (Friess and Yadigaroglu, 2002):

- monolayer deposits, where particles adhere directly to the wall and are not in contact one another;
- multilayer deposits, where the particles are sitting on top of other particles and form a granular medium.

In the first case, the resuspension of monolayer deposits plays an important role in the clean technologies and in the semiconductor industry.

The clean substrate surfaces in the fabrication of semiconductor microelectronic devices is of great importance. This is so because the device performance, reliability and product yield of silicon circuits are critically affected by the presence of chemical contaminants and particulate impurities on the wafer of a device surface (Kern, 2008). Effective techniques for cleaning silicon wafers initially and for oxidation and patterning are now more important than ever before because of the extreme sensitivity of the semiconductor surface and the submicron size of the device features. As a consequence, the preparation of ultraclean silicon wafers has become one of the key technologies in the fabrication of ULSI silicon circuits. The term "ultraclean" may be defined in terms of chemical contaminants on the silicon surface. According to this, particles larger than 0.1 μm in size should be less than 1 particle per 10 cm^2 wafer. These extremely low numbers indicate challenges for the cleaning technology (Gradon, 2009).

Another aspect of the problem relates to the reemission of particles under the atmospheric and indoor environmental conditions. Single and multilayer structures of particulate deposits are exposed to external forces causing their re-entrainment. Following an accidental or planned airborne release and after deposition, the resuspension of small particles is an important mechanism which may pose an inhalation hazard, and lead to the redistribution of contaminants (Ould-Dada and Baghini, 2001). During dry windy periods, contaminated forests, streets and buildings, may act as sources of a resuspended material subject to secondary wind transfer to adjacent areas. In the case of radionuclides and other carcinogens, this process could represent a long pathway of environmental exposure, especially for long lived isotopes and organic compounds (Wu et al., 1992).

Similar effects are observed for indoor contaminants, including airborne dust, bioaerosols and aeroallergens. When disturbed by human activity, contaminated reservoir dust

releases carrier particles containing allergens, leading to occupant inhalation exposure, allergic sensitization and asthma diseases development in susceptible individuals (Gomes et al., 2007).

The resuspension of multilayer deposits, which involves several effects that do not occur in monolayer deposits (mutual obstruction of particles, clustering effect, influence of resuspension on the deposit structure), is observed at the aerosolization of pharmaceutical powders in dry powder inhalers (DPI). This type of inhalers is currently used by almost 40% of patients with asthma and chronic obstructive pulmonary disease (COPD) (Atkins, 2005). An aerosol is typically created via dispersing in the air an inhaled aliquot quantity of possibly loose powder. The amount of respirable particles depend on the primary size of micronized powder grains, the cohesive forces acting among the particles in the powder and the energy of the flowing air required to re-entrain the particles into the air stream and to break apart particle clusters (Telko and Hickey, 2005).

The nuclear industry shows interest in the study of the mechanism of the resuspension for both cases of particle deposits. This thesis will however focus only on multilayer deposit, since the complex mechanisms of multilayer resuspension are relatively under investigated.

1.3 Graphite dust

The current nuclear core technology termed "Generation III" focuses more on industrial reliability than on security. For this reason new technologies are being invented so that they could improve the efficiency as well the overall security.

The so-called "Generation IV" is composed of numerous types of fission power plant, including the High Temperature Reactors (HTR), which were among the first studied reactors of that kind. Since the early 70s', several projects of experimental HTRs (also known as PBR for Pebble Bed Reactors - see Fig. 1.1) have been planned: in China (HTR-10), in Russia, in the USA (Fort St. Vrain HTR) and in Germany, the well known AVR, a reactor formerly based on Jülich, which was of great interest because of its long-time running. The HTRs' technology is based, like every other current nuclear reactors, on the fission of radioactive elements (mostly Uranium). The main difference from older generations' reactors is that in a HTR the temperature used (750 °C for HTR and around 1000 °C for VHTR -Very High Temperature) can provide a better efficiency (up to 50%).

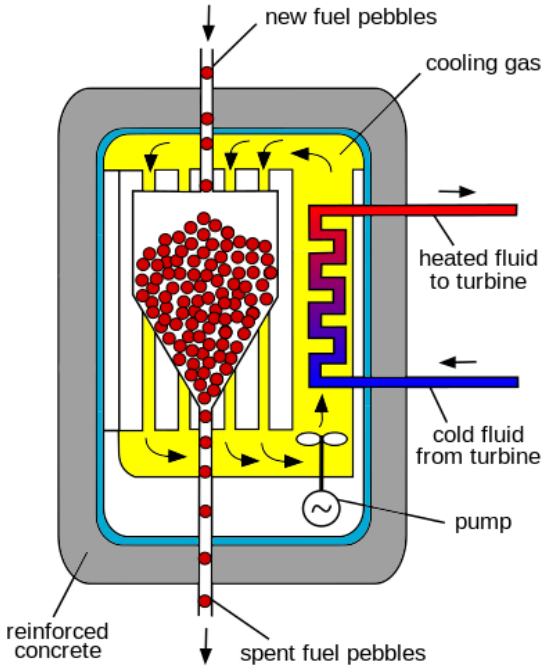

Figure 1.1: Sketch of a Pebble Bed Reactor.

Every HTR uses graphite embedding for the fuel elements (spherical or prismatic - see Fig. 1.2), with the pebble bed core consisting of about 100,000 tennis-sized fuel pebbles.

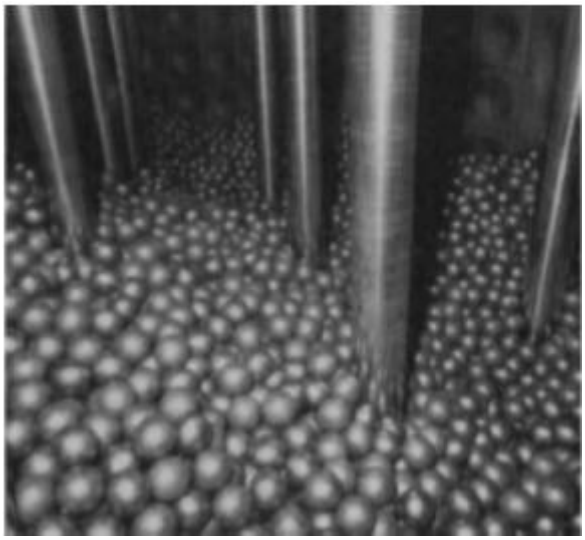

Figure 1.2: Graphite spheres in a HTR.

The graphite layer is the origin of the carbonaceous dust (Rostamian et al., 2012). This graphite is used as moderator to stabilize the chain reaction. The Uranium Dioxide is

completely embedded in the graphite (the small fuel spheres are called TRISO fuel - see Fig. 1.3). When the reactor is operating, some dust is transferred by the coolant gas in the primary circuit and deposits on the inner surface of the pipes through several layers. The reentrainment of those fine deposited particle can be a hazard in case of an accident (case of sudden and heavy depressurization, after a pipe breaking or cracking). The LOCA (Loss Of Coolant Accidents) case is a standard accident case where radioactive particles can be released in the environment (Stempniewicz and Komen, 2010).

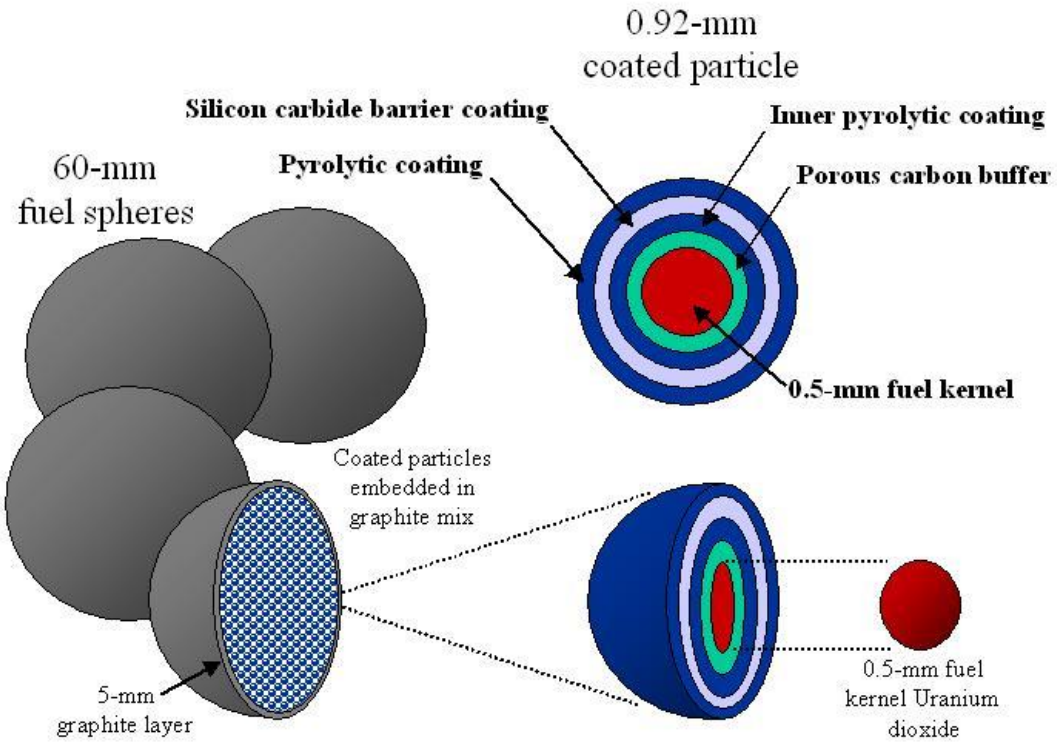

Figure 1.3: Pebble bed TRISO fuel sphere cross section.

Data provided over the years can give a good start to study the amount and the characteristics of the produced dust. An analysis on dust deposition (Stempniewicz et al., 2012) that has been conducted in a pebble bed NGNP (Next Generation Nuclear Plant) showed that approximately 1630 kg of graphite dust would enter the primary helium flow during the nuclear plant's lifetime (60 years). Moreover, the initial activity of the dust would be approximately 5 - 10^{10} Bq/kg due to the presence of cesium Cs-137 (One Bq is defined as the activity of a quantity of radioactive material in which one nucleus decays per second).

Other experiments conducted on the AVR reactor (Moormann, 2008) showed that the amount of dust produced was about 5 kg/year. This accumulating dust in the circuit is a safety hazard.

1.4 Helmholtz-Zentrum Dresden-Rossendorf

Located near Dresden in Germany, the story of HZDR (see Fig. 1.4) began in 1956 and was initially named "Zentralinstitut für Kernphysik". It was focused on nuclear research and safety as the name indicates. This was the major nuclear research center in the German Democratic Republic. After the reunification of Germany, it was established as "Forschungzentrum Rossendorf" (FZR) with new fields of studies including medical (pharmaceutical) and material research. In 2011 the center incorporated to the Helmholtz Association so it took its current name: "Helmholtz-Zentrum Dresden-Rossendorf".

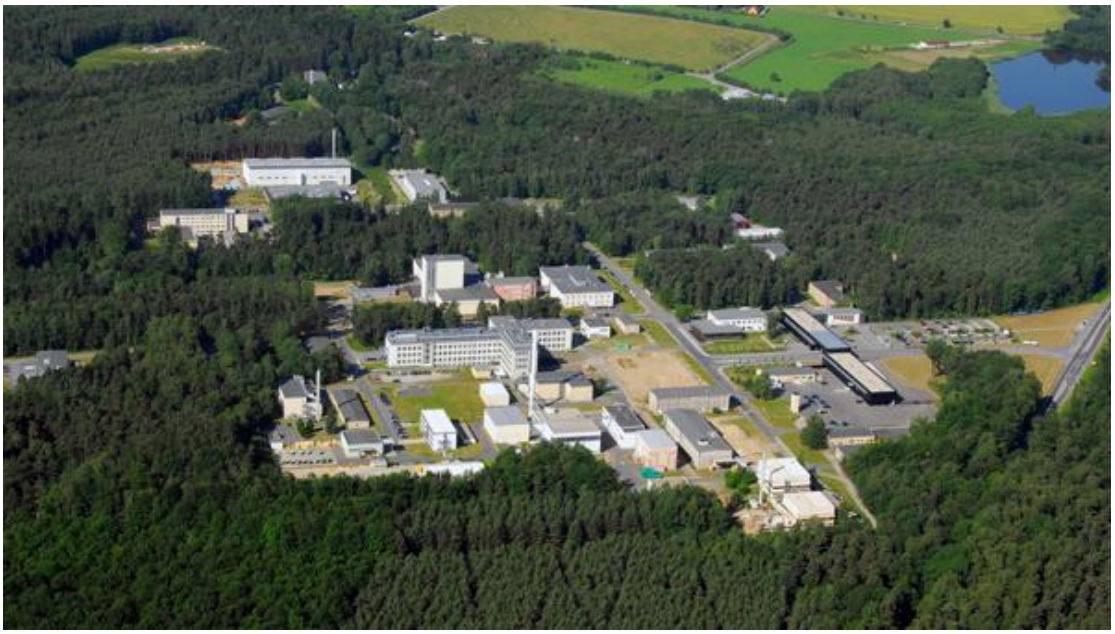

Figure 1.4: Aerial view of HZDR research institute

Several reactors for nuclear research were built in the center like RFR ("Rossendorfer Forschungsreaktor"), RAKE ("Rossendorfer Anordnung für kritische Experimente") and RRR ("Rossendorfer Ringzonenreaktor").

The following are some of the innovative installations/institutes that are settled in the HZDR:

- Institute of Ion-Beam Physics and Materials Research
- High Magnetic Field laboratory
- Institute of Radiopharmaceutical Cancer Research
- Institute of Fluid Dynamics
- Institute of Radiation Physics
- Institute of Radiooncology
- Institute of Resource Ecology

Nowadays, almost one thousand people work in the center.

Chapter 2

State of the Art

2.1 Forces acting on a particle

When a particle is deposited on a wall or over other particles, several forces are acting on it (see Fig. 2.1). The aerodynamic forces (i.e. lift, drag, etc) tend to remove the particle from the surface, whereas forces such as adhesive, gravitational, etc resist to the resuspension of the particle and hold the particle to the surface.

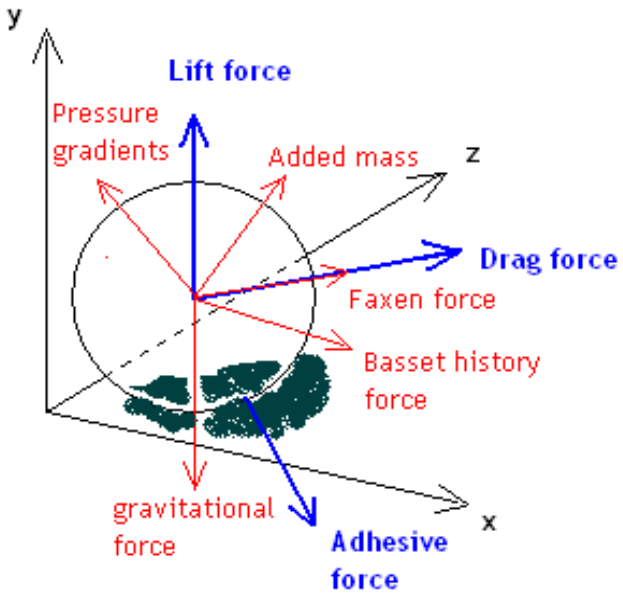

Figure 2.1: Forces acting on a particle (Zhang, 2011).

2.2 Resuspension models

The particle resuspension is usually indicated in terms of resuspension rate (Λ) and resuspension mass flux (Φr). According to Fauske (1984), the resuspension rate and mass flux are defined as, respectively:

$$\Lambda = \lim_{\Delta t \to 0} \frac{\Delta M / S}{\left(M_0 / S\right)\Delta t} = \frac{1}{M_0}\frac{dM}{dt} \tag{2.1}$$

$$\Phi_r = \Lambda \frac{M_0}{S} = \frac{1}{S}\frac{dM}{dt} \tag{2.2}$$

where, M_0 is the initial mass load of particles deposited on a surface with area S, and ΔM is the mass of the particles resuspended during a time interval Δt.

All the theoretical models for the simulation and prediction of the resuspension properties that have been developed so far, can be divided into two categories: one is based on a balance of forces which concerns the resultant force from aerodynamic and adhesive forces acting on a particle and the other is based on energy accumulation that describes particle removal with regards to accumulation of kinetic energy from the flow.

In the next sections of this chapter the force balance model and the energy balance model will be discussed.

2.3 Models based on Force balance

The force-balance model is based on a simple concept where particle resuspension is assumed to take place instantaneously when the aerodynamic forces exceed the surface adhesive force. Three types of force balance models have been developed - statistical models, kinetic models and Lagrangian models.

2.3.1 Statistical Models

Cleaver and Yates (1973) developed the first isolated-particle resuspension model to combine the statistical character of turbulent bursting with particle resuspension by using the visual observations on burst distribution in space and time. Although it is statistical in nature, it retains the essential character of a force-balance model. The resuspension depends on both the lift force caused by burst flow and the adhesive force from the surface (see Fig. 2.2).

The burst is modeled by Cleaver and Yates as an axisymmetric stagnation-point flow and the lift force acting on a particle is given by the formula

$$F_L = 0.608\rho_f \nu_f^2 \left(\frac{r u_\tau}{\nu_f} \right)^3 \tag{2.3}$$

where, ρ_f is the fluid density, ν_f is the fluid kinematic viscosity, u_τ is the wall friction velocity and r the particle radius.

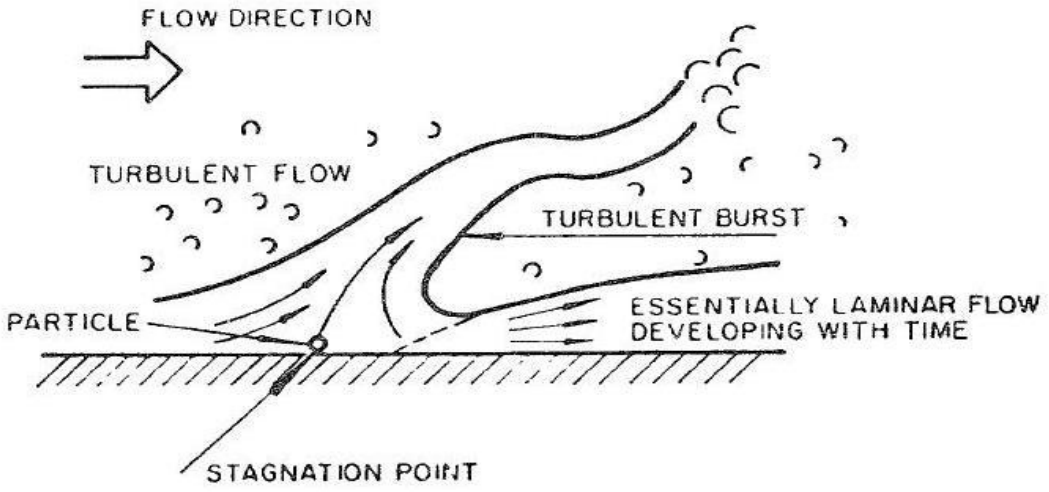

Figure 2.2: Schematic diagram of turbulent burst in the wall region (Cleaver & Yates, 1973).

Following Zimon (1964) they assumed that all types of adhesive forces are proportional to the particle diameter. Particle resuspension can occur if the lift force is greater than the adhesive force leading to the following criterion:

$$\rho_f \nu_f^2 \left(\frac{r u_\tau}{\nu_f} \right)^3 > const. \quad \Rightarrow \quad \tau_w r^{4/3} > \beta \tag{2.4}$$

where τ_w is the wall shear stress, β is a constant and the rest variables as in Eq.(2.3).

Ziskind et al. (1997) analyzed particle detachment from a surface by considering the aerodynamic and adhesion force (or moment). By using the JKR adhesion model (Johnson et al., 1971), they defined the conditions of particle resuspension from a perfect smooth surface which is similar to Eq.(2.4) and from a two-asperity rough surface.

$$\tau_w r^{4/3} > \frac{\gamma^{4/3}}{5.37\kappa^{1/3}} \qquad smooth\, surface \tag{2.5}$$

$$\tau_w r^3 > \frac{\gamma r_\alpha^2}{35.7} \qquad rough\,surface \tag{2.6}$$

where κ is elastic constant of the particle, γ is the surface energy and r_a is the asperity radius.

The aerodynamic force for the particle resuspension is given by turbulent burst based on an analysis of experimental data. Cleaver and Yates suggested that a typical burst diameter is of the order of $20\nu_f/u_\tau$ and that bursts are separated by a distance of about $630\nu_f/u_\tau$ in the streamwise direction, and $135\nu_f/u_\tau$ in the cross-stream direction (Fig. 2.3).

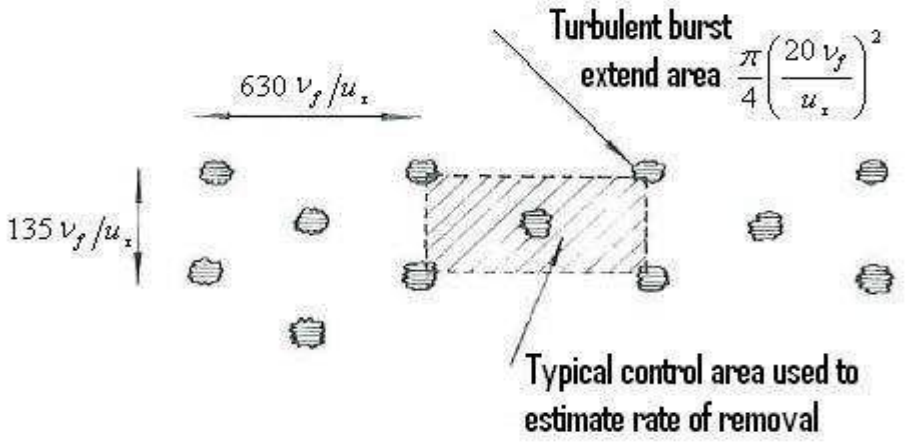

Figure 2.3: Turbulent burst distribution on the surface (Cleaver & Yates, 1973).

The mean time period between bursts is approximately $75\nu_f/u_\tau^2$. Assuming that some fraction α of the particles exposed to a turbulent burst on the surface of the deposit are removed, in other words all the particles in an area of $\alpha(\pi/4)(20\nu_f/u_\tau)^2$ will be removed from the surface in any one burst, the fraction of the particles resuspended as a function of time is given by:

$$f_c(t) = 1 - \left(1 - \frac{\alpha(\pi/4)(20\nu_f/u_\tau)^2}{630\nu_f/u_\tau \times 135\nu_f/u_\tau}\right)^{\left(u_\tau^2/75\nu_f\right)t} = 1 - \left(1 - \frac{\alpha}{270}\right)^{\left(u_\tau^2/75\nu_f\right)t} \tag{2.7}$$

The initial resuspension rate defined at the moment when the surface is first exposed to a turbulent burst is given by

$$\Lambda(0) = \left.\frac{df_c}{dt}\right|_{t=0} = -\frac{u_\tau^2}{75\nu_f}\ln\left(1-\frac{\alpha}{270}\right) \tag{2.8}$$

Cleaver and Yates assume that the constant α is approximately of the order 1/100.

Braaten et al. (1990) developed a Monte-Carlo particle resuspension model which was capable of simulating the unsteady nature of resuspension and compared the results with those obtained from a resuspension experiment using Lycopodium particles (count-median diameter 27.8 μm). They considered the random nature of turbulent-burst effect and used an approximate mean time ($300\nu_f / u_\tau^2$) between bursts. For each time step, Braaten et al. generate a random number from a probability distribution to calculate surface fluid force; if it is larger than the minimum required for resuspension, a fraction of particles removed is determined by a particle adhesion function (which is given by a log-normal distribution) and compared to the current cumulative removal fraction. If the calculated fraction removed is larger than the current cumulative removal fraction, the latter is replaced.

Braaten et al. concluded that the fraction of particles removed from the wall in a turbulent boundary layer with a constant streamwise velocity as a function of time was found to be governed by two regimes which both can be fitted to exponential functions. The first occurs in the first few minutes (nearly 60% particles removed in first 5 minutes) and then the fraction gets a constant value around 60% - 70%.

2.3.2 Kinetic Models

Matsusaka and Masuda (1996) studied the resuspension of aggregates from a fine powder layer in an accelerated flow and presented a new model to explain the time dependence of the resuspension of aggregates. An experiment was also provided by resuspending fly-ash particles (mass median diameter ~3 μm) in air flow. The experimental results showed that the distribution of adhesive strength (wall shear stress which calculated from the mass flux) was approximated by a log-normal distribution.

The resuspension phenomena is described as consisting of two types, the short delay resuspension (due to small fluctuation in the shear flow) and long delay resuspension (due to large fluctuation caused by turbulent burst), where the resuspension flux of both cases is approximated by simple exponential functions. It is also shown that the resuspension flux increased in an accelerated flow with elapsed time being approximately proportional to flow acceleration α (see Fig. 2.4).

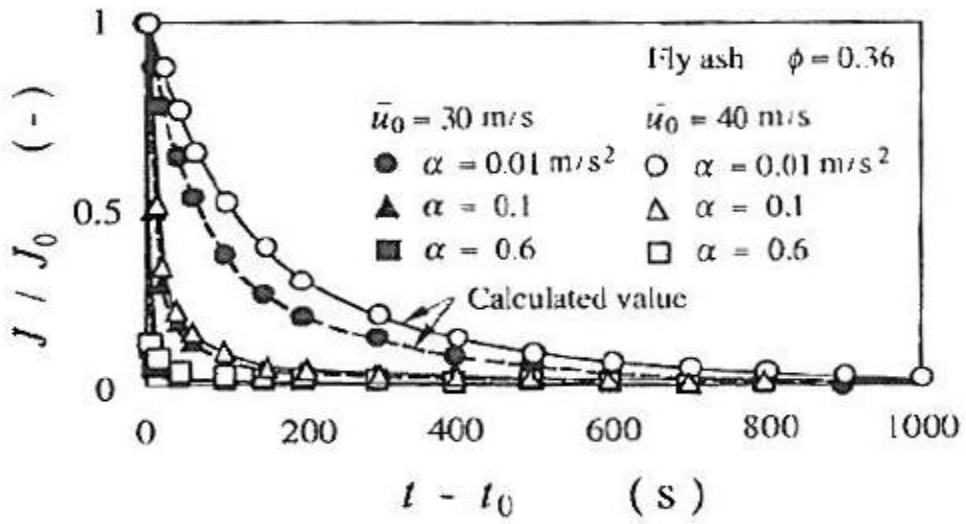

Figure 2.4: Resuspension flux with different flow acceleration (Matsusaka & Masuda, 1996).

2.3.3 Lagrangian Models

Hontañón et al. (2000) developed a force-balance resuspension model by using a 2D Lagrangian particle tracking method, which calculates the trajectory of the particles within the viscous sublayer of turbulent pipe flow. The model was conceived to deal with small particles (up to a few microns) so the gravitational force was neglected. The particles were assumed to be hard smooth spheres, sitting on a rough surface consisting of asperities with the same radius of curvature, and a height distribution given by a polynomial approximation.

The formula for the drag force for a small particle close to a wall in turbulent pipe flow, included corrections due to both inertial and wall effects, and the lift force used in the model is that derived by Cherukat and McLaughlin (1994). The adhesive force acting on the particle is derived using the Lennard-Jones (LJ) potential (Lennard-Jones, 1931) to describe the intermolecular interaction of the particles and surface. The equation includes both the attractive and repulsive terms.

The model was used to simulate resuspension in the STORM experiment (see Section §2.6) conditions. There is an initial phase (see Fig. 2.5), lasting a few milliseconds, in which most of the material is resuspended, and then the resuspension rate falls very rapidly. This agrees qualitatively with experimental observations, but the initial resuspension rate is higher than that measured in the experiments. One possible explanation for this is that this is a single layer model, in which all the particles are exposed to the flow directly and it does not include cohesion between particles.

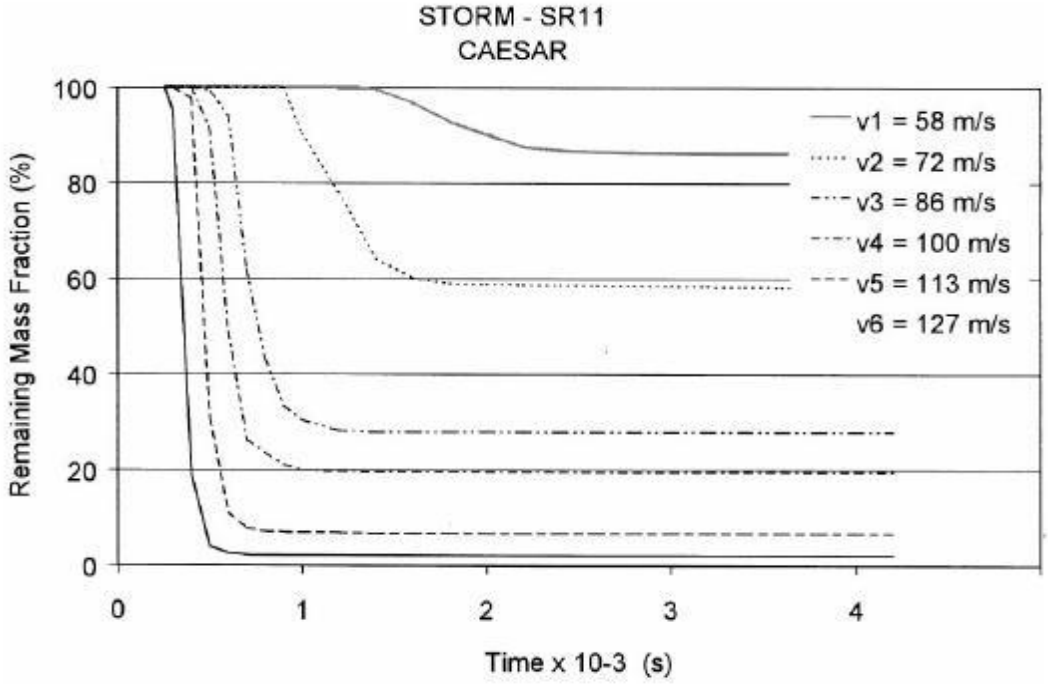

Figure 2.5: Remaining mass fraction vs. time prediction (CÆSAR model) (Hontañón et al., 2000).

Guingo and Minier (2008) proposed a new model aiming at simulating the resuspension of spherical particles in turbulent air flow using stochastic Lagrangian methods. In this model, particles are considered to be resuspended when the drag moment exceeds the adhesion moment. The drag force is taken as 1.7 times the Stokes drag. In this model the surface of the wall consists of a mixture of large and small scale roughness elements, and the adhesive force then depends on the size of the particle relative to the size of the roughness elements and the spacing between them. Three different cases are possible (see Fig. 2.6).

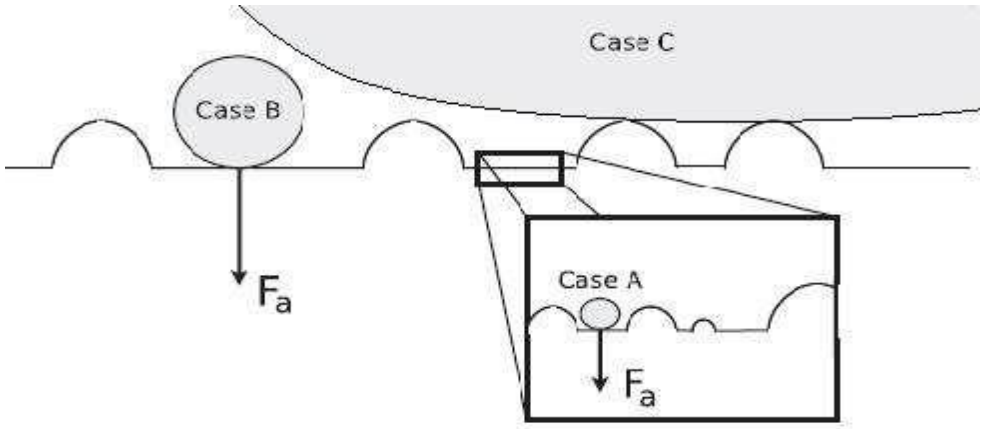

Figure 2.6: Adhesion model in three different cases of particle size (Guingo & Minier, 2008).

Case A: small particles

In this case, the wall is considered as smooth. According to the JKR theory (Johnson et al., 1971), the adhesive force is given as

$$F_\alpha = 3\pi r\gamma \tag{2.9}$$

where γ is the surface energy.

Case B: mid-sized particles

The particle is large enough to be in contact with several small asperities; to evaluate the number of these asperities, the contact radius (r_c) needs to be defined using the JKR theory.

$$r_c = \left(\frac{12\pi\gamma r^2}{K}\right)^{1/3} \tag{2.10}$$

where K is the composite Young's modulus defined by

$$K = \frac{4}{3}\left(\frac{1-\nu_1^2}{E_1} + \frac{1-\nu_2^2}{E_2}\right)^{-1} \tag{2.11}$$

where ν_1, ν_2 are Poisson's ratio for the particle and the substrate, respectively, and E_1, E_2 are Young's modulus.

If the mean asperity radius is denoted for the small scale roughness by r_{fine}, and the surface density of the small scale elements by ρ_{fine}, then the adhesive force is given by:

$$F_\alpha = P\left(\rho_{fine}\pi r_c^2\right)\frac{H_c L\left(r_{fine}\right)}{6H_0^2} \tag{2.12}$$

where P is generated from a Poisson distribution, L is generated from a log-normal distribution with the standard deviation equal to the mean, H_c is the Hamaker constant and H_0 is the equilibrium distance (0.3nm), i.e., the particle-surface gap.

Case C: large particles

A large particle will be in contact with several large-scale asperities and the number of contact points is estimated as a Poisson distribution with mean $2r/L_{large}$ where L_{large} is the mean distance between two large-scale asperities. Then the total adhesive force is given by:

$$F_\alpha = \sum_{i=1}^{l} P_i\left(\rho_{fine}\pi r_c^2\right)\frac{H_c L_i\left(r_{fine}\right)}{6H_0^2}, \qquad where\ l = P\left(2r/L_{large}\right) \tag{2.13}$$

In all three cases the aerodynamic drag force is taken as 1.7 times the Stokes drag. The model was used to simulate the experiments of Ibrahim et al. (2003) and it reproduces the main features of their results (see Fig. 2.7, dot: alumina particles r = 36μm, square: alumina particles r = 16μm).

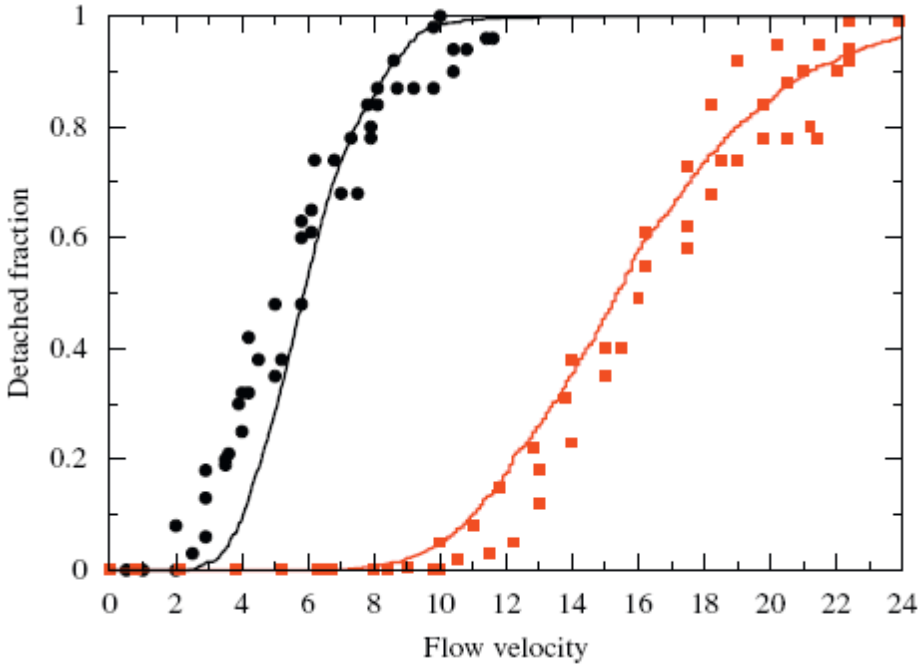

Figure 2.7: Results of G&M model and Ibrahim's experiments (Guingo & Minier, 2008).

The model was also used to simulate Hall's experiment (Reeks & Hall, 2001) with 10μm graphite particle resuspension (see Fig. 2.8). Based on these comparison, Guingo and Minier concluded that the surface roughness and Hamaker constant, which are input variables for their model, do represent physical quantities or material properties and have strong intrinsic physical meaning which are important aspects of particle resuspension.

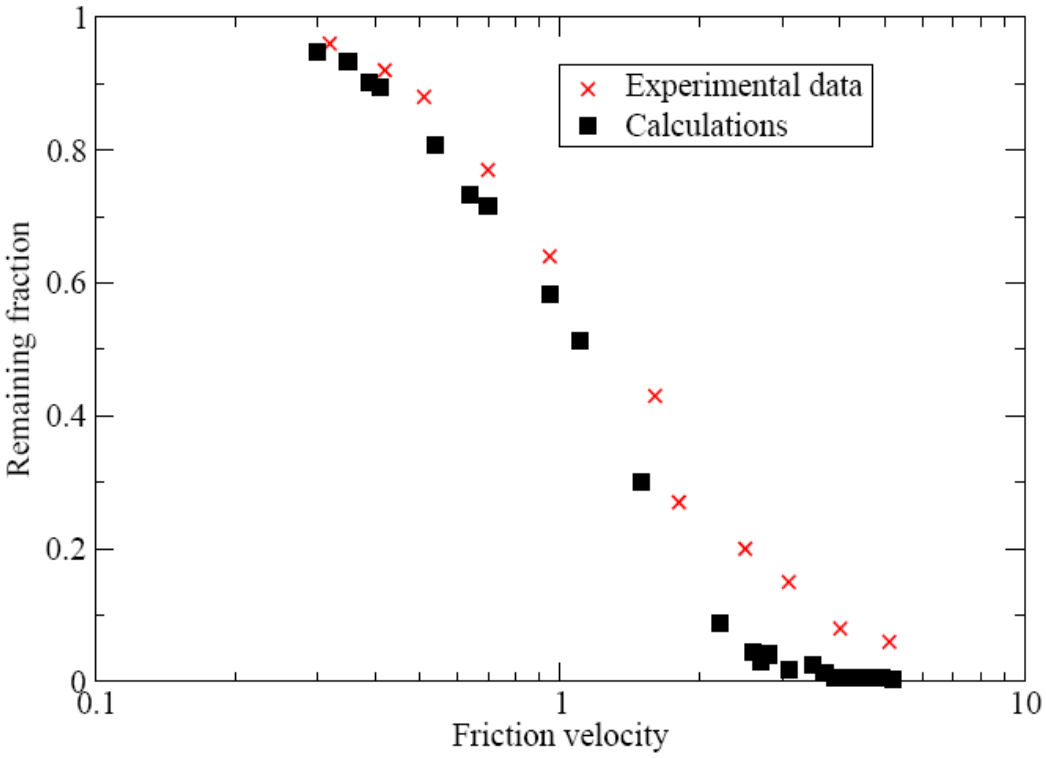

Figure 2.8: Results of G&M model and Hall's experiment (Guingo & Minier, 2008).

2.4 Models based on Energy Accumulation

Force-balance approaches imply that particles are resuspended instantaneously from a wall when the aerodynamic forces exceed the resistance forces (adhesion, etc.). However, Sehmel (1980) showed from experimental measurements that particle resuspension from a surface was not instantaneous but evolved with time. According to Corn and Stein (1965), the removal of nominally identical small particles from a smooth surface in high-velocity air also depends on the time of exposure. Based on the observation that small particles can be resuspended, even when the adhesive force exceeds the aerodynamic force, Reeks, Reed and Hall (1988) (hereafter RRH) proposed a new model, based on the idea that the adhesion of the particle to the substrate can be represented as a particle in a potential well, with a potential that decreases as the particle moves away from the surface. The action of the unsteady turbulent flow on the particle then causes it to vibrate – to oscillate within the well – until it acquires enough vibrational energy to escape from the well, and becomes resuspended. They defined a resuspension rate constant p, for a long-term resuspension of the form

$$p = \omega_0 \exp\left(-\frac{Q}{2\langle PE\rangle}\right) \tag{2.14}$$

where ω_0 is the typical natural frequency of the system, Q is the height of the surface adhesive potential well and $<PE>$ is average potential energy of a particle in a well. Later, Reeks and Hall (2001) developed this model to include aerodynamic drag, applied using a quasi-static analysis of the particle at the top of the potential well; thus has become known as the Rock'n'Roll model.

Since in this thesis, the model that will be developed will be based upon the force balance method, the equations that form the energy balance models (RRH and Rock'n'Roll) are omitted. These could be found in the literature (Reeks et al., 1988) as well as to (Vainshtein et al., 1997), (Biasi et al., 2001), and (Zhang et al., 2013) where the latter ones are presenting improvements of the former energy balance models.

The modeling results (see Fig. 2.9) show that the resuspension of particles (radius around 25-50μm) from a rough surface can be divided into two regimes: the initial resuspension in which many particles are resuspended within a very short time; and the long-term resuspension where its rate is proportional to approximately $t^{-1.1}$. This relationship is observed for wide variations of particle diameter, flow conditions and surface roughness and this behavior of reverse time relationship has also been confirmed by other models and experiments (Wen and Kasper, 1989), (Jurcik and Wang 1991).

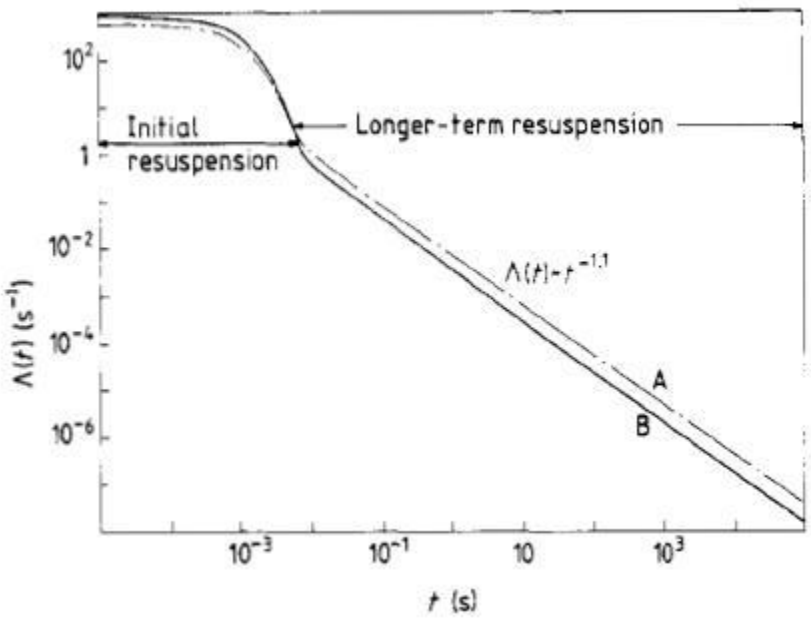

Figure 2.9: Resuspension rate vs. time (Reeks et al., 1988)

Reeks and Hall reported 20 resuspension experiments that used both alumina and graphite particles. The parameters for adhesive force log-normal distribution in the RRH and the R'n'R models are produced based on Reed and Rochowiak (1988). The results for 10μm alumina (in diameter) and graphite particle are shown in Fig. 2.10 and Fig. 2.11, respectively. It can be seen from the figures that the Rock'n'Roll model gives much better agreement with experimental values of the resuspension than the original RRH model, the agreement being fairly good considering the large uncertainty in the adhesive force measurement. Furthermore, the comparison between the Rock'n'Roll model results with and without resonant energy transfer shows only a slight difference. This means that the resonant energy transfer only makes a very small contribution to resuspension and the quasi-static version (without resonant energy transfer) can be used for certain conditions.

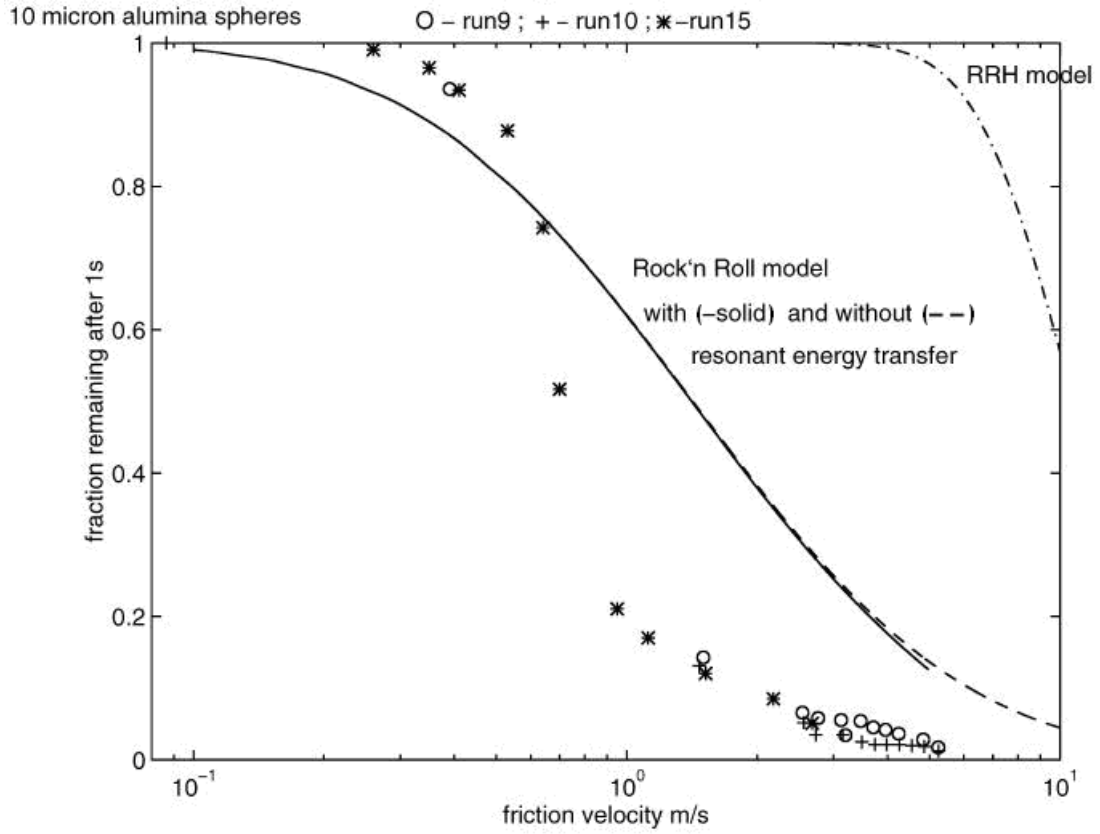

Figure 2.10: Comparison of alumina particle fraction remaining (Reeks & Hall, 2001).

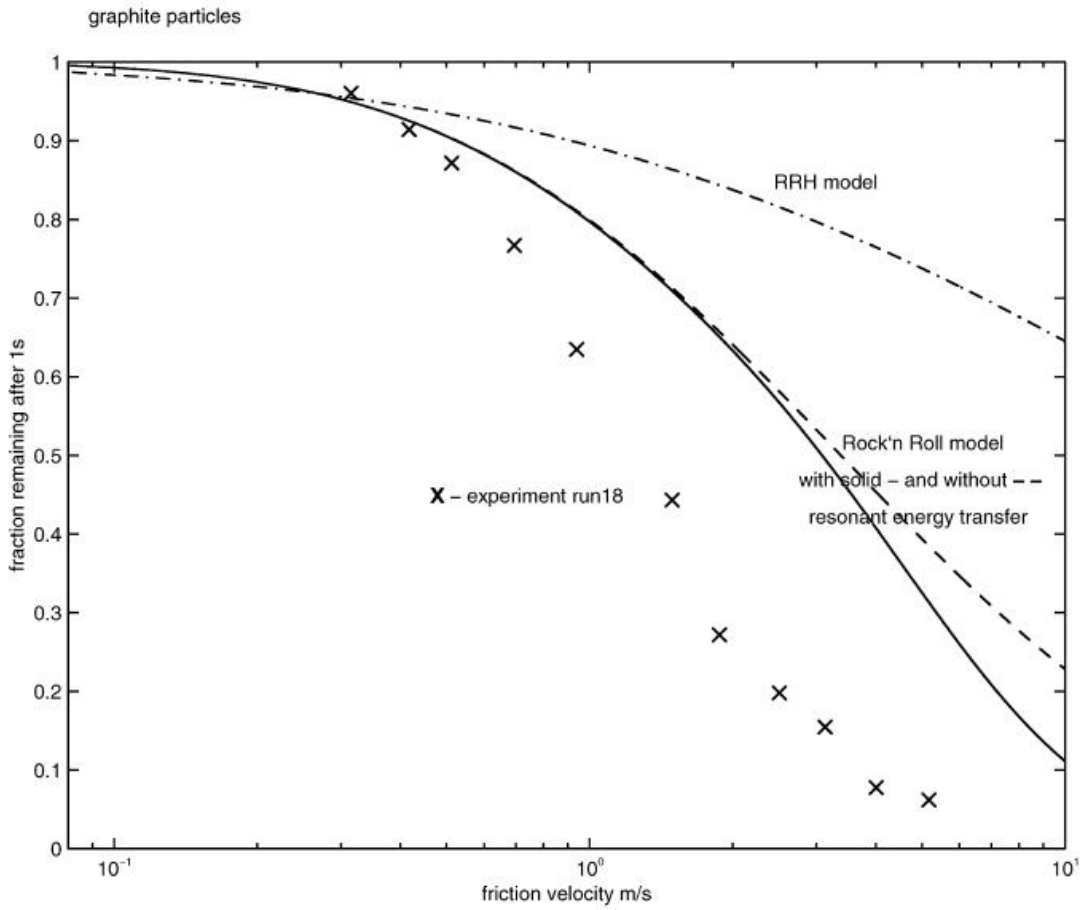

Figure 2.11: Comparison of graphite particle fraction remaining (Reeks & Hall, 2001).

Vainshtein et al. (1997) observed resuspension due to rolling and they concluded that the drag force is a more effective agent than lift for the transfer of turbulent energy from the flow to a particle on a surface. The Vainshtein et al. model used the potential-well approach and considered the particle wall effect as though the particle is connected to the wall by a spring. They defined a tangential pull-off force which pulled the particle off against the spring. Compared with the RRH model, the ratio of the height of the potential well to the average potential energy in Eq.(2.14) ($Q/2<PE>$) was rewritten as the ratio of the pull-off force to turbulent drag force.

Stempniewicz et al. (2008) compared the results of the Rock'n'Roll model (Reeks and Hall, 2001) and Vainshtein model (1997) with the experiments of Reeks and Hall and STORM experiments (see Fig. 2.12), and concluded that the Vainshtein model gave better agreement with the experiment results whereas the Rock'n'Roll model somewhat overestimated the resuspension at low value of the friction velocity. They also concluded that

the adhesive force and its distribution for dust particle deposited on a rough surface were very important in successful resuspension predictions.

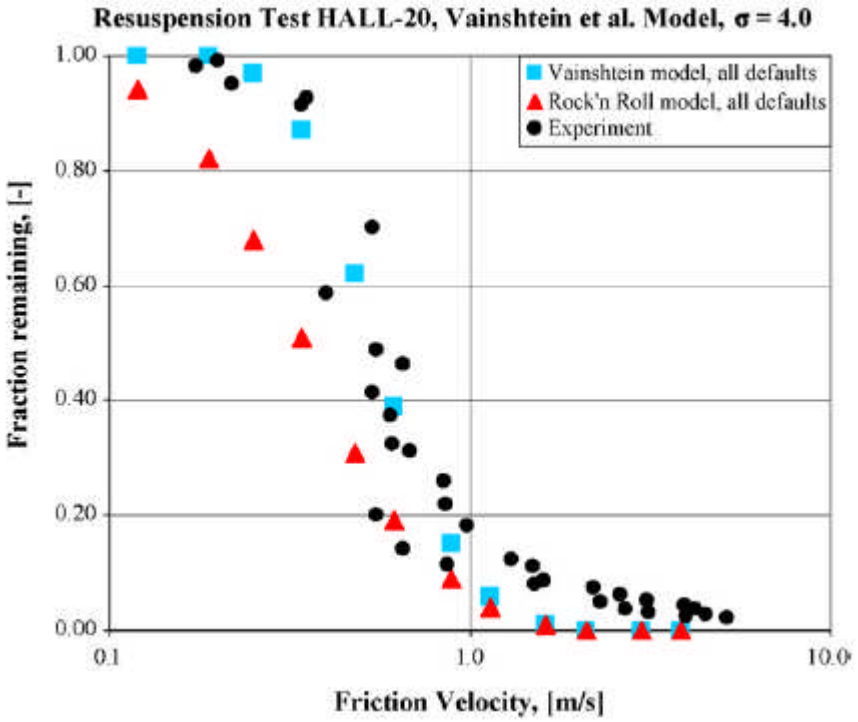

Figure 2.12: Remaining fraction for R'n'R and Vainshtein model (Stempniewicz et al., 2008).

Biasi et al. (2001) took the Rock'n'Roll model for resuspension with an empirical log-normal distribution of adhesive force to reproduce the resuspension data of a number of experiments. Some adhesion-force parameters were tuned to fit the data of the most highly-characterised experiments, i.e., those of Hall (Reeks & Hall, 2001) and Braaten (1994). Then, using an enlarged dataset including STORM and ORNL ART (Aerosol Resuspension Test) resuspension results, they obtained a global correlation for geometric mean adhesive force and geometric spread as a function of particle geometric mean radius (in microns).

They also concluded that the measurements of adhesive force (Boehme et al., 1962) show that the distribution of adhesive forces is close to a log-normal distribution, but that the validity of assuming a Gaussian distribution for the drag force might be questionable (i.e. there is no physical basis justifying the particular form of the Gaussian distribution). They also pointed out that, in reality, the geometric ratio of particle radius to average separation of asperities, *r/a*, appearing in the R'n'R model, rather than being a constant, has a spread as with the actual adhesive force.

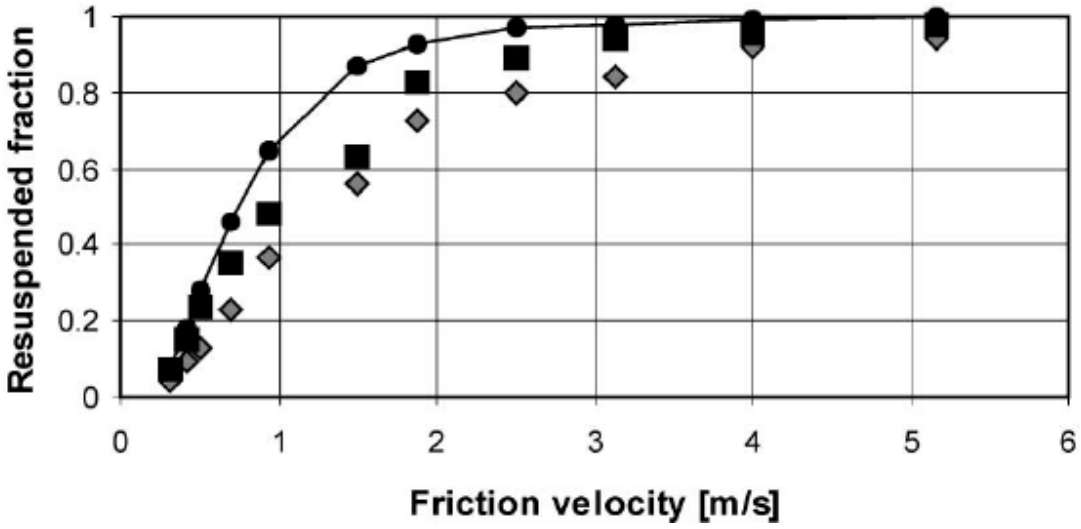

Figure 2.13: Biasi's result compare with Reeks and Hall's experiment (Biasi et al., 2001).

2.5 Models for Resuspension from a Multilayer Deposit

In most nuclear accidents, particles will first be deposited on the walls, forming multilayer deposits, before being resuspended. But all the models reviewed so far consider the resuspension of an isolated particle from a clean surface. In reality, particles will be in contact with other particles and will form agglomerates or clusters, and it may be argued that particles will be resuspended in "clusters" rather than individually. In the multilayer deposit, bulk density (related parameter, porosity) has been used to characterize the structure (i.e. how dense the deposit structure is) (Schmidt & Löffler, 1991). Coordination number (which is the average number of contacts of a particle) is an important parameter for the structure of agglomerates (Weber and Friedlander, 1997). Furthermore, the aerodynamic contribution should be taken into account through the shielding effect by existence of other particles in the deposits. The aerodynamic drag force acting on each constituent particle should be definitely smaller than that without other particles. Iimura et al. (2009) concluded that the morphology of deposits much affects the resuspension of particles and the steric-bulky deposit undergoes the stronger aerodynamic force and is easy to be resuspended and consequently a smaller number of particles remain attached to the surface.

The first multilayer model was probably that of Paw U (1983) which was initially an extension of the model of Cleaver and Yates (1973). In this model, the multilayer deposit ensures a continuous supply of particles for resuspension, so the resuspension fraction becomes:

$$f_c(t) = \frac{1}{270}\frac{u_\tau^2 t}{100\nu_f} \tag{2.15}$$

where $100\nu_f / u_\tau^2$ is the average time between turbulent bursts in Cleaver and Yates (1976), ν_f is the fluid kinematic viscosity and u_τ is the wall friction velocity. Paw U concluded that the model required further development to include saltation, and the physics of the atmospheric surface boundary layer and rebound/net-deposition phenomena. One can observe that it is a rough model since the resuspension fraction is determined as a resuspension probability constant (1/270) multiplied by the total number of bursts.

Fromentin (1989) set up a two-step experiment PARESS (PArticle RESuspension Study) in which the first step was deposition of different aerosols and the second step was resuspension. Experiments were performed with a range of mean flow velocities, between 5 and 20m/s. Throughout the experiments, the long-term resuspension flux (time > 2s) decreased with time of exposure to the flow and could be modeled by an expression of the form where A and B are empirical coefficients.

$$\Lambda = A \cdot t^{-B} \tag{2.16}$$

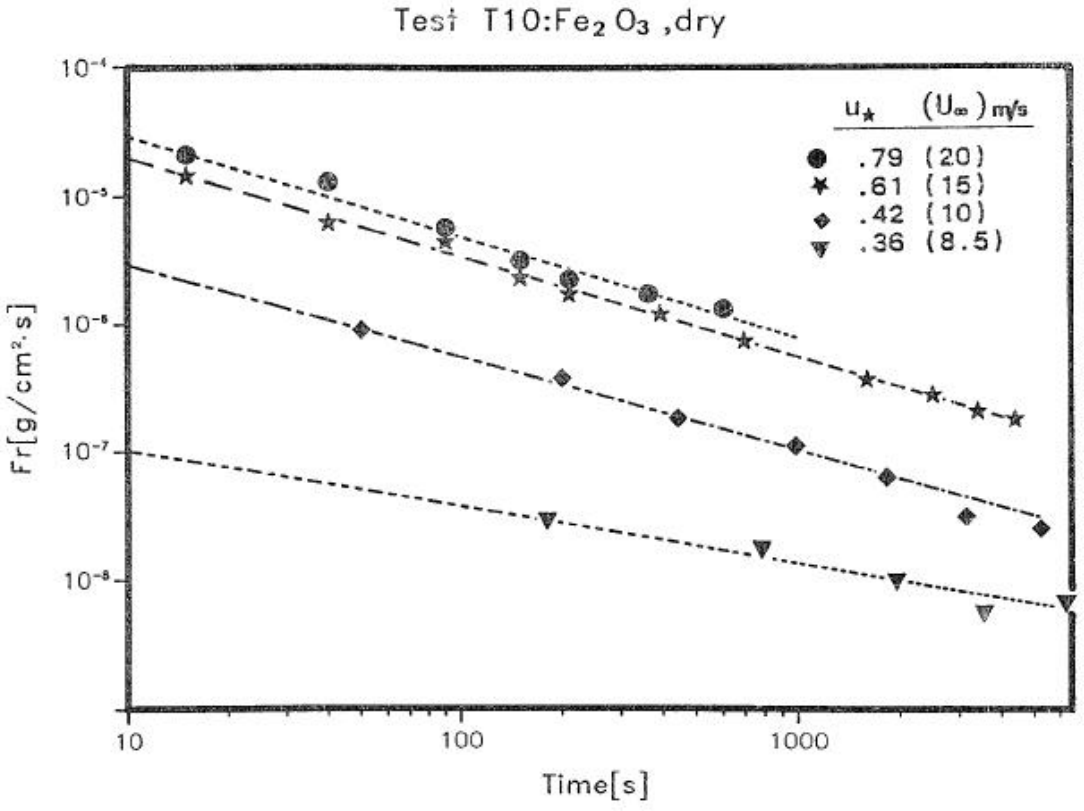

Figure 2.14: Resuspension flux vs. time of Fromentin's model (Fromentin, 1989).

Fromentin showed that the constants A and B are proportional to the wall friction velocity u_τ. Therefore, the resuspension flux could be written as a function of time and wall friction velocity.

$$\Lambda = 0.025\left(u_\tau - 0.29\right)^3 t^{-1.2\sqrt{u_\tau}} \tag{2.17}$$

which is valid for 2s < t < 10000s, and 0.3m/s < u_τ < 1m/s.

Lazaridis and Drossinos (1998) derived an expression for the total particle resuspension rate from a multilayer deposit in terms of the fixed resuspension rate from each layer, calculated using the RRH model. An interaction potential is considered between each layer and particle-particle interactions in the same layer are neglected (i.e. no particle interaction in the streamwise axial direction). The formula for interaction energy between a particle and the surface or between particles are developed and used to evaluate the natural frequency of vibration in the RRH model. In order to obtain an analytical solution for the particle fraction remaining on the surface as a function of time, the deposit was limited to two layers.

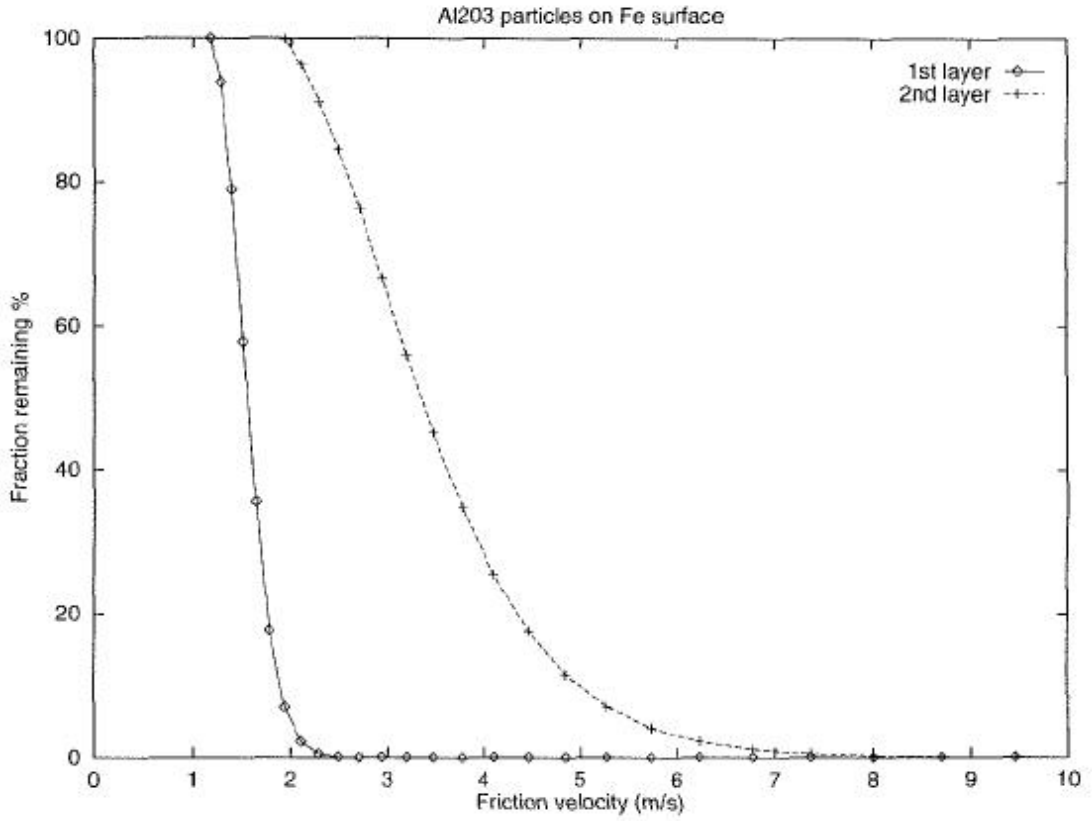

Figure 2.15: Two-layer 10μm Al_2O_3 particle fraction remaining (Lazaridis and Drossinos, 1998).

Friess and Yadigaroglu (2001) provided a generic model which uses a recursion relation for the resuspension rate of the first layer (i = 1) to calculate the resuspension rate of the layers below ($i \geq 2$).

The particle resuspension rate of the current layer i, based on the previous layers derived by:

$$\Lambda_i(t) = \int_0^t \Lambda_1(t-t')\Lambda_{i-1}(t')dt' \quad i \geq 2 \tag{2.18}$$

The total resuspension rate for L layers ($L \geq 2$) deposit was given by:

$$\Lambda_L(t) = \Lambda_1(t) + \sum_{i=2}^{L}\int_0^t \Lambda_1(t-t')\Lambda_{i-1}(t')dt' = \Lambda_1(t) + \int_0^t \Lambda_1(t-t')\Lambda_{L-1}(t')dt' \tag{2.19}$$

They compared their model with that of Lazaridis and Drossinos (1998) and found that the exposure time required to resuspend half of the deposit predicted by their generic model (i = 150, typical value of STORM test) is 2.4 times longer than that computed by L&D's model.

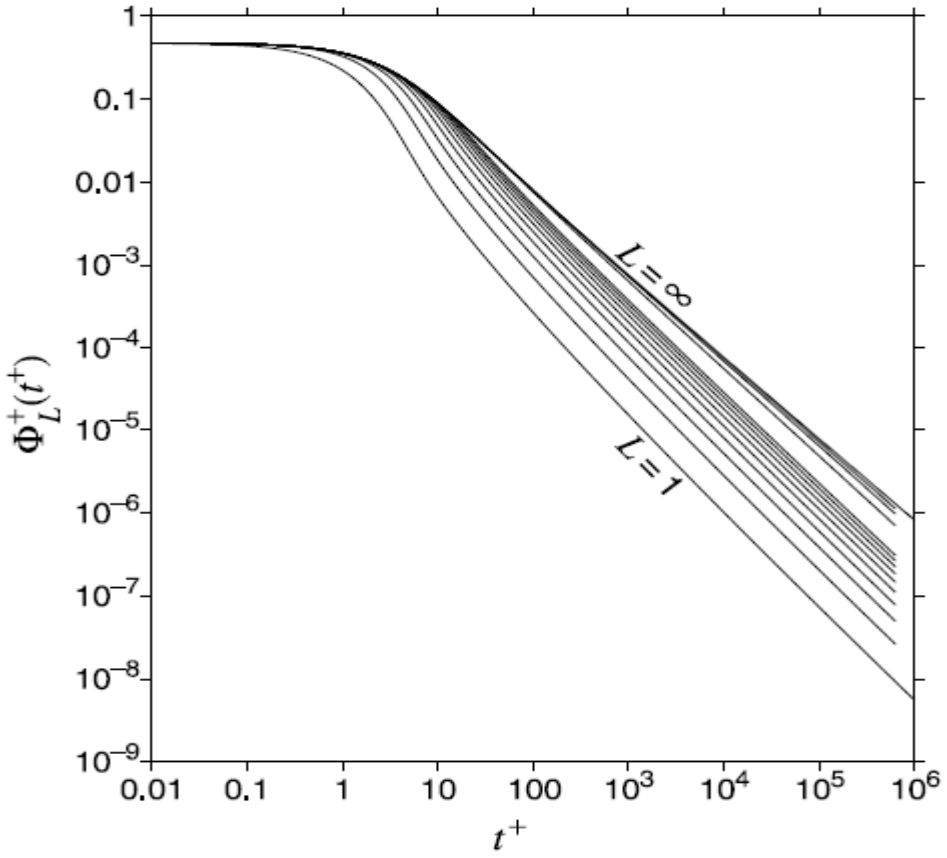

Figure 2.16: Dimensionless resuspension flux (Friess & Yadigaroglu, 2001)

Figure 2.16 shows the dimensionless resuspension flux vs. dimensionless time for the various thickness deposits (L = 1, 2, 3…, 10, 20, 30, 40, infinity). Friess and Yadigaroglu (2001) mentioned that the fact that the resuspension flux is predicted to always become zero after an infinite time might seem paradoxical: One might expect that eroding an infinitely thick deposit by means of a fluid of constant velocity eventually leads to a stationary state with a nonzero value of the resuspension flux.

The main conclusion of Friess and Yadigaroglu (2001) is that major discrepancies between theory and experiment are to be expected if a monolayer model is used for a wide range of initial deposit thicknesses. The monolayer models also over predict the resuspension mass and the short term resuspension flux. For long-term flux, the results of a monolayer model are acceptable.

In order to investigate the influence of the deposit structure on particle resuspension, Friess and Yadigaroglu (2002) developed a new simulation tool, in which individual particles were first deposited on a wall, to build up a multilayer deposit. Each particle is deposited with a "sticking probability" (s) which is used to determine, randomly, whether a particle will stick to another deposited particle or slide over it. This sticking probability directly determines the porosity, ε, of the bed that is formed. When the sticking probability is very low (s = 0) the bed is closely packed and the porosity tends to its minimum value; as the sticking probability increases the bed tends to grow in bifurcating chains of particles, and the porosity increases.

Every cluster is associated with a resuspension probability per unit time, pc, which is based on a balance between adhesion forces and the forces exerted by the turbulent bursts (which the distribution of burst forces exerted on a cluster is assumed to be Gaussian). It is similar to the model that originally proposed by Fromentin (1989) and later refined by Friess and Yadigaroglu (2001). The resuspension mass flux is then derived as:

$$\varphi_r(t) = -\frac{d}{dt} m(t) = \frac{\pi}{6} \rho_p D_m p_c \frac{d}{dt} \int_0^t e^{-p_c t'} \sum_{i=0}^{L_n - 1} \frac{(p_c t')^i}{i!} dt' \tag{2.20}$$

where $m(t)$ is the remaining mass per unit wall surface area as a function of time, D_m is the mass mean diameter of deposited particles, and L_n is the quantity layer number, defined as the number of particles intersected on average by a line normal to the wall (Friess and Yadigaroglu, 1998).

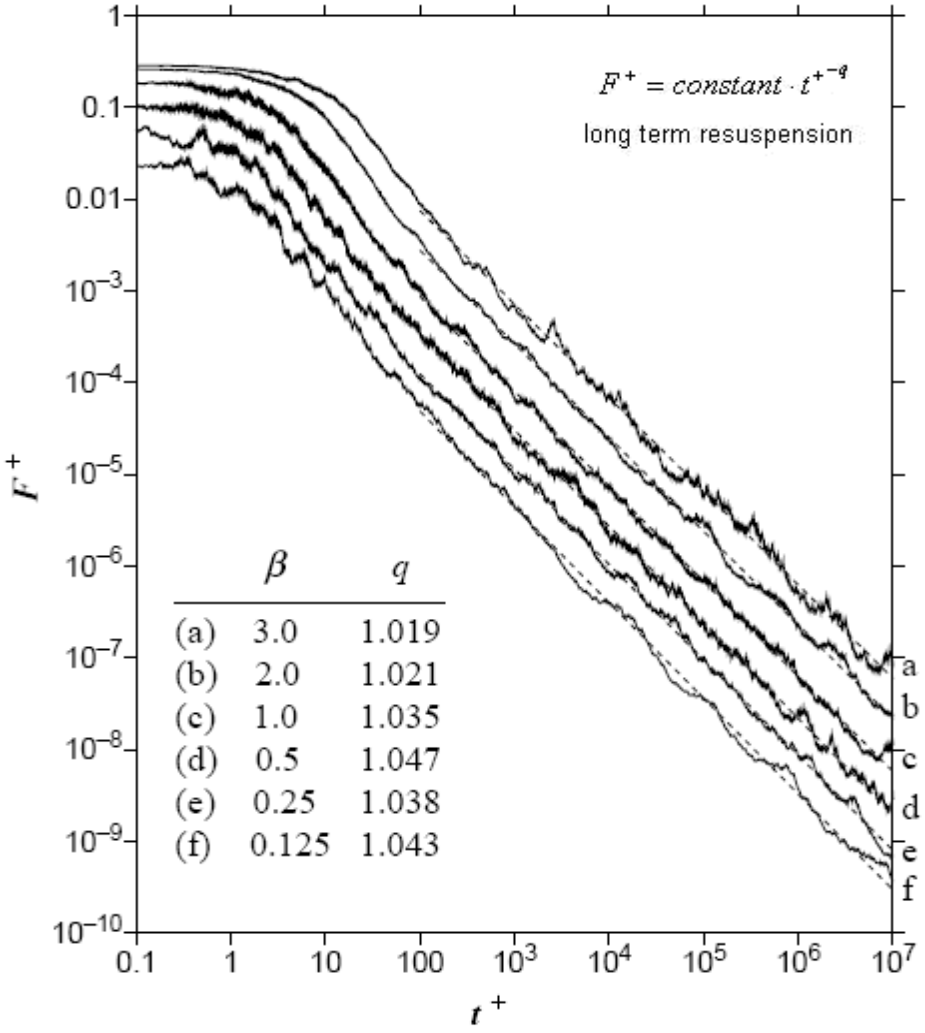

Figure 2.17: Dimensionless resuspension flux (Friess & Yadigaroglu, 2002).

Friess and Yadigaroglu (2002) showed that the model predictions confirm the 1/t law for long-term resuspension (in Fig. 2.17, β is the relative burst strength which is the ratio of the average burst force on a particle to this particle's adhesion force on a flat base) and conclude that the values of exponent q = 0.8 (see equation in Fig. 2.17) from the PARESS experiments are still theoretically unexplained. They also analyze the sensitivity of the model to bed porosity, using the data from STORM experiment. The characteristic shape of model responses can be seen to depend strongly on the bed porosity. The model results offered an explanation for the difference in resuspendability between the deposits in the PARESS (Fromentin, 1989) and STORM (Agrati et al., 1991) experiments.

2.6 Resuspension Experiments

2.6.1 Main resuspension experiments

Many experiments have been performed to investigate different aspects of the resuspension of small particles by a turbulent flow. These experiments can be divided into two main groups; those aimed at improving the detailed understanding of specific physical processes involved in the resuspension of a small particle from a clean surface, and those designed to provide data concerning the collective resuspension of a large number of particles from a deposit. Often these latter experiments have been performed in conditions that are as close as possible to those that might occur in a real resuspension event in a nuclear circuit. Data from both types of experiment have been used in the development and validation of resuspension models, but the very wide range of conditions and experimental techniques that have been used makes it difficult in some cases to obtain general agreement on the influence of certain parameters and effects (Zhang, 2011).

It should also be emphasized that the conditions in a real resuspension event in a nuclear circuit are likely to be so extreme (temperature, velocities, radioactivity...) that it is not possible to envisage simulating them directly in an experiment. So the only way of extrapolating from laboratory experiments to these extreme conditions is with models which reproduce the basic physical processes correctly.

Parozzi et al. (1995) reviewed several nuclear process based resuspension experiments in detail:

- The Marviken Experimental Intermediate Program (Ström, 1986) which investigated the possible effect of the resuspension mechanism on the aerosol deposition in pipes and concluded that no resuspension effect had influenced the tests previously performed.

- The LWR Aerosol Containment Experiments (LACE) (Rahn, 1988) which focused on providing a representative database for thermal-hydraulic and aerosol codes in the scenarios of containment failures.

- PARESS (PArticle RESuspension Study) (Fromentin, 1989) which gave preliminary indications about the main characteristics of the resuspension phenomenology although it did not produce data bases representative of RCS (Reactor Coolant System) conditions because of the lack of accurate measurements of the initial mass in RCS condition.

- AEA Winfrith Experiments (Benson and Bowsher, 1988) which confirmed the importance of the physical resuspension process in severe accident analyses although the conditions of those tests were again quite far from LWR accident conditions.

- Oak Ridge Experiments (Wright et al., 1986) which is the most systematic experimental approach to dry aerosol resuspension within the RCS and the results showed that the resuspension became significant (~90%) at high velocity (~ 60m/s).

- STORM Program (Simplified Tests On Resuspension Mechanisms) (Agrati et al., 1991) in which the experiments were designed to investigate two processes considered to be important in the primary cooling circuit – thermophoretic deposition and mechanical resuspension.

Only a few experiments have been performed using multilayer deposits. The PARESS experiment (Fromentin, 1989) includes two steps:

- Deposition phase in which particles (Fe2O3, Sn, Si and NaCl) are generated with an AMMD (Aerodynamic Mass Median Diameter) between 2 and 4.3 μm and STD (Geometric Standard Deviation) is around 2.

- Resuspension phase in which the mean velocity of the flow could be selected from 5 to 20 m/s.

Fromentin determined a fraction of resuspended particles which he expressed in terms of the mean flux, calculated from the difference between the mass of the deposit before and after resuspension. From these experimental data, Fromentin established a relationship between resuspended flux, the exposure time and the friction velocity near the surface. He also concluded that the resuspended flux was approximately proportional to the surface friction velocity. Also, the study showed that the mechanical resuspension of dry particles reveals two distinct aspects: erosion and denudation. If erosion occurs, the dust is removed steadily layer by layer, while if denudation occurs, the deposit is suddenly lifted and holes are produced on the deposited surface.

Raunio (2008) produced a resuspension experiment funded by VTT (Technical research center of Finland). The experimental data showed that there are only about 50% of the particles resuspended after approximately 100 minutes. Raunio concluded that their resuspension results suffered from large uncertainties and are largely inconclusive.

2.6.2 Experiments at HZDR

For the work presented in this thesis, the resuspension will be validated with experimental data from experiments performed in HZDR (Barth et al., 2013).

The experiments were performed in an air-driven small-scale test facility (Figure 2.18). This Gas Particle Loop is an open-loop wind tunnel consisting of an inlet with a particle filter, a nozzle contracting the flow into a flow formation zone and a subsequent test section. The profile of the test section is a square with a hydraulic diameter of about d_{hyd} = 10 cm. 15 steps were placed on the bottom of the channel characterized by the step height h and the streamwise distance between the steps P. The aspect ratios of the arrangement were adjusted to previous works so as to allow comparability to their results (d/h = 10, P/h = 10). The test section is followed by a diffuser stage and an electrostatic precipitator to remove the particles from the gas stream before the flow enters the power unit consisting of one radial fan. The turbulent flow field is fully developed after the 10th step.

Streamwise periodicity of the particle multilayer was rechecked by comparing the layer thickness of two consecutive areas (step 13-14 versus 14-15) and the difference was less than one standard deviation of the measurement signal. Thus, the particle multilayer deposition process was studied in the middle of the test section (step 13-14) where the flow field and the particle mixing are fully developed. The wall segment between step 13 and 14 was designed as a flush mounted removable steel tile. This wall segment was grounded to remove electrostatic charges. The entire tile could be extracted as a whole to be placed on an external measurement table for the layer thickness scan.

During the particle deposition experiment the graphite particles were dispersed into the turbulent flow field upstream of the flow formation zone using a solid aerosol generator (SAG). Note that the reservoir of the SAG was heated prior and during the experiment to remove humidity from the graphite particles and the laboratory was heated and ventilated to keep the relative humidity of the air below 30%. Thus, particle agglomerations originating from moisture could be excluded. The aerodynamic particle size distribution of the graphite particles was measured by means of the isokinetic sampling technique in combination with an Aerodynamic Particle Sizer spectrometer. The uncertainty in the aerodynamic particle size distribution is less than 1% and the counting efficiency is better than 85% for solid particles.

The measurement of the surface layer thickness was done using a laser distance sensor with a three component positioning system. The data acquisition and the synchronisation of the measurement system were performed by in-house C++ software. The measurement uncertainty was determined in two ways. Considering all sources of error the

measurement uncertainty of the graphite layer thickness is less than 5% and the uncertainty of the computed volume is less than 10%.

Radiographic methods were used to characterize the particle bed properties in terms of the volume porosity. The measurements were performed by means of an x-ray microscope. This measurement instrumentation has been chosen due to its high spatial resolution and the vertical orientation of the x-rays.

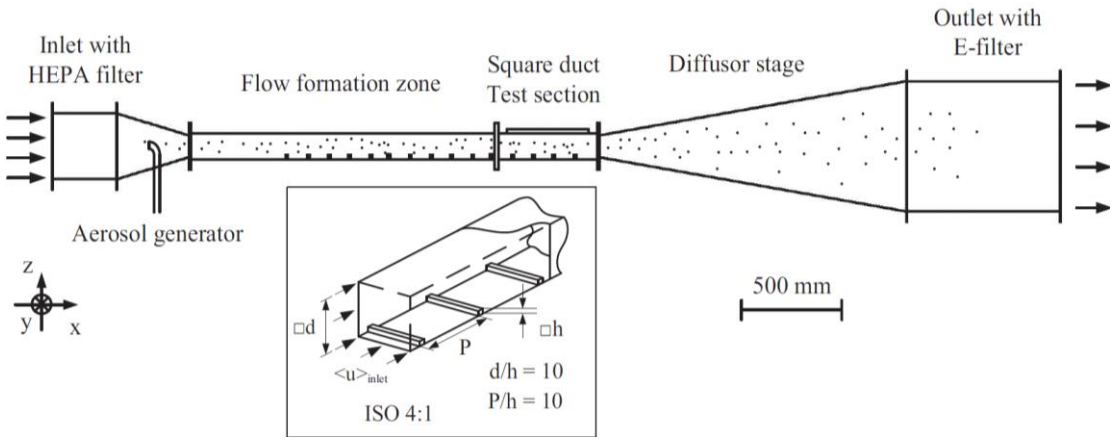

Figure 2.18: Schematic drawing of the Gas Particle Loop (Barth et al., 2013).

Figure 2.19 shows the cumulative frequencies of the graphite particles. The AVR (Arbeitsgemeinschaft Versuchsreaktor) dust was sampled over several years of filter experiments at the pebble bed HTR in Julich (Germany). Moormann (2008) report the number related particle size distribution with a mean particle size of d = 0.5 µm. Rott and Wahsweiler (1991) present results from filter experiments of the Thorium High Temperature Reactor (THTR). This distribution is a volume related particle size distribution with a mean diameter of about d = 7 µm. In the present experiments technical graphite dust 23061 (Thielmann Graphite GmbH & Co. KG) has been chosen. The particle size distribution of the 23061 was recorded using an Aerodynamic Particle Sizer (APS) spectrometer and the volume related aerodynamic mean diameter is about d = 5.3 µm which is in between the two AVR and THTR particle size distributions, respectively.

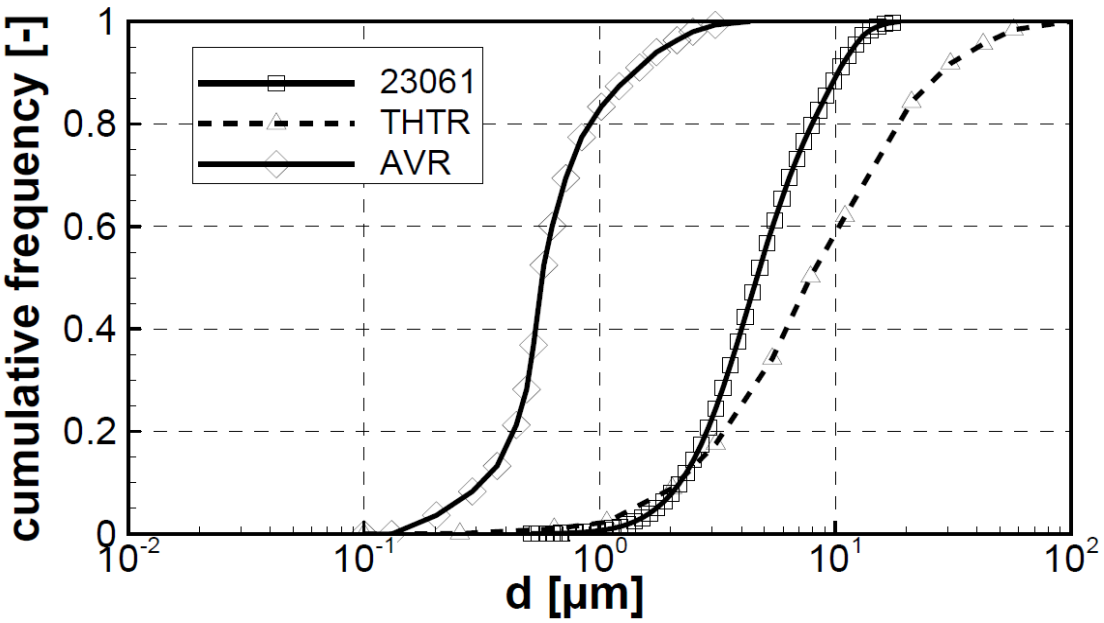

Figure 2.19: Cumulative distribution of AVR, THTR and 23061 graphite dust.

The deposition experiment was carried out by dispersing the graphite dust 23061 into the inlet zone over several hours. The fluid velocity was kept constant at a bulk Reynolds number Re_d = 8900 corresponding to a friction velocity u* = 0.08 m/s. The experiment was intercepted each hour to scan the surface layer thickness. Figure 2.20 shows a snapshot of the particle multilayer between the steps 13-14 generated after t = 4 h exposition to the particle laden flow field. It can be seen that the most part of the graphite particles accumulate upstream of the step and less particle material is found downstream. Furthermore, axial periodicity of the particle multilayer with respect to the channel midsection (xz-plane, y = d/2) is clearly visible.

Figure 2.20: Multilayer particle deposits between step *13-14* after *t = 4 h*, flow direction from left to right (Barth et al., 2013).

The spatial distribution of the particle multilayer build up against time is shown in Figure 2.21. The entire wall surface is covered with dust and independent of the time step several areas are remarkable. The region 0 < x < 20 mm is characterized by a rather low multilayer thickness followed by a particle plateau of higher thickness up to x = 70 mm. The areas directly upstream of the step (80 mm < x < 90 mm) and close to the channel side walls (y < 5 mm) show a considerable increase in the multilayer thickness.

Comparing the time mean averaged turbulent flow field between the periodic steps with the spatial distribution of the graphite multilayer it is assumed that most of the larger particles pass the step and settle on the floor between the reattachment line at x = 35 mm and the consecutive step. Only smaller particles of higher aerodynamic mobility are caught by the recirculation vortex downstream of the step and deposit directly behind it (0 < x < 20 mm). The area up to x = 70 mm shows a plateau like layer thickness indicating that the particles homogeneously deposit due to gravitational settling. The strong accumulation of deposits right upstream of the step (85 < x < 90 mm) and close to the channel walls (y < 5 mm) is related to particle deposition due to inertia impaction. The larger particles simply impact on the front side of the step due particle inertia. Fractions of these particles drop down from the wall and re-deposit on the floor, again. The smaller particles are likely caught by the recirculation vortex and being deposited right downstream of the step due to turbulent dispersion. A spatial correlation of the single components of the turbulent flow field (<u>, <w> ,u' ,w') with the multilayer thickness supports these assumptions. It is found that the time averaged mean velocity <u> weakly correlates with the layer thickness δ. The other flow field components do not correlate with the multilayer thickness distribution showing different deposition mechanisms at different locations between the steps.

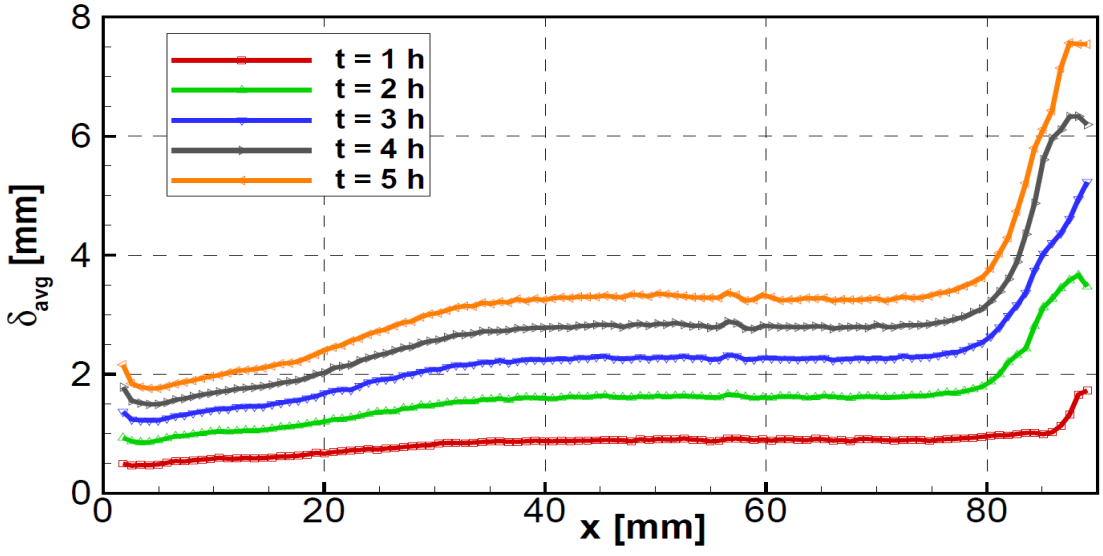

Figure 2.21: Spanwise averaged layer thickness (Barth et al., 2013).

The particle multilayer resuspension experiment was performed by generating an initial deposition layer over t = 4 h. This initial layer was exposed to discrete flow transients by the stepwise increase of the fluid velocity. Note, the entire flow path upstream of the steel tile (steps 13-14) was cleaned from graphite particles to avoid the re-deposition of graphite material originating from the upstream flow path of the channel during the resuspension experiment. The surface layer thickness was scanned before and after each flow transient using the laser distance sensor system. Figure 2.22 displays a snapshot of the multilayer between steps 13-14 after a flow transient corresponding to a friction velocity of about u* = 0.36 m/s. The axial symmetry of the multilayer with respect to the channel mid-plane is clearly visible. Two major resuspension areas are found nearby the recirculation zones. The multilayer is completely removed over the entire channel width at the reattachment line (x = 38 mm). The second cavity appears in channel mid-plane upstream of the subsequent step. The multilayer interface forms dune like surface structures as observed by Mantz (1978).

Figure 2.22: Multilayer particle deposits after a flow transient corresponding to a friction velocity *u* = 0.36 m/s*, flow direction from left to right (Barth et al., 2013).

Figure 2.23 displays the spanwise averaged layer thickness with respect to different friction velocities. Increasing the velocity from the initial deposition up to u* = 0.39 m/s the cavity at x = 30 mm continuously progresses down to the channel floor. Furthermore, the deepening directly upstream of the step (x > 80 mm) also increases. In contrast, the layer thickness in the region below x < 10 mm grows with increasing fluid velocity which is related to the re-deposition of graphite material due to the recirculation vortex. The turbulent flow field data at Re_d = 27950 was correlated with the corresponding graphite multilayer thickness to explore the relations between the single components of the flow and the multilayer. It was found that the layer thickness slightly correlates (0.5) with the mean velocity <u> and the wall

normal velocity <w>. Furthermore the correlation coefficient between the layer thickness and the turbulent velocity components is about 0.34. According to that the multilayer particle resuspension seems to be influenced by the mean flow components as well as by the turbulent structures. Especially close to the recirculation and the reattachment zones the mean velocities are rather low. Nonetheless, the removal of the particles begins at these places first and proceeds to the channel floor indicating that the turbulent bursts may trigger the particle resuspension. In the plateau region (40 mm < x < 70 mm) the resuspension begins at higher friction velocities and does not proceed to the channel floor as fast as it takes places in the recirculation zones. Therefore, it is assumed that the particle resuspension in this region is rather influenced by the mean flow field components than by the turbulent structures.

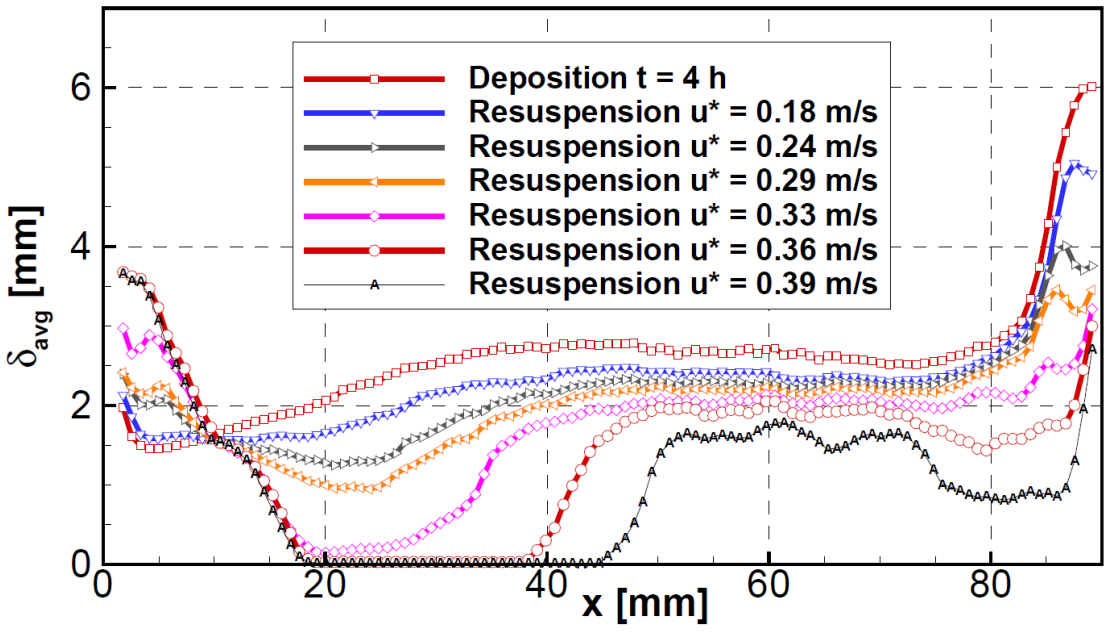

Figure 2.23: Spanwise averaged thickness after different flow transients (Barth et al., 2013).

The overall resuspension process was quantified by the fraction of remaining particle material against the mean friction velocity of the flow transient. As can be seen in Figure 2.24 the remaining fraction against the friction velocity follows an s-shaped tendency. In principle, particle deposits tend to resuspend when a critical friction velocity is exceeded. This behaviour is also visible in the present data set. Below a friction velocity u* < 0.1 m/s the multilayer remains unmodified. Exceeding this velocity the material starts to resuspend. Note that at friction velocities larger than u* > 0.3 m/s almost the entire multilayer is removed. Figure 2.24 also displays resuspension curves of other particle resuspension studies. Reeks and Hall (2001) observed the resuspension of 10 to 20 µm in diameter particles. The particles

started to resuspend at friction velocities larger than u* > 0.3 m/s and the entire resuspension process was not accomplished at u* = 3 to 4 m/s. Furthermore, Hontanon, et al. (2000) report about the resuspension of d = 0.4 µm in diameter large particles in the framework of the STORM project. Here, considerably larger friction velocities up to 7 m/s were necessary to remobilise the particles. Ahmadi et al. (2007) observed a tendency between the particle size and the necessary friction velocity. Upon their results larger particles resuspend at much lower friction velocities than smaller particles which might explain the higher friction velocities in the STORM project in comparison to the results of Reeks and Hall (2001). Comparing the present multilayer resuspension to these two studies it can be concluded that the resuspension of multilayers requires less aerodynamic forces than single particle resuspension. Reason for this may be found in the adhesion forces. Particle-to-particle contact forces are much less than the adhesion forces between a single particle and a flat wall (Friess & Yadigaroglu, 2002). In principle, the characteristics of single particle resuspension such as the friction velocity and the particle size dependency are also found in the results of the multilayer particle resuspension.

The bed porosity was measured for the resuspension probe Re_d = 39870 by means of gravimetric and radiographic methods. It was found that the volume porosity ε slightly decreased from 0.94 (Re_d = 8900) down to 0.90. This reduction is related to the removal of the loose particle agglomerates by the turbulent flow field. During the inceptive resuspension the turbulent flow has a kind of polishing effect on the interface before dune like structures are formed.

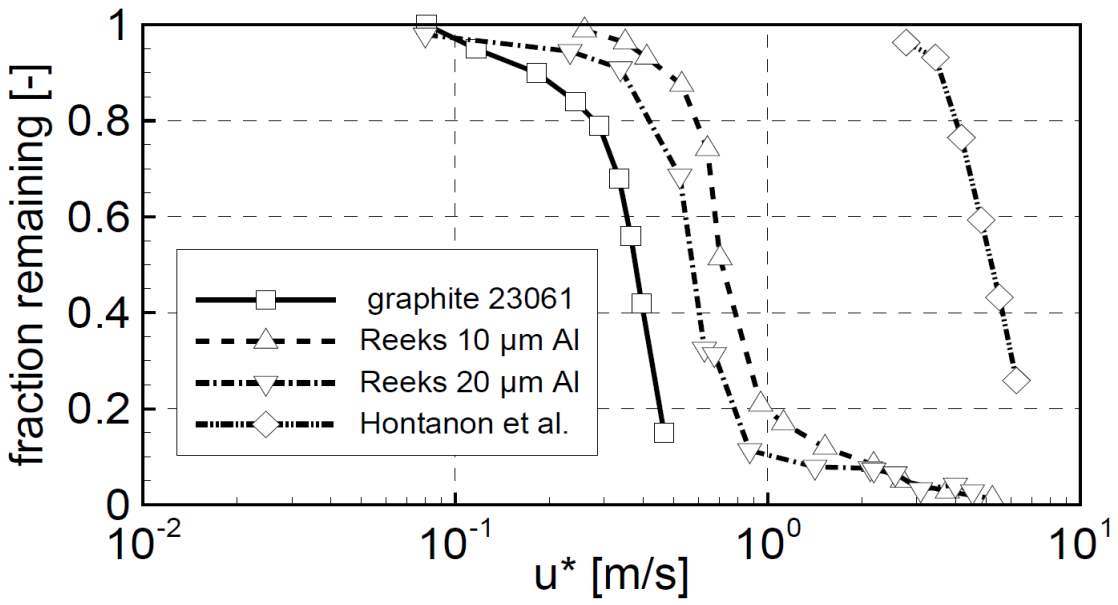

Figure 2.24: Comparison of the remaining fraction of the initial multilayer against the friction velocity (Barth et al., 2013).

Chapter 3

Methods

3.1 Multilayer particle bed reconstruction

3.1.1 Artificial deposition mechanisms

This section focuses on the resuspension of solid particles from a multilayer deposit, which presupposes the existence of granular bed on a wall surface subject to a sudden gas flow increase. There has been evidence (Friess & Yadigaroglu, 2002) that mechanisms of particle detachment from multilayer deposit strongly depends on deposit structure (for instance, fluffy deposits are removed easier than compact ones). Porosity of the deposit greatly influences particle detachment since it determines particle arrangement across the deposit. It is a measure of the unoccupied space in the multilayer deposit. The present section seeks to create a fast and versatile artificial deposition algorithm. It will generate various deposits made of a large number of polydisperse particles with variable porosity and in complex geometries.

The artificial deposition process is based on the assumption that each solid particle either sticks or glides upon collision with a wall or another particle (Friess & Yadigaroglu, 2002). Particles are released sequentially, one after the other, from the highest altitude in the domain of a cavity that has to be filled. Every particle has a random diameter (taken from a pre-defined size distribution), a horizontal position and a sticking probability. A sticking probability equaled to unity ($p_s = 1$) indicates pure sticking. A zero probability ($p_s = 0$) indicates pure gliding. Particles, after being assigned all initial values, move downwards, under the influence of a gravity-like force.

Whenever a falling particle hits a wall surface it remains fixed on the ground irrespective of the sticking probability. However if a particle collides with another particle of the deposit, a new particle trajectory must be worked out. If the falling particle shows a pure sticking probability ($p_s = 1$) and it collides with another already deposited particle, then it remains fixed at this position (Fig. 3.1a). However, if the falling particle shows a pure gliding behavior and collides with another particle, then it will roll down its surface in the downslope direction and one of the following four cases will be realized:

Case 1: as the falling particle rolls down the surface of the deposited particle, it collides with a third particle, leading to a stable position (local minimum) that stops the freefall. It remains fixed at this location (Fig. 3.1b).

Case 2: it collides with a third particle, but the position is unstable (not a local minimum), the falling particle starts to roll down the surface of the third particle, and the control of these four cases is repeated.

Case 3: the falling particle loses contact (the centers of both particles are at the same height). It starts to fall again and previous steps are reiterated (Fig. 3.1c, middle sub-picture),

Case 4: as the falling particle rolls down the surface of a deposited particle, it touches the ground. It reaches a stable position (Fig. 3.1c, last sub-picture).

The next injected particles are treated likewise until the particle bed is completed. The particle bed is considered complete, if either a user-defined number of particles has been injected or the desired particle bed thickness has been achieved.

The multilayer particle build-up for a two-dimensional system is sketched below. The falling particle is with a dotted line, while fixed particles (being in their final position) are drawn with a solid line.

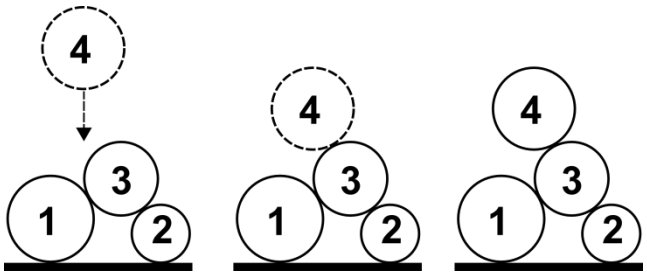

Figure 3.1a: Particle 4 (sticking probability p_s=1) moves downwards until it collides first with particle 3. Since particle 4 has a sticking attribute, it remains fixed at this position.

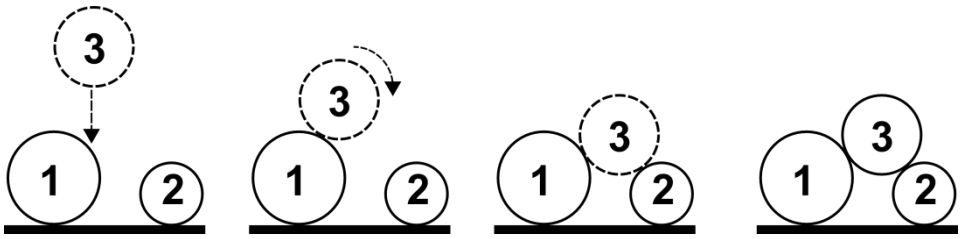

Figure 3.1b: Particle 3 (gliding) is inserted and moves downward until it collides with particle 1. It then naturally rolls to the right until it collides with another one, particle 1. This position is stable (local minimum), as particle 2 prevents particle 3 to move closer to the wall. The particle stays fixed there.

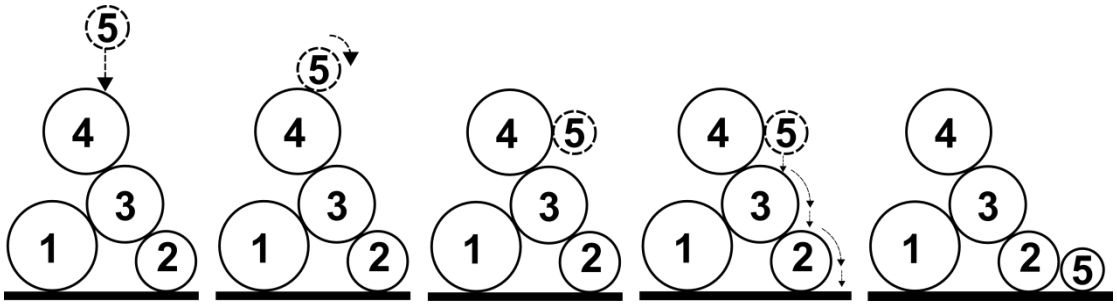

Figure 3.1c: Particle 5 (gliding) first collides with particle 4 and starts to roll to the right until it loses contact when the centers of both particles are at the same height. Then the particle starts falling again until it collides with particle 3. This position is unstable, thus, particle 5 starts rolling on it until it loses contact again. Eventually particle hits the ground and remains fixed there.

The multilayer deposition algorithm developed in this work allows a fine control of the particle bed porosity by adjusting the sticking probability of each particle. This probability is user-defined, and allows creation of fluffy structures (highly porous deposit) by setting the sticking probability high enough ($p_s = 1$), and creation of compact deposit (low porous) by setting a low sticking probability ($p_s = 0$).

Another advantage of the multilayer deposition algorithm described previously is the flexibility to create a deposit on complex ground shapes, and also the capability to adjust the thickness of the particle bed along the channel.

The flowchart of the previously described multilayer particle bed reconstruction algorithm is shown in Figure 3.2.

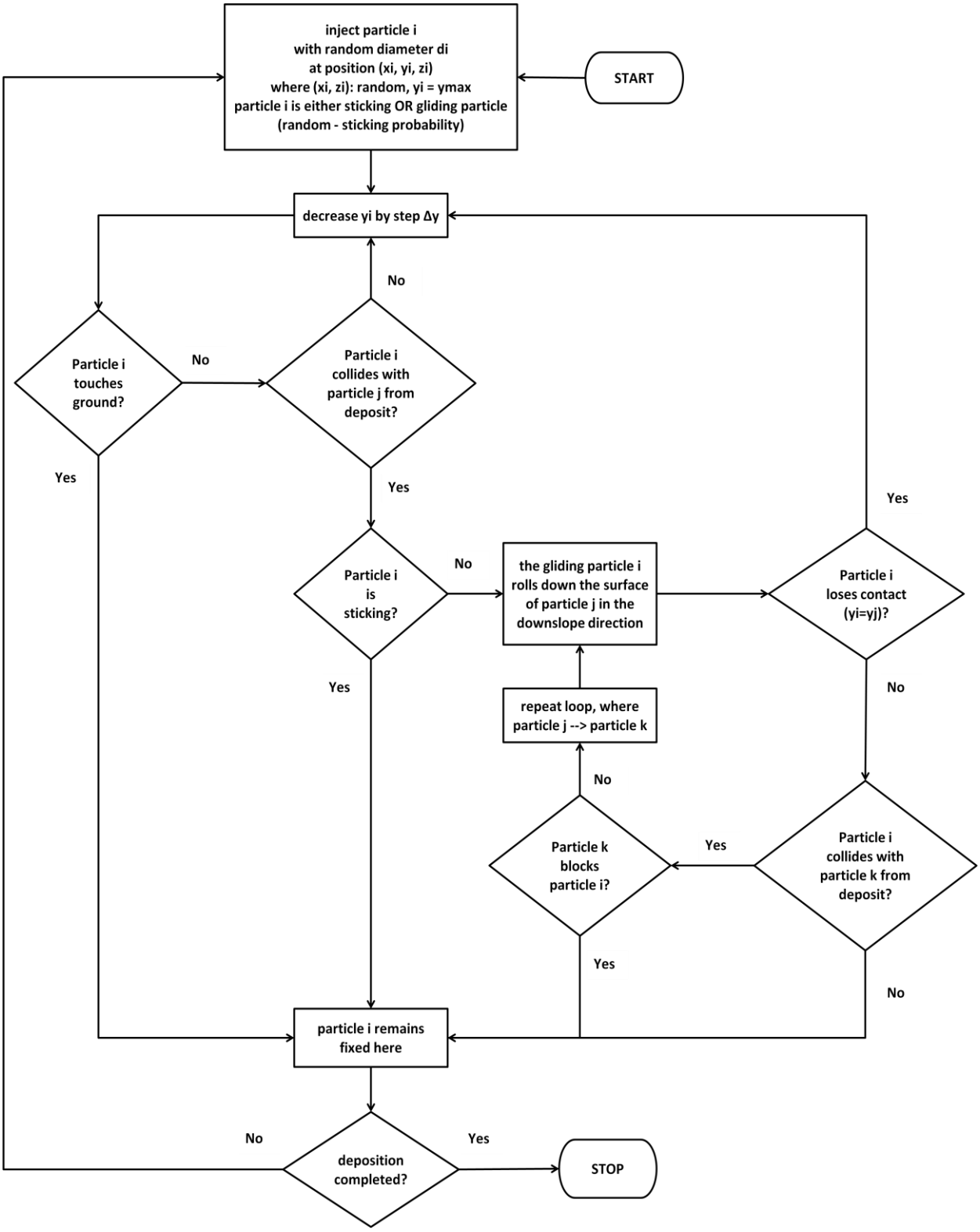

Figure 3.2: Flowchart of the multilayer particle bed construction algorithm.

Two versions of the same algorithm were developed. In the first version each falling particle was checked if it was colliding with another particle by looping through all the

already deposited particles, as a result the computational cost was overwhelmingly high by raising the number of the injected particles. The second version following the bottom-to-top reconstruction model (Pöschel and Schwager, 2005) greatly reduced the computational cost by looping only through the nearby particles. The comparison of the computational cost between these two versions can be seen in Figure 3.3:

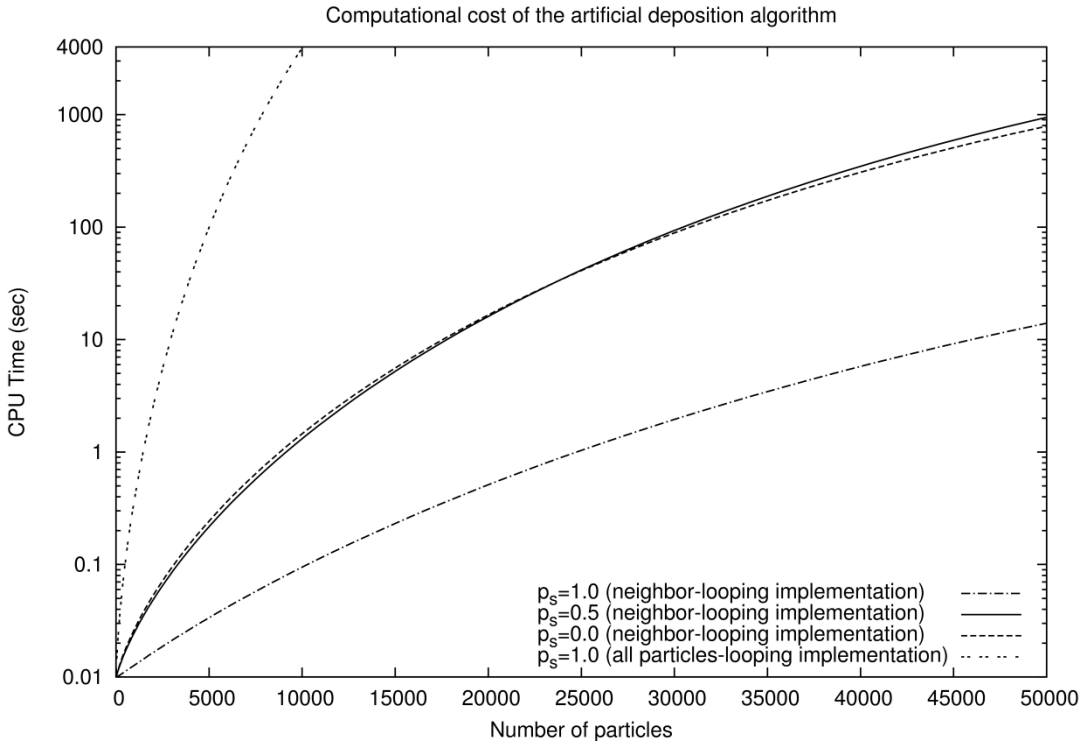

Figure 3.3: Computational cost (CPU time) of the artificial multilayer deposition algorithm against number of particles.

It is clear that the computational cost for reconstruction of a multilayer deposition is unaffordable in the first version of the algorithm, which is why this case is no longer examined in the present work. The second version of the algorithm that solely loops through all neighboring particles for a possible collision is much faster than the first one. In this version one may see the effect of porosity in the execution time. For a high porous deposit of half a million particles (p_s=1) the execution time equals 10 seconds. The same experiment with the initial implementation would have probably required a few hours to a few days. A decrease in the sticking probability results in an increase of the computational time. Note that the creation of a mid-porous structure (p_s=0.5) takes more execution time than a low porous one (p_s=0). This happens because in the case of the mid-porous sediment, the combination of sticking and gliding particles creates multiple gaps, so when a gliding particle falls it should

roll on the surface of a lot of particles until it finds a stable position. If all the particles are gliding, then these particles are just rolling on the surface of very few particles that are found at the top of the sediment, thus reducing the computational cost.

3.1.2 Particle bed porosity

Porosity ε (epsilon) is a measure of the void (i.e., "emptiness) in a granular material, and is a fraction of the volume of voids over the total volume, ranging from $\varepsilon = [0..1]$, or as a percentage $\varepsilon = [0..100\%]$. The term is used in multiple fields including pharmaceutics, ceramics, metallurgy, materials, manufacturing, earth sciences, soil mechanics and engineering.

According to Friess and Yadigaroglu (2002) the mass per unit wall surface area associated with an artificial deposit is given by:

$$m_0 = \frac{\pi}{6}\frac{\rho}{w}\sum_{i=1}^{J} d_i^3 \tag{3.1}$$

where w is the area of the domain, J is the number of the particles, and ρ is the particle density (in this work, the density of graphite particles is 2200 kg/m^3).

The porosity ε is, thus, defined as:

$$\varepsilon = 1 - \frac{volume\,of\ particles}{total\,deposit\,volume} = 1 - \frac{\pi}{6}\frac{1}{wh}\sum_{i=1}^{J} d_i^3\,, \tag{3.2}$$

where the deposit volume is the product of the wall surface area w and the deposit thickness h (averaged thickness along the wall) which is defined as twice the average distance between particle centers and the wall:

$$h = \frac{2}{J}\sum_{i=1}^{J} y_i \tag{3.3}$$

The above equations stand for the three-dimensional model of an artificial deposit. These equations are simplified in the case of a 2D deposition. The mass load is simplified as follows:

$$m_0 = \frac{\pi}{6}\frac{\rho}{\upsilon}\sum_{i=1}^{J} d_i^2 \tag{3.4}$$

where υ is the length of the wall where the deposition takes place.

The porosity in a 2D configuration, is derived from the following equation:

$$\varepsilon = 1 - \frac{\pi}{6}\frac{1}{\upsilon h}\sum_{i=1}^{J} d_i^2 \tag{3.5}$$

3.1.3 Two-dimensional deposition

According to the artificial deposition algorithm explained in §3.1.1, two artificial deposits on a flat plate corresponding to the limiting values of the sticking probability (all the particles are either sticking or gliding) are shown in Figure 3.4:

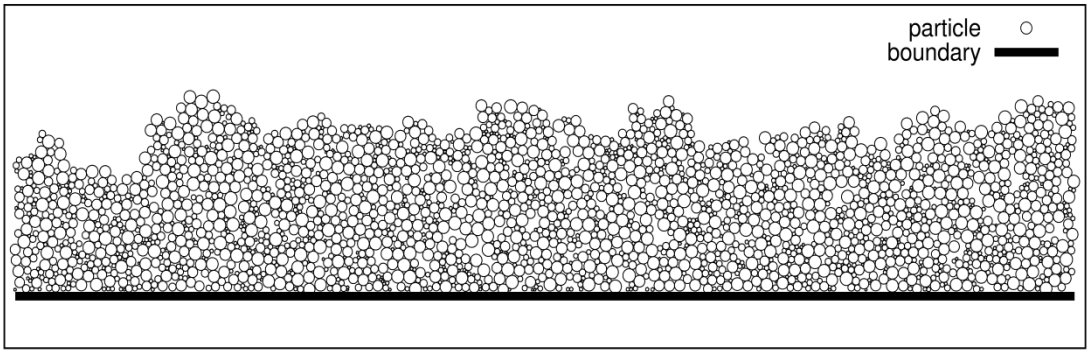

Figure 3.4a: An artificial multilayer deposit on a flat plate (N=2500 particles, p_s=0, ε=0.37).

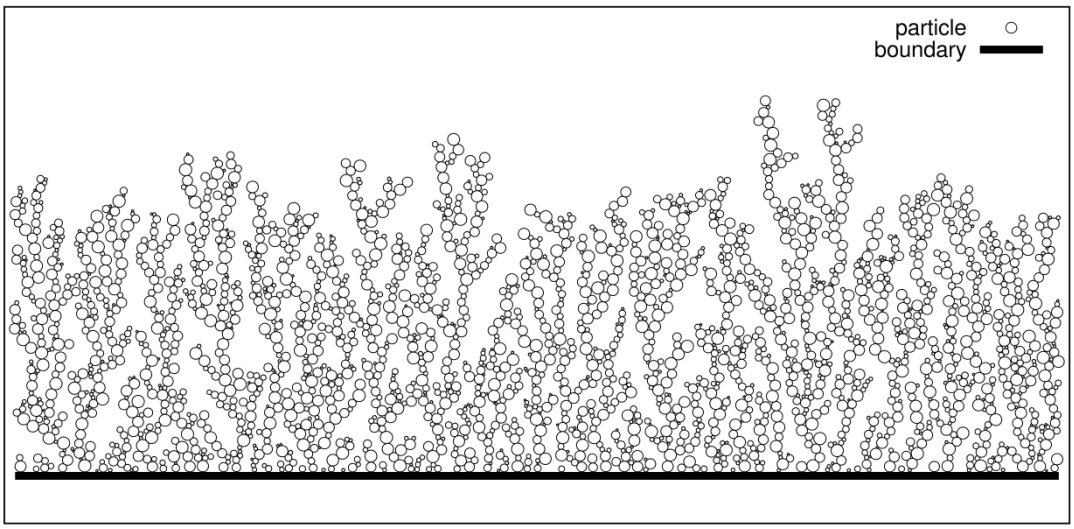

Figure 3.4b: An artificial multilayer deposit on a flat plate (N=2500 particles, p_s=1, ε=0.75).

As already mentioned, the geometry of the boundary surface where the multilayer particle deposit will be created can take any complex shape. In Figure 3.5 one may see two artificial deposits with limiting values for the sticking probability (all the particles of the deposit are either gliding or sticking) on a curved geometry that is given by a sinusoidal function:

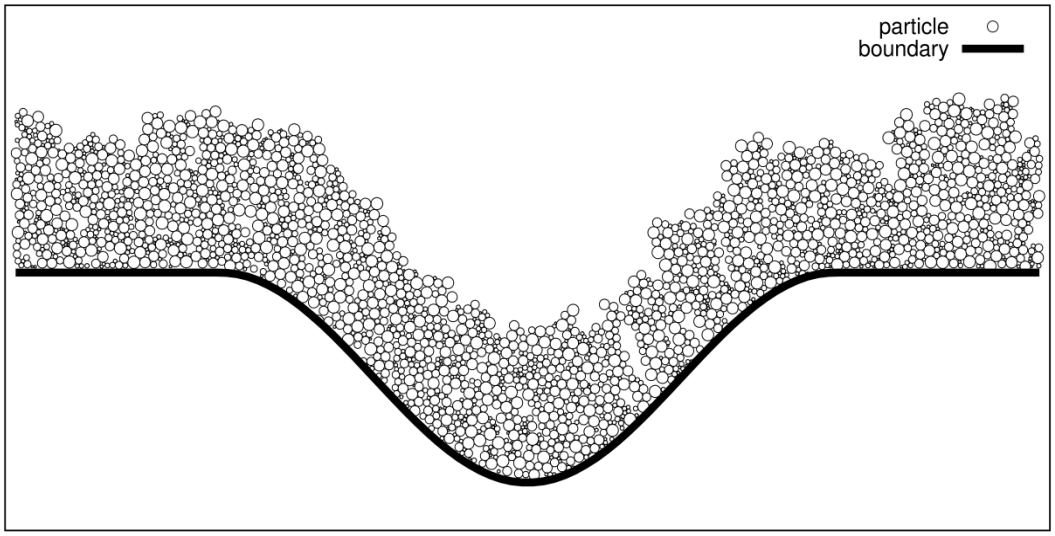

Figure 3.5a: An artificial multilayer deposit on a curved plate (N=2500 particles, p_s=0, ε=0.43).

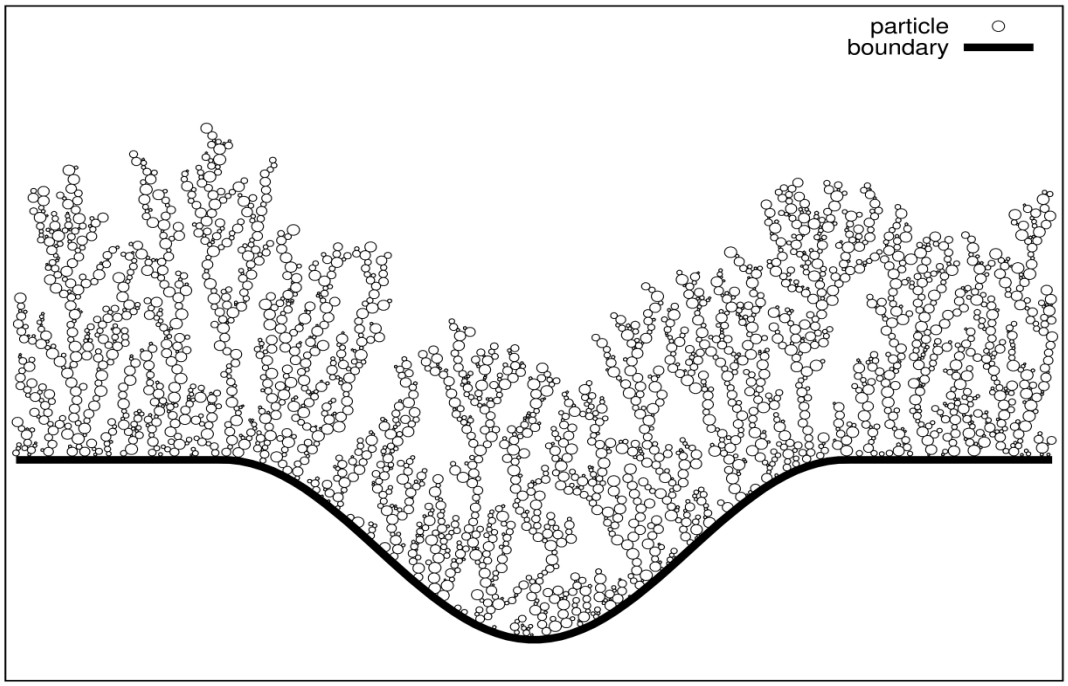

Figure 3.5b: An artificial multilayer deposit on a curved plate (N=2500 particles, p_s=1, ε=0.83).

The aim of this thesis is to simulate the phenomenon of particle resuspension and validate this model with the existed experimental data (see Section §2.6.2). Hence, an initial particle bed must be reconstructed to reproduce the average (in the vertical cross section) thickness layer after 4 hours of sedimentation (see Fig. 2.23). This structure (Fig. 3.6) will be the initial state of the particle bed before any resuspension takes place.

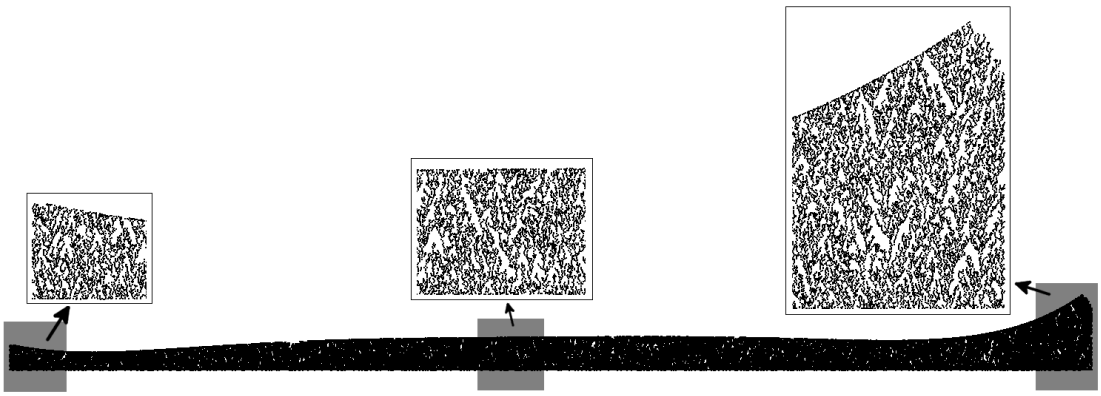

Figure 3.6: Initial thickness layer of a deposition that resembles the experimental data for a pure sedimentation after 4h (at Re = 8900) in cavity (N=778,919particles, p_s=0.95, ε=0.85).

In the above cavity, the diameter size distribution is in the range of [1..20]μm, as in the experiments (Figure 2.19) and requires about 800,000 particles. In the zoomed sub-images (Figure 3.6) one may see the tree-like formations of this high porous (ε = 85%) deposit. This porosity of the granular bed roughly equals that measured experimentally (ε = 94%). One may see summarized all the (experimental and numerical) data of the granular bed in Table 3.1:

	Experimental	**Simulation**
Bed porosity	94%	85%
Particle size range	From 1 to 20 μm	From 1 to 20 μm
Number of particles	unknown	778,919
Material	Graphite	Graphite
Particle density	2.2 g/cm^3	2.2 g/cm^3

Table 3.1: Summarized data of the granular bed in the experiments and in the simulation.

3.1.4 Three-dimensional deposition

The deposition (and the resuspension) algorithm is not limited only to a two-dimensional domain, it has been extended to the third dimension. It is obvious that this requires the injection of a lot more particles, so the computational cost increases significantly. The dimensions of the domain that will be simulated in this work are big enough and the diameter size of the particles is very small, leading to an injection of more than ten million particles (depending on the desired porosity). For this reason the 3D implementation is out of the scope in this work.

In Figure 3.7 one may see the deposition structure in the three-dimensional domain, where the injected particles are colored by its diameter size.

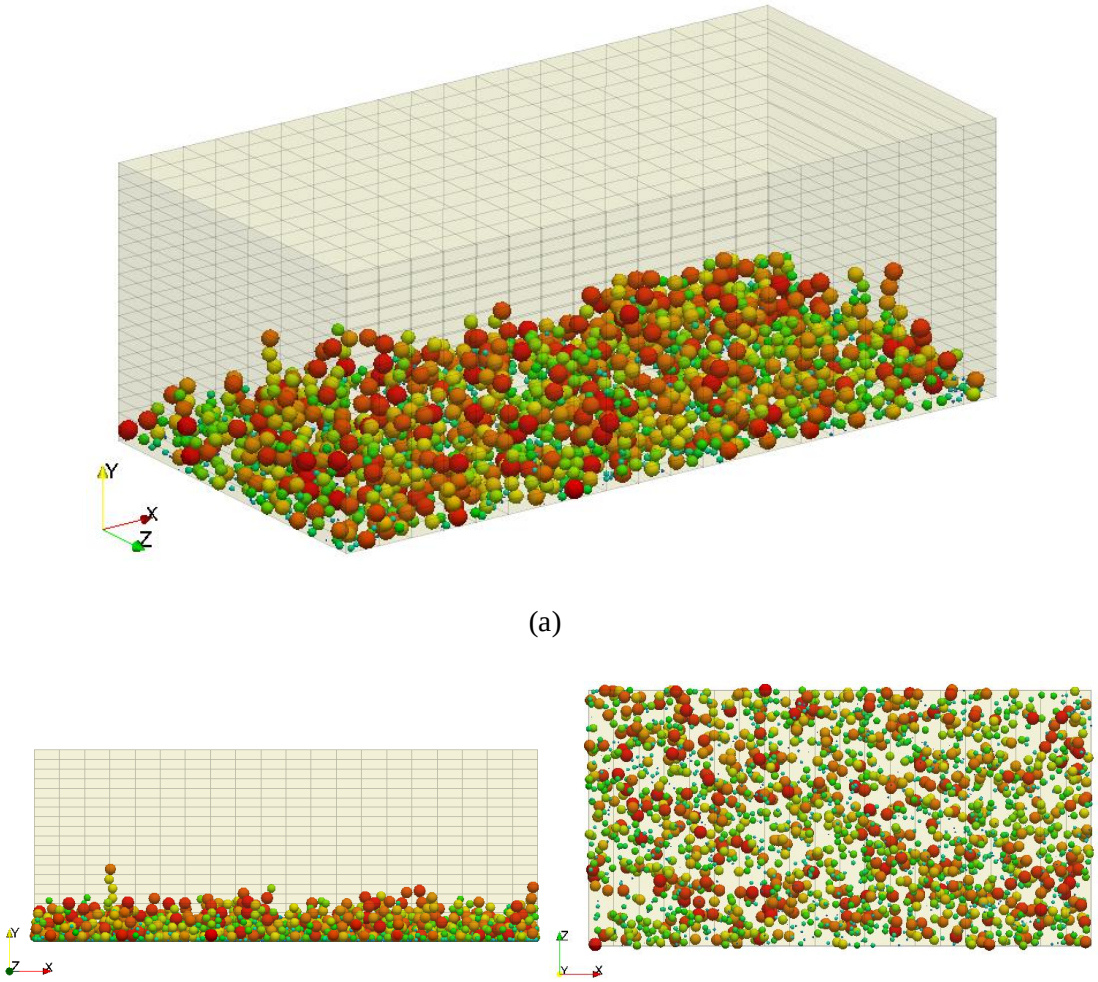

(a)

(b) (c)

Figure 3.7: a) Isometric view, (b) side view, and (c) top view of a three-dimensional deposition (2500 particles) with variable diameter (color).

3.2 Particle re-entrainment

3.2.1 Background

As previously stated, the purpose of this work is to simulate the resuspension of deposited solid particles in a turbulent channel flow. The results of the simulation will be compared with the experimental data from HZDR (§2.6.2). In those experiments (Barth et al, 2013) it was observed that the particle resuspension was accomplished at lower friction velocities than that necessary for single particle resuspension. The phenomenon of cluster resuspension that occurs only in the resuspension of multilayer deposits was observed first in the STORM experiments (§ 2.6.1) and has been described and initially analyzed by Friess & Yadigaroglu (2002), developing a model based on the assumption that the particles are resuspended as in clusters rather than as sole. Also, in Wang et al (2012) it was found that large and loose particle clusters were resuspended first and smaller particle formations needed higher fluid velocities for the removal.

The aerodynamic forces acting on a particle are proportional to the square of particle's diameter, whereas the adhesive forces developed between two particles is proportional to the diameter size of the smaller particle. Hence, a simple argument on force balance suggests that large particles are easier to resuspend. Moreover, if one considers that the mean diameter of the particles examined here is about 10 μm then it is obvious that the adhesive forces between two particles are much stronger than the removable ones, making this way the resuspension as in clusters much more feasible (Friess & Yadigaroglu, 2002).

In this work, the phenomenon of cluster resuspension will be taken into consideration. Firstly, there will be an identification of the resuspendable clusters in the deposit. In each cluster it will be assigned a resuspension probability p_r derived from the force balance model (Cleaver & Yates, 1973). Every cluster, that fulfills resuspension criteria, is removed from the deposit without tracking its following trajectory. It is assumed that re-deposition of resuspended particles does not take place.

3.2.2 Cluster identification

Since in a multilayer deposit the particles can be interconnected in various ways depending on the porosity of the particle bed, there should be a mathematical definition of the term "cluster". In this work we will examine a fairly simple description of the cluster similar in shape to a chain of particles. Every particle of the chain-like cluster has exactly two neighbours (one on top and the other at the bottom of it), apart from the first particle of the

cluster that is in the top (and is connected with only one particle at the bottom of it) and the last particle of the cluster that it is either connected with more than two particles or with only one if it happens to be in contact with the wall.

Although in a deposit at a certain time step there may be a lot of clusters, not all of them are tracked by the cluster identification algorithm, since some of them are unlikely to resuspend at this time step. The non-resuspendable clusters are the ones non dislodgeable, i.e. if one tries to remove them by an upwards movement then they would collide with other particles of the deposit. The resuspendable clusters of a deposit may be seen in Figure 3.8 (gray color). It is obvious that there are much more clusters in this sediment, but there is no reason for tracking them in the current time step as they are blocked by other particles.

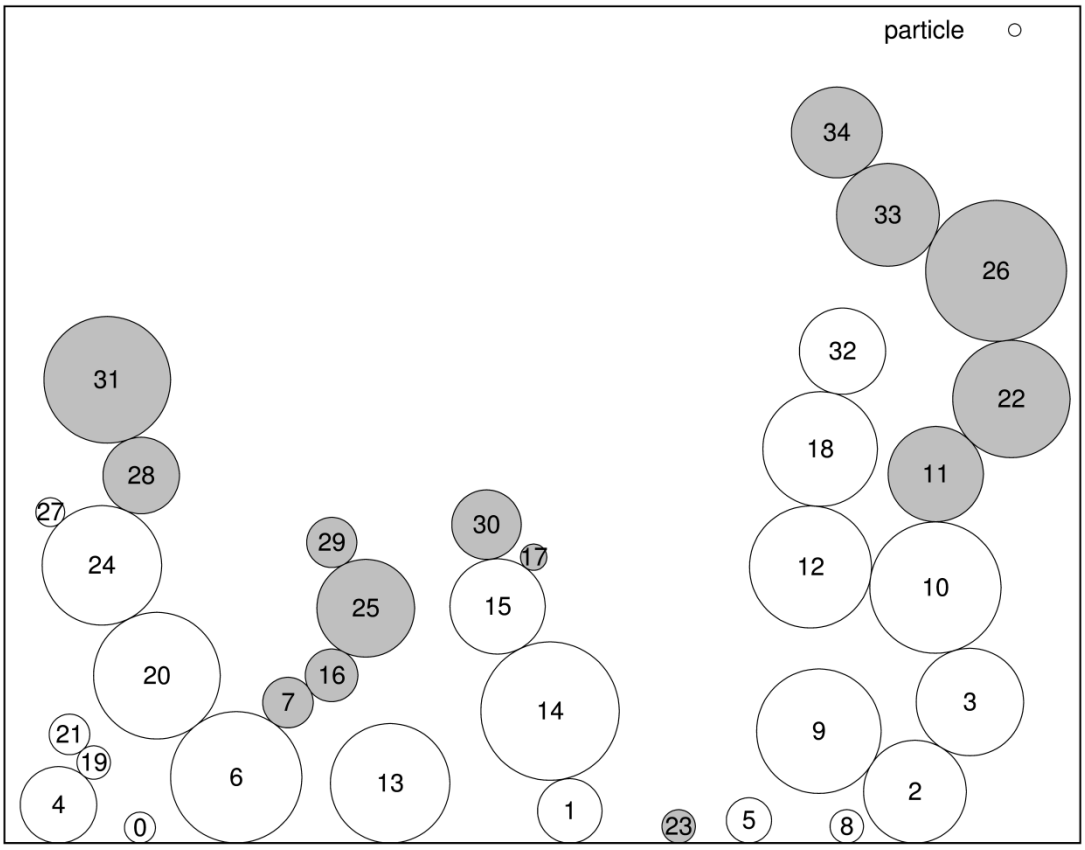

Figure 3.8: Resuspendable clusters (gray color) of a deposit.

Each resuspendable cluster (see Fig. 3.8) is assigned a resuspension probability p_r based on a force balance model. If clusters do resuspend, the topology of the sediment will change, so the cluster identification algorithm will identify a new set of resuspendable clusters.

The cluster identification algorithm (see Fig. 3.9) starts from first tracking these particles that are on top of all other particles and are unobstructed. Then each one of these particles starts to form its cluster by adding the consecutive particle that fulfills the condition of this chosen version of the cluster. The resuspendable cluster may consist of only one particle, especially in low porous particle beds.

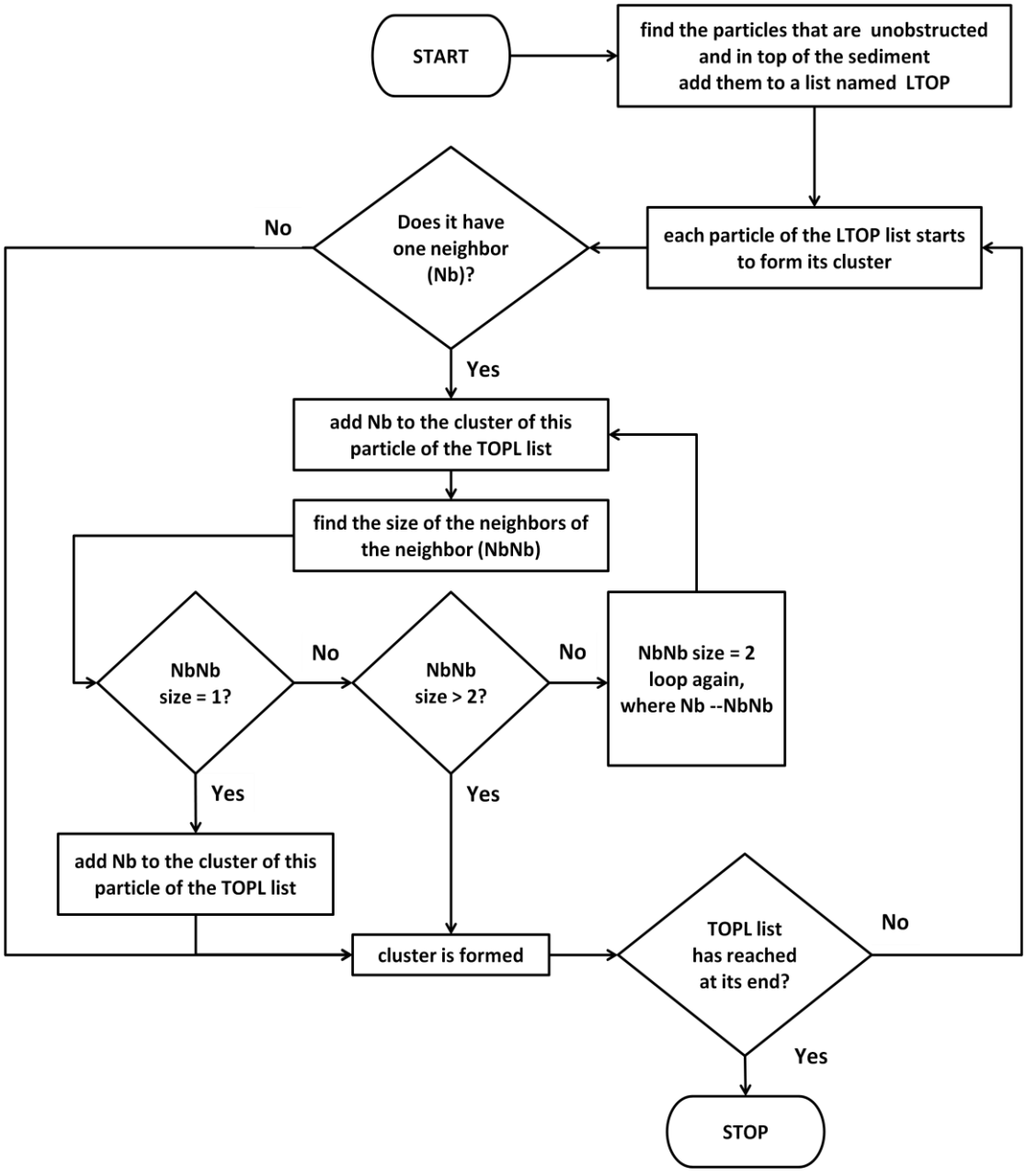

Figure 3.9: Flowchart of the cluster identification algorithm.

3.2.3 Cluster re-entrainment

As previously mentioned (see Section §3.2.1), in each time step, the cluster identification algorithm creates a list of clusters at the granular interface that are potentially resuspendable. The next stage involves the association of each cluster with a resuspension probability to determine which ones will re-enter the flow in the current time step. This resuspension probability is considered as the resultant of two distinct probabilities that are applied to each cluster, one probability derived from a force balance model whereas the other one derives from the temporal evolution of the resuspension process.

One of the conclusions drawn from experiments performed at HZDR, was that the particle resuspension shows a strong dependency on fluid friction velocity (Barth et al, 2013). This assumption is going to be studied further in this work, by constructing a model based on this clue. This comes also in good agreement with the most force balance models from the literature that was reviewed in Chapter 2. For instance, the model proposed by Cleaver and Yates in Eq.(2.4) is based on a formula of the wall shear stresses and the diameter size of the particles. Here this formula is simplified to include just the wall shear stresses acting on a cluster, as the diameter size may lead to erroneous conclusions, since it is not feasible to reconstruct exactly the same deposit as in the experiments. Although the size distribution is identical, it is not known from the experiments how the polydisperse particles are distributed in the problem domain, meaning that there are no data for the exact position and diameter of each particle. Hence, particles with big diameter could deposit by using the artificial deposition algorithm in areas where in the experiments particles with small diameter were deposited, thus affecting the resuspension process. For this reason, this factor is left aside. The inaccuracy of this simplification is balanced by the exact computation of the wall shear stresses, a variable that was assumed as constant in previous models.

Since the higher friction velocity at a given location corresponds to a higher resuspension probability, a Cauchy-like probability density function is employed to model this resuspension probability. In each time step, there is an exact computation of the field of the wall shear stresses (or of the friction velocity u_*) along the interface of the particle bed. From this field, it is then calculated the mean u_*^{mean} and the maximum friction velocity $u_*^{\max}$. The cluster that is found at the point of the maximum friction velocity will likely resuspend, while clusters that are found in areas where friction velocity is below the average, they have slim chance of being resuspended. This is described by the following formula:

$$\mathrm{P}_{resusp,u_*} = \frac{1}{\pi}\arctan\left(s_1 \cdot \frac{u_* - u_*^{mean}}{u_*^{mean}}\right) + \frac{1}{2} \tag{3.6}$$

where s_1 is an adaptable dimensionless parameter that controls the steepness of the curve (in this problem an appropriate value is about 15 to 25).

The resuspension probability of the cluster against the friction velocity (Eq. 3.6) can be seen in Figure 3.10, where it is obvious that clusters with low friction velocity are unlikely to resuspend (p_r close to 0).

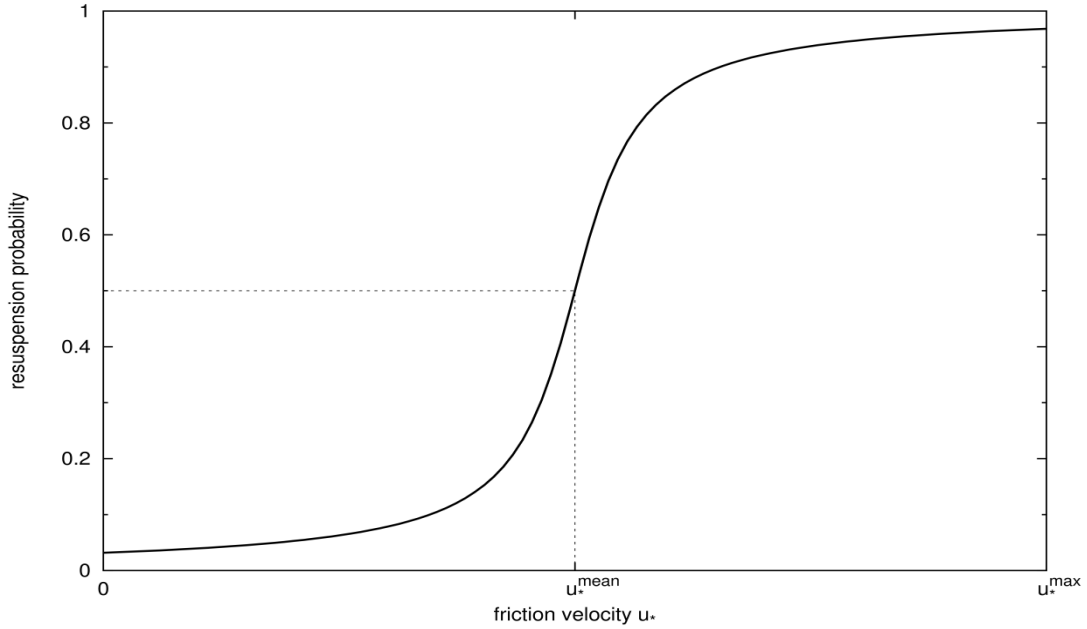

Figure 3.10: Resuspension probability of a cluster versus the friction velocity at this point.

This novel approach has the physical meaning that in a deposit the location with higher friction velocity will erode faster than the low friction areas. What is not physical, is the infinite removal of particles of high friction velocity areas. In reality, it has been observed from experiments that although resuspension has an intermittent nature, the material removal stops after a certain exposure time (Yuan et al, 2009). The temporal evolution of the phenomenon is implemented through the association of an inverse time law. This second component of resuspension probability is formed by a similar formula like Eq. (3.6), and is given by:

$$P_{resusp,t} = -\frac{1}{\pi}\arctan\left(s_2 \frac{t - t_{stop}}{t_{stop}}\right) + \frac{1}{2} \tag{3.7}$$

where s_2 is an adjustable dimensionless parameter (it is set to have a value between $5 \cdot 10^{-4}$ to $10 \cdot 10^{-4}$), t_{step} is the time step, and t_{stop} is the time after which the resuspension is becoming

increasingly unlikely (this variable is a function of the dimensionless number Reynolds and the mass fraction remaining).

One may see in Figure 3.11 the contribution of the time parameter to the resuspension probability. After the exposure time exceeds t_{stop}, the resuspension probability rapidly decays to zero.

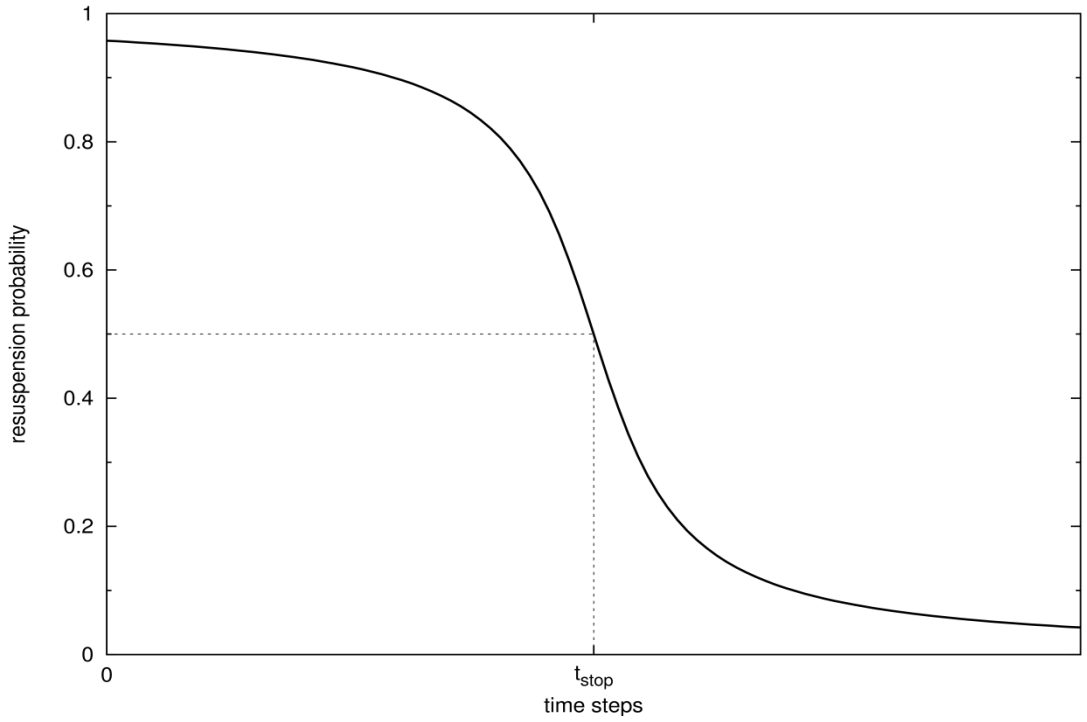

Figure 3.11: Resuspension probability of a cluster versus time.

The combination of these two components (time and friction velocity) will define the overall resuspension probability of each resuspendable cluster. Once a cluster fulfills the probability to resuspend, then it is subtracted completely from the particle bed without taking into consideration its following trajectory as it is assumed that does not re-deposit.

As resuspension evolves over time, in each time step, the remaining mass $m(t)$ per unit wall surface area is calculated by Eq.(3.4). So, the resuspension mass flux (kg/m^2 s) is computed by the formula:

$$F(t) = -\frac{d}{dt} m(t) \tag{3.8}$$

3.3 Flow simulation

3.3.1 Large Eddy Simulation

Large eddy simulation (LES) is a mathematical model for turbulence used in computational fluid dynamics. This turbulence model will be used in this work. It was initially proposed in 1963 by Joseph Smagorinsky to simulate atmospheric air currents. LES grew rapidly and is currently applied in a wide variety of engineering applications, including combustion, acoustics, and simulations of the atmospheric boundary layer. LES operates on the Navier-Stokes equations to reduce the range of length scales of the solution, reducing the computational cost.

The principal operation in large eddy simulation is low-pass filtering. This operation is applied to the Navier-Stokes equations to eliminate small scales of the solution. This reduces the computational cost of the simulation. The governing equations are thus transformed, and the solution is a filtered velocity field. Which of the "small" length and time scales to eliminate are selected according to turbulence theory and available computational resources.

Large eddy simulation resolves large scales of the flow field solution allowing better fidelity than alternative approaches such as Reynolds-averaged Navier-Stokes (RANS) methods. It also models the smallest (and most expensive) scales of the solution, rather than resolving them as direct numerical simulation (DNS) does. This makes affordable the computational cost for practical engineering systems with complex geometry or flow configurations, such as turbulent jets, pumps and vehicles. In contrast, direct numerical simulation, which resolves every scale of the solution, is prohibitively expensive for nearly all systems with complex geometry or flow configurations.

To separate the large from the small scales, LES is based on the definition of a filtering operation. Formally, one may think of filtering as the convolution of a function with a filtering kernel G (Pope, 2000):

$$\overline{u}_i\left(\vec{x}\right) = \int G\left(\vec{x} - \vec{\xi}\right) u\left(\vec{\xi}\right) d\vec{\xi}\,, \tag{3.9}$$

resulting in

$$u_i = \overline{u}_i + u_i' \tag{3.10}$$

where $\overline{u}_i$ is the resolvable scale part and u_i' is the subgrid-scale part. However, most practical (and commercial) implementations of LES use the grid itself as the filter (the box

filter) and perform no explicit filtering. The box filter, that is used here, cuts off the values of the function beyond a half filter width away.

$$G(x) = \frac{1}{\Delta} H\left(\frac{1}{2}\Delta - |x|\right) \tag{3.11}$$

where, $G(x)$ is the filtering kernel in physical space, Δ is the filter width, and H is the Heaviside function.

For incompressible flow, the continuity equation and Navier-Stokes equations are filtered, yielding the filtered incompressible continuity equation,

$$\frac{\partial \overline{u}_i}{\partial x_i} = 0 \tag{3.12}$$

and the filtered Navier-Stokes equations of a Newtonian fluid,

$$\frac{\partial \overline{u}_i}{\partial t} + \frac{\partial}{x_j}\left(\overline{u}_i \overline{u}_j\right) = -\frac{1}{\rho}\frac{\partial \overline{p}}{\partial x_i} + \nu \frac{\partial^2 \overline{u}_i}{\partial x_j \partial x_j} - \frac{\partial \tau_{ij}}{\partial x_j} \tag{3.13}$$

The filtered Navier-Stokes equations written above govern the evolution of the large, energy-carrying, scales of motion. The effect of the small scales appears through a subgrid-scale (SGS) stress term,

$$\tau_{ij} = \overline{u_i u_j} - \overline{u}_i \overline{u}_j \tag{3.14}$$

that must be modeled to achieve closure of the system of equations.

Two classes of SGS models exist; the first class is functional models and the second class is structural models. Some models may be categorized as both. Functional (eddy-viscosity) models are simpler than structural models, focusing only on dissipating energy at a rate that is physically correct. These are based on an artificial eddy viscosity approach, where the effects of turbulence are lumped into a turbulent viscosity. The approach treats dissipation of kinetic energy at sub-grid scales as analogous to molecular diffusion. In this case, the deviatoric part of τ_{ij} is modeled as:

$$\tau_{ij} - \frac{1}{3}\tau_{kk}\delta_{ij} = -2\nu_T \overline{S}_{ij} \tag{3.15}$$

where ν_T is the turbulent eddy viscosity and $\bar{S}_{ij} = \frac{1}{2}\left(\frac{\partial \bar{u}_i}{\partial x_j} + \frac{\partial \bar{u}_j}{\partial x_i} \right)$ is the strain-rate tensor.

The eddy viscosity has units of $\left[\frac{length^2}{time} \right]$. Most eddy viscosity SGS models, model the eddy viscosity as the product of a characteristic length scale and a characteristic velocity scale. The first SGS model developed (Smagorinsky, 1963) and used in the first LES simulation by Deardorff (1970), is the one used also in this work, was the Smagorinsky-Lilly SGS model. It models the eddy viscosity as:

$$\nu_T = \left(C_S \Delta\right)^2 \sqrt{2\bar{S}_{ij}\bar{S}_{ij}} \tag{3.16}$$

where Δ is the filter width that is associated with the grid size and is taken to be

$$\Delta = \left(Volume\right)^{\frac{1}{3}} \tag{3.17}$$

and C_s is the Smagorinsky constant, in this simulation was set $C_s = 0.158$.

3.3.2 Interaction with multilayer particle bed

The flow field variables affect the deposited particles, since the friction velocity is the main resuspension mechanism. Yet there is in reality a two-way interaction between these two distinct events. The way that the deposit affects the flow field, could be conceivable if one makes the assumption that there is no gas flow through the deposited particles, even if the porosity is very high. This means that the gas flow conceives the interface of the particle bed as a wall. Since the surface of the granular interface is very rough and could lead to complex flow structures, it is smoothed out by using Bezier splines.

Ideally, every time clusters resuspend, the topology of the interface should be modified so as to calculate the new flow field variables and thus define the new resuspendable clusters according to them and so on. Although there is a follow-up project to improve the developed algorithm for this feature of using a dynamic mesh in the domain of the problem, it will not be carried out due to time constraints.

The friction velocity will be calculated at the smoothed interface of the deposit, according to the following equation:

$$u_* \equiv \sqrt{\frac{\tau_w}{\rho}} \tag{3.18}$$

where ρ is the fluid density at the wall (incompressible) and τ_w is the wall shear stress that is given by the equation:

$$\tau_w = \mu \left(\frac{\partial u}{\partial y} \right)_{y=0} \tag{3.19}$$

where μ is the dynamic viscosity, u is the flow velocity parallel to the wall and y is the distance to the nearest wall.

3.3.3 Near-wall treatment

The standard Smagorinsky model eddy viscosity is nonzero at solid boundaries, which is contrary to the notion that the eddy viscosity should be zero where there is no turbulence. The easy fix for this situation is to add a Van Driest-style damping function into the length scale (Berselli et al, 2006):

$$D\left(y^+; A^+, m, n\right) = \left[1 - \exp\left(-y^{+n} / A^{+n}\right)\right]^m \tag{3.20}$$

Various different values for A^+, m, n have been used (for this case it was used $m = 1$, $n = 1$, $A^+ = 26$). The use of this formulation requires the accurate computation of wall shear (in order to compute y^+), which has generally been accomplished by high grid resolution in near-wall regions.

3.3.4 OpenFOAM platform

The OpenFOAM (Open source Field Operation And Manipulation) CFD Toolbox is an open source CFD software package. It has a large user base across most areas of engineering and science, from both commercial and academic organizations. OpenFOAM has an extensive range of features to solve anything from complex fluid flows involving chemical reactions, turbulence and heat transfer, to solid dynamics and electromagnetics. It includes tools for meshing, and for pre- and post-processing. Almost everything (including meshing, and pre-

and post-processing) runs in parallel as standard, enabling users to take full advantage of computer hardware at their disposal.

OpenFOAM is on the one hand a C++ library, on the other hand a collection of applications (created using these libraries). The applications can be divided into two different categories: *solvers* and *utilities*, of which the former perform the actual calculations to solve a specific continuum mechanics problem and the latter provide a range of functionalities for pre- and post-processing.

In this thesis, a solver was developed that was responsible for the injection, tracking and resuspension of the solid particles based on the lagrangian library that is supplied by default. This solver was coupled with an already existed solver named *channelFoam* (an incompressible LES solver for flow in a channel). Moreover, a set of other applications and utilities were developed and/or used (e.g. calculation of the friction velocity, generation of the initial turbulent conditions).

3.4 Coupling

3.4.1 Solution domain

The present numerical experiment takes place in a three-dimensional horizontal duct flow having a rib-roughened bottom wall surface. A sketch of the obstructed wind tunnel can be seen in Figure 3.12. The channel height, the channel length, the rib height and the rib pitch are denoted by H, L, e and p, respectively. The channel height equals H = 0.1 m and the ratio of the channel length to height is set to L/H = 20. The height of the square rib obstructs the channel by e/H = 10%. The rib pitch, defined as the distance from one leading edge to the next leading edge, is p = H. A total of 17 ribs are placed in the virtual channel. The dimensions of the channel and of the obstruction are chosen to match the geometry of experimental test facility built on-site (Lecrivain et al, 2013). The flow variables will be solved only between two consecutive steps (13-14), as it will be taken into account only the fully developed flow field and there are periodic boundary conditions between the steps.

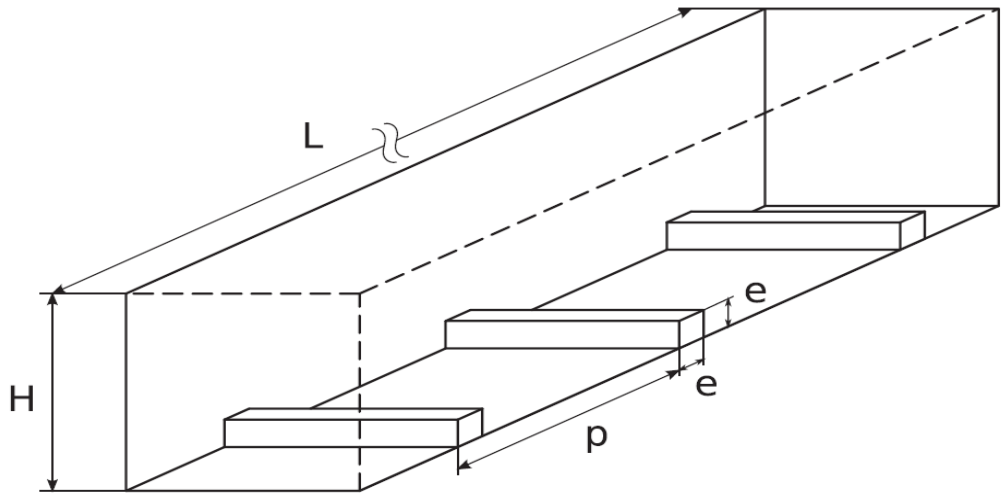

Figure 3.12: Schematic representation of the obstructed square channel, flow direction from left to right (Lecrivain et al, 2013).

3.4.2 Mesh generation

The above geometry was meshed with structured grid using the meshing software ICEM CFD and then this mesh was imported in OpenFOAM to compute the flow field variables.

A hexahedral structured 3D mesh was chosen for the discretization in space of the domain (Figure 3.13).

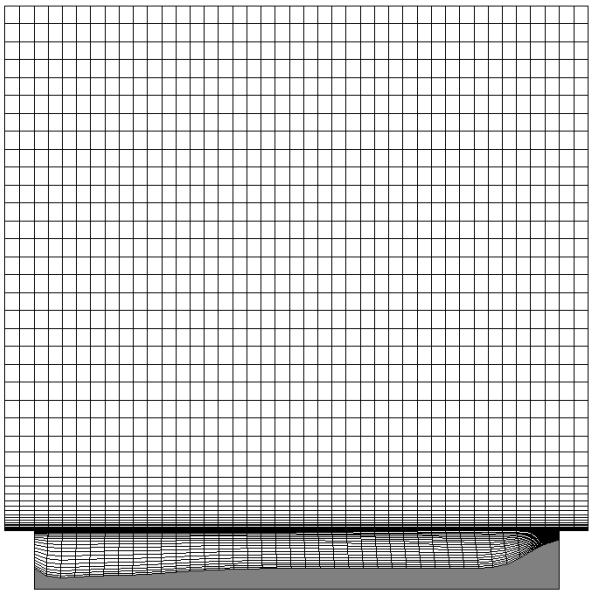

Figure 3.13: Mesh of the computational domain (xy-plane).

After a grid independence study, the coarser mesh that was providing invariant solutions comparing to the ones of finer meshes, was a 3D grid made up of 41x48x21 cells in flow, vertical and streamwise direction.

In Figure 3.13 one may see the mesh of the domain and also a multilayer deposit of solid particles at the bottom of it (gray color). As it has been already stated the fluid flow perceives this sediment as a wall, so the mesh should be properly modified so as the bounding line to coincide with the granular interface. This is performed by moving the bottom boundary line to the deposit's interface and smoothing so as to reduce the roughness. Ideally, the mesh should be dynamic, adjusting each time the new thickness of the deposit, but this is out of the scope of this work. It however not the case here.

3.4.3 Initial conditions

All the fields (pressure, stress tensor, kinematic turbulent viscosity) were set to zero value, apart from the velocity field where an OpenFOAM utility named perturbU generated the initial turbulent conditions (adds a decreasing sinusoidal random noise to the parabolic profile of the velocity).

3.4.4 Boundary conditions

All the boundary surfaces were considered as a wall, so the flow field variables were set to have zero gradient at the boundary, except for the inlet, outlet and the two side surfaces in the spanwise direction. In these surfaces the boundary conditions were set to cyclic (enables two patches to be treated as if they are physically connected) as of the flow periodicity between the virtual steps.

3.4.5 Numerical schemes

The scheme (backward) used for the time discretization is second-order and implicit. The Gauss linear numerical scheme was used for all the other terms (such as gradient ∇, divergence $\nabla\bullet$, laplacian ∇^2 of the equations' terms). A linear scheme was chosen for the interpolation of various variables.

3.4.6 Numerical methods

The solver that was used for the numerical solution of the system of the pressure equations was the PCG (Preconditioned Conjugate Gradient) method, with the DIC (Diagonal incomplete-Cholesky) symmetric preconditioner. For the numerical solution of the velocity the PBiCG (Preconditioned Bi-Conjugate Gradient) method was chosen, with the DILU (Diagonal incomplete-LU) asymmetric preconditioner.

Before solving an equation for a particular field, the initial residual is evaluated based on the current values of the field. After each solver iteration the residual is re-evaluated. The solver stops if the residual falls below the solver tolerance, or if the ratio of current to initial residuals falls below the solver relative tolerance, or eventually if the number of iterations exceeds a maximum number of iterations.

For this application in OpenFOAM the pressure-implicit split-operator (PISO) algorithm was used for the coupling of velocity and pressure. The algorithm is based on evaluating some initial solutions and then correcting them, the number of correction that were set for the PISO was 2 (usually more than 1 correction, but no more than 4).

Chapter 4

Results

4.1 Gas phase

4.1.1 Turbulent flow field

In this work, two different approaches are used for the calculation of the friction velocity u^* that is essential for evaluation of resuspension probability. On one hand, the unsteady friction velocity is computed directly from the Large Eddy Simulation (LES) model. On the other hand, the mean friction velocity $\overline{u^*}$ is calculated from the time-averaged flow field.

Before the resuspension process takes place, the flow simulation runs 40 flow cycles, so that turbulence can be considered as fully developed. The time of a flow cycle is defined as the bulk flow velocity divided by the channel lentgh: U_{bulk}/L. The Courant number never exceeded 0.5, ensuring this way the convergence of the system of equations.

One may observe the magnitude of the mean velocity for the time-averaged LES model after 40 cycles in Figure 4.1, as well as the instant velocity of the LES model at the same moment for a Reynolds number $\mathrm{Re} = 26670$.

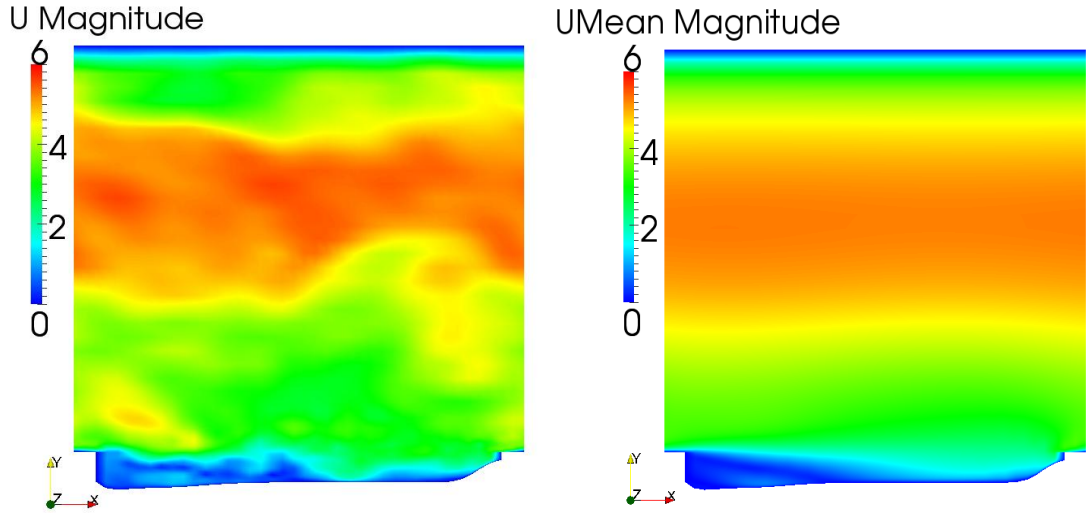

Figure 4.1: Instantaneous (left) and time averaged velocity field (right) after 40 flow cycles.

The y-axis <Uy> and z-axis <Uz> component of the mean velocity after 40 cycles for Re = 26670, are shown on Figure 4.2.

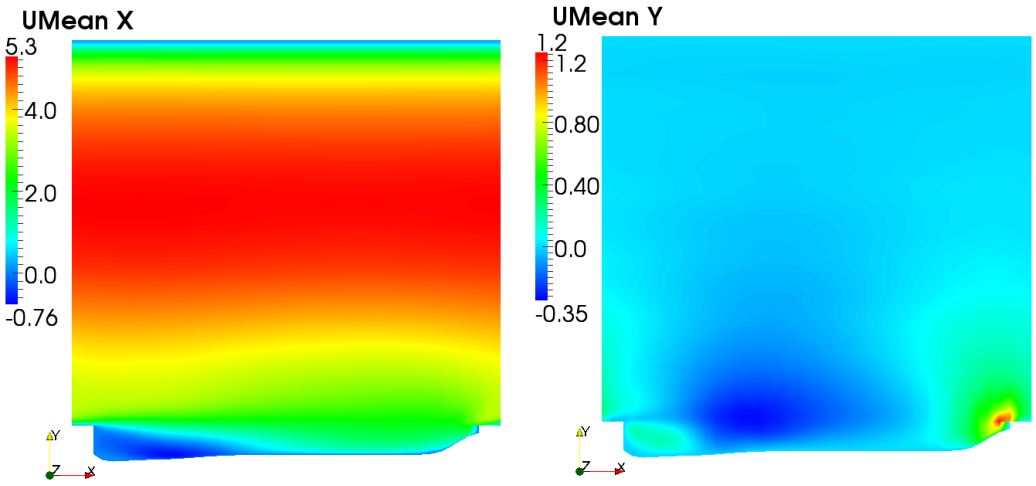

Figure 4.2: Components of the mean velocity after 40 flow cycles.

The flow field is characterized by a large recirculation area downstream of the domain, stated by a negative horizontal mean flow component <Ux>. The area found upstream of the domain is characterized by an increase of the vertical flow component <Uy>, as a consequence of the flow tendency to bypass the subsequent step.

Figure 4.3 offers a close view of the bottom part (half-height) through the mid-section of the channel. The vectors and the colors correspond to the magnitude of the time-averaged mean velocity.

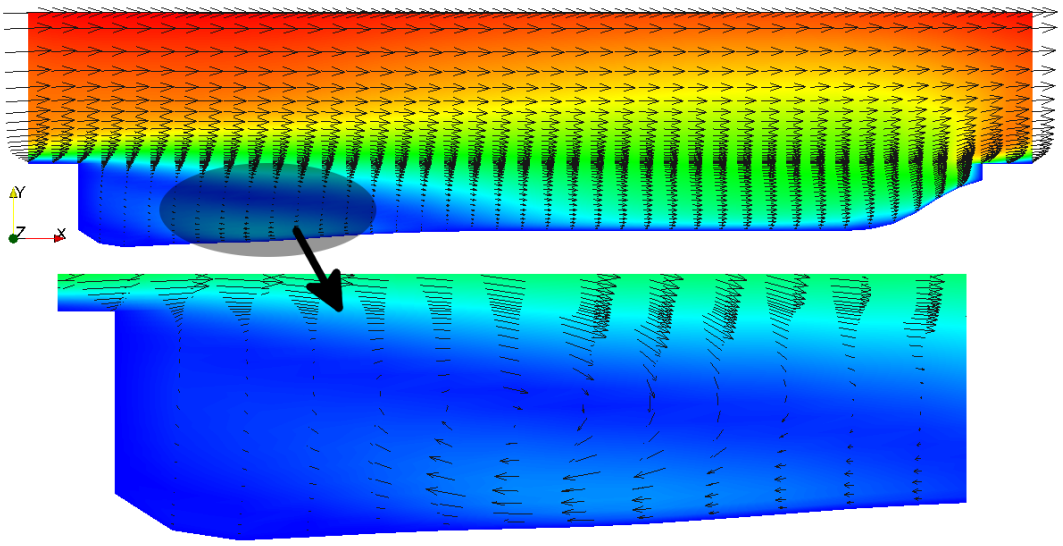

Figure 4.3: Time-averaged mean velocity next to the multilayer deposit.

One may see the parabolic evolution of the velocity profile (Fig. 4.3) as one departs from the walls (no-slip boundary condition). Downstream of the rib, the vectors do have an opposite direction as a result of the flow recirculation. This recirculation can be clearly seen also from the streamlines colored by the magnitude of the mean velocity that are displayed in Figure 4.4:

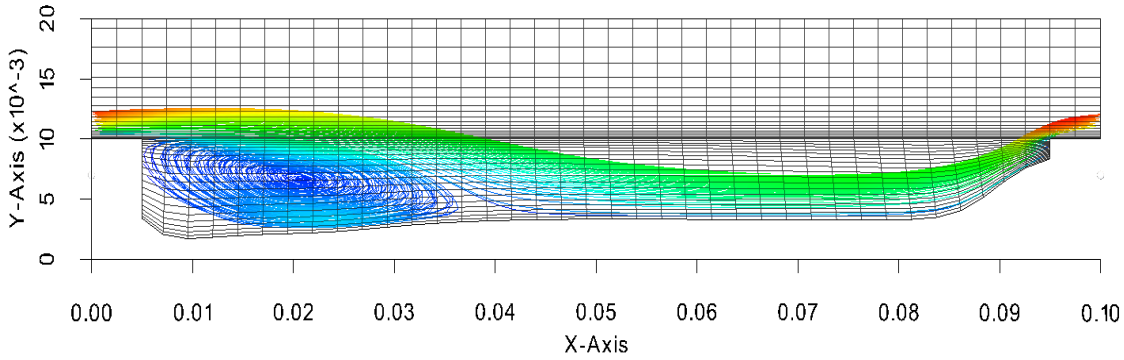

Figure 4.4: Streamlines of the time-averaged mean velocity at the half-height of the channel.

The recirculation zone is found downstream of the obstacle (Fig. 4.4). The flow separates at the back end of the rib and reattaches at $x/e \simeq 4$ (where e the height of the rib) downstream of the rib. This value is in good agreement with the experiments carried out in HZDR (Barth et al, 2013) and to the ones by Shafiqul et al (2002), as well as to the findings by the numerical simulations performed by Lecrivain et al (2013) and by Viswanathan and Tafti (2005).

4.1.2 Friction velocity field

As previously mentioned, two different approaches are applied to study resuspension. In the first case the friction velocity will be computed by time-averaging the LES solutions, leading to a mean friction velocity profile that will solely depend on space and not on time. In the other case, the resuspension criterion takes into consideration the unsteady solutions of the friction velocity in every time step. The friction velocity depends on space and time.

In Figure 4.5 one may see the friction velocity u^* along the interface between the deposit and the fluid flow. Four cases are depicted, one stands for the time-averaged mean friction velocity after 40 flow cycles, while the other three cases show the instant friction velocity after 40, 41 and 42 cycles.

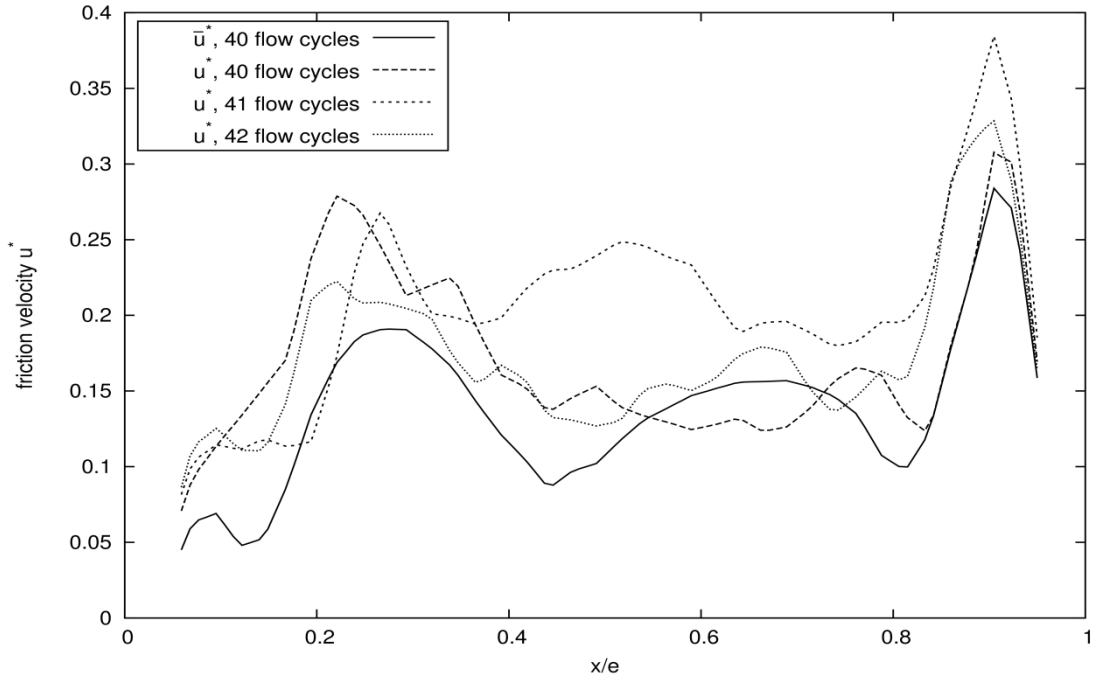

Figure 4.5: Friction velocity along the granular interface at the bottom of the channel.

It can be seen from the previous figure, that for the time-averaged model, the resuspension criterion that decides which particles are to re-enter the flow is based upon an almost "static" profile of the friction velocity since it has been averaged for a wide range of time steps, so a change of the friction profile in the next time step, only slightly affects the mean value.

By taking into consideration the unsteady solutions of the flow field, the resuspension criterion is adapted to the current time step distribution of wall shear stresses rather than following a purely space-dependant change. This should better reproduce multilayer resuspension.

4.2 Re-entrainment of the deposit

4.2.1 Time-averaged LES

The resuspension process, following the experimental one, is performed for various Reynolds number (Re). The initial state of the resuspension corresponds to a thick layer of deposited particles that have been injected in the domain under the influence of a fluid flow at

$\mathrm{Re} = 8900$ as it was discussed in the previous Chapter (Fig. 3.6). After the particle bed of the experiments has been re-constructed, the flow velocity is increased suddenly and the field is properly perturbed so that a turbulent flow is successfully generated.

The velocity increment causes an increase in the wall shear stress, that is considered the main resuspension mechanism in this work. By gradually increasing the flow velocity, more and more particles re-enter the flow. Since in the present model there is no concern for re-deposition, the resuspended particles are removed entirely from the deposit. Figure 4.6 depicts the resuspension process of a deposit by gradually increasing the Reynolds number. The gray colored particles correspond to the simulation, while the dashed line displays the spanwise averaged thickness line of the experimental data.

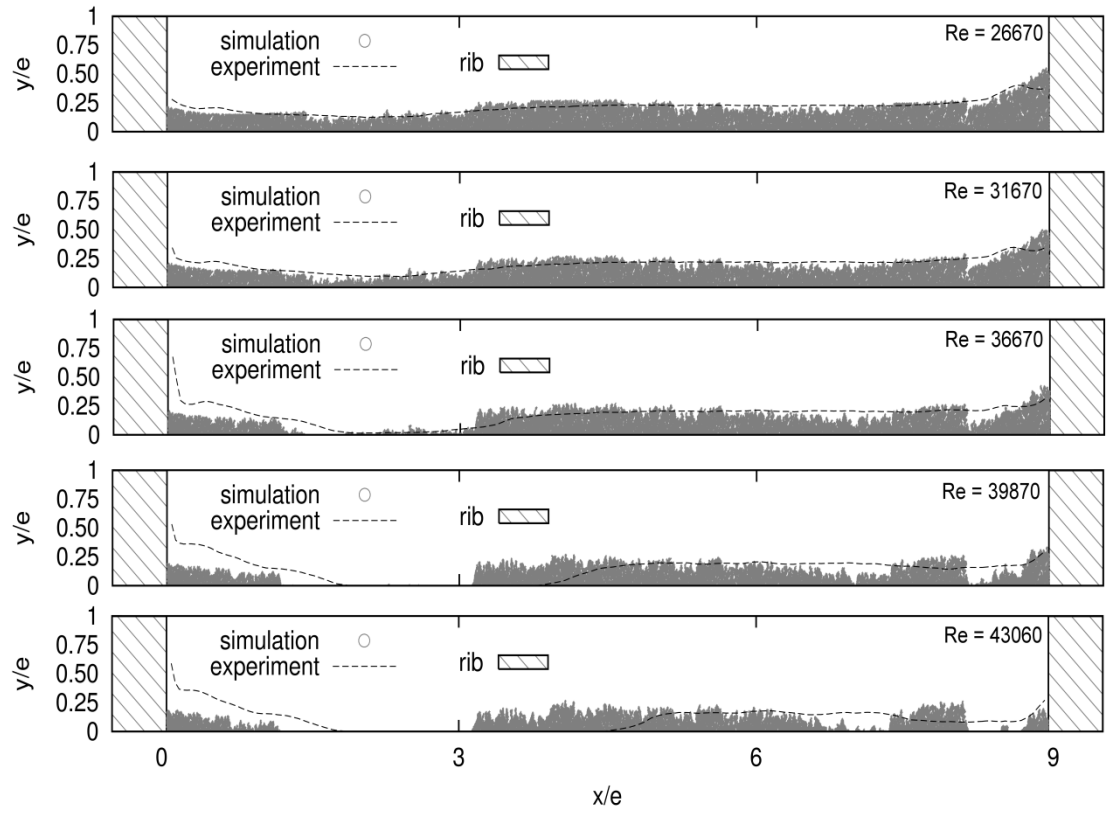

Figure 4.6: Resuspension process of the deposit at various Reynolds numbers (time-averaged LES). The dashed line depicts the spanwise averaged thickness layer of the experimental data.

Looking at the resuspension process (Fig. 4.6) of the time-averaged LES solutions, one may observe a good fit between the experimental and the numerical solution for a Reynolds number between $\mathrm{Re} = 26670$ and $\mathrm{Re} = 36670$. By increasing more the flow velocity ($\mathrm{Re} = 39870$), three areas are being constantly eroded, leading to the full exposure

of their surface ($\mathrm{Re} = 43060$). These three areas correspond to the high friction velocity areas (Fig. 4.5), and for this reason their particles are removed almost layer-by-layer while in nearby areas of low friction velocity areas, no resuspension takes place. This makes sense as by time-averaging the flow field, a prominent profile of the mean wall shear stresses guides the resuspension process. This is the main drawback of this approach.

Figure 4.7 displays the overall comparison of the thickness layer of the deposit between the numerical and the experimental data, for various Reynolds numbers. It should be noted, that the filled curves of the simulation results have being formed by joining the particles of the granular interface with Bezier splines, for this reason no zero thickness is depicted along the cavity as it should be (like in Fig. 4.6).

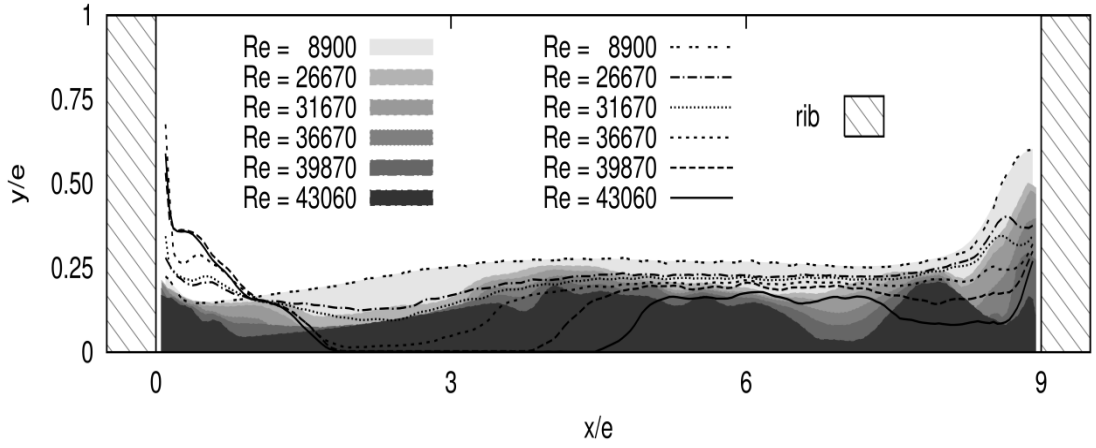

Figure 4.7: Overall comparison of the resuspension process for the time-averaged LES between the simulation (grayscale filled curves) and the experiments (dashed and dotted lines).

4.2.2 Unsteady LES

Aiming at resolving the issue of a prominent wall shear stress profile during the resuspension process, the unsteady solution of the LES are taken into account to compute the instantaneous friction velocity and, thus, predict particle resuspension. This will hopefully (Figure 4.8) result in better predictions.

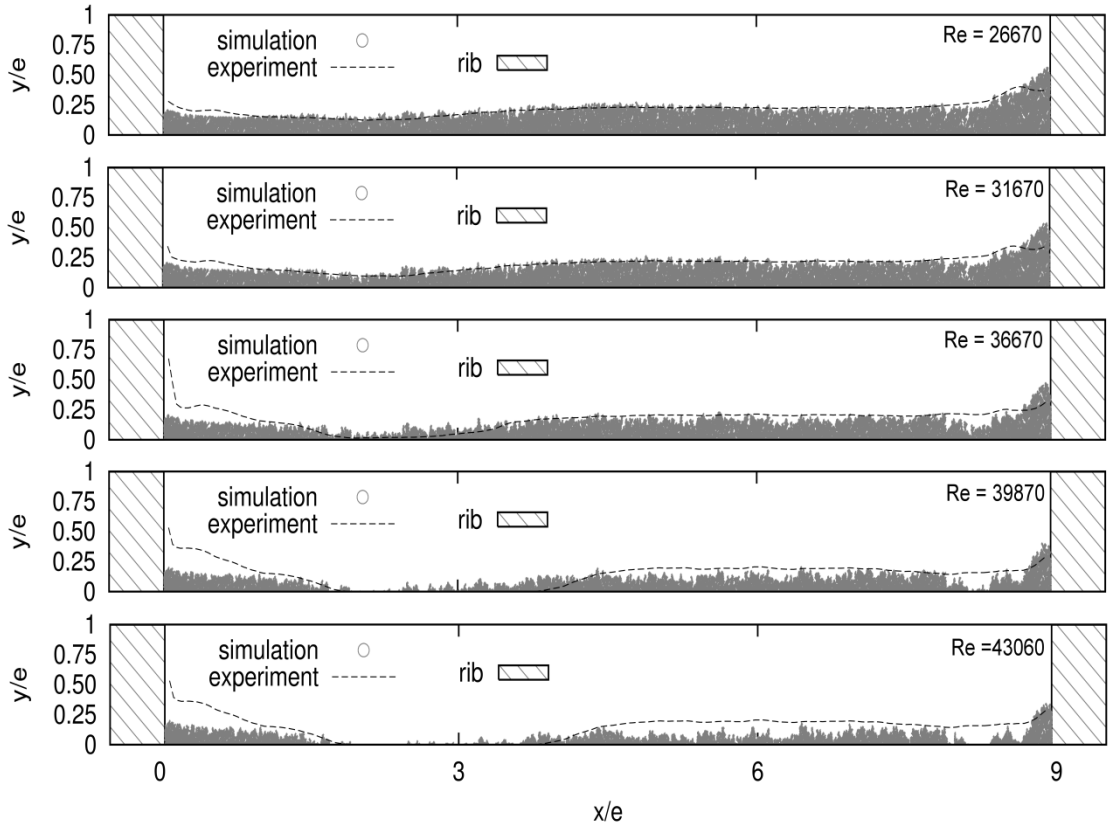

Figure 4.8: Resuspension process of the deposit at various Reynolds numbers (unsteady LES). The dashed line depicts the spanwise averaged thickness layer of the experimental data.

In Figure 4.8 the results of the unsteady LES simulation (gray deposit) seem to fit remarkably well experimental data (dashed line). There is an over-estimation in the resuspension of the upstream area ($x/e \simeq 8.5$) for the high Reynolds number ($\mathrm{Re} = 43060$), but there is a good agreement in the area $x/e \simeq 2-4$. The over-predicted resuspension upstream of the domain occurs because of the lack of a dynamic mesh, since in the initial mesh the flow is fully attached at this location, but as the clusters of this area are keeping to be resuspended, an eddy should have appeared there, leading to lower friction velocities and, thus, lower resuspension probability.

In Figure 4.9 the particles on the particle bed interface are interconnected with smooth Bezier splines forming the thickness layer of the simulation (filled grayscale curves) along the interface in contrast to the experimental data (dashed and dotted lines) of the spanwise averaged thickness layer.

One may observe from the experimental data the tendency for increasing thickness downstream of the domain with increasing the Reynolds number. This could be perceived as a

result of the re-deposition process, as a result of the recirculation area that appears right next to this location. In other words, the resuspended particles of the zone between $x/e \simeq 2$ and $x/e \simeq 4$ are re-entering the flow, that happens to be a big eddy moving them back right in front of the step. This behavior however can not be captured by the model developed in this work, since there is no concern for re-deposition, leading to a discrepancy of the layer thickness in this area between experimental measurements and numerical predictions.

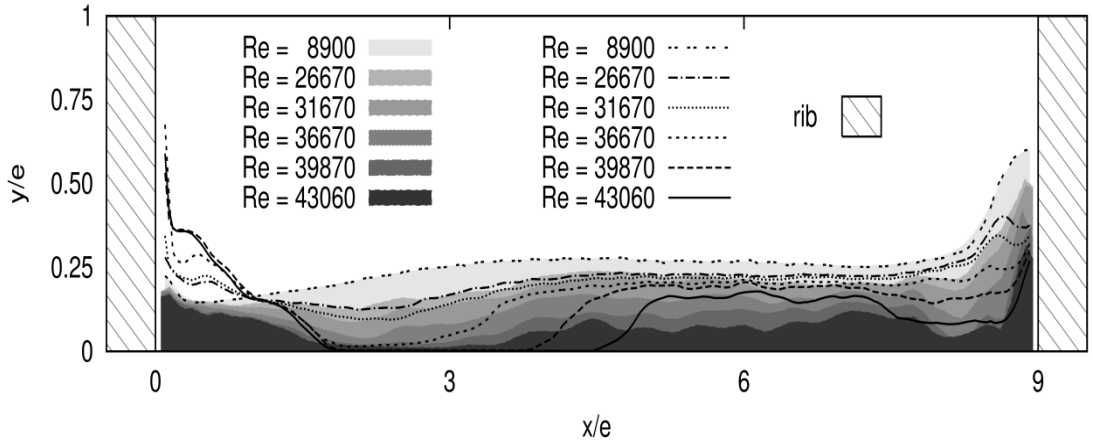

Figure 4.9: Overall comparison of the resuspension process for the unsteady LES between the simulation (filled grayscale curves) and the experiments (dashed and dotted lines).

It is noted that in the above figures, the experimental data are referring to the spanwise averaged thickness layer of a three-dimensional deposit, while the simulation refers to a deposit of just one three-dimensional row placed in the midsection of the channel's floor. So, any comparison between them carries a certain amount of inaccuracy.

4.2.3 Integral analysis of the resuspension process

The overall resuspension process was quantified by the fraction of remaining particle material against Reynolds number of a transient flow. In principle, particle deposits tend to resuspend when a critical friction velocity is exceeded. This behavior is also visible in the present data set (see Fig. 4.10). Below a mean friction velocity that a flow of Reynolds number $\mathrm{Re} = 8900$ creates, the multilayer remains unmodified. Exceeding this velocity the material starts to resuspend. Note that at Reynolds number $\mathrm{Re} > 43060$ almost the entire multilayer is removed. The shape of this curve (Figure 4.10) is in good agreement with the experimental data, Experiment I and II, performed at HZDR (Reiche, 2012), (Barth et al, 2013).

Figure 4.10 displays also curves for other particle resuspension experiments. Reeks and Hall (2001) reported about the monolayer resuspension of 10 micron alumina spheres (RH01-Al) and graphite particles (RH01-C), while Hontanon et al. (2000) reported about the resuspension of particles with diameter 0.4 μm in the framework of the STORM project. In those last two experiments (RH01, STORM-SR11) larger friction velocities were necessary to remobilise the particles. Comparing the multilayer resuspension simulation (time-averaged and unsteady LES) and the multilayer resuspension experiments performed at HZDR (Experiment I and II) to these two studies it can be concluded that the resuspension of multilayer deposits requires less aerodynamic force than single particle resuspension. Reasons for this may be found in the adhesion forces. Particle-to-particle contact forces are much less than the adhesion forces between a single particle and a flat wall as in monolayer deposits (Friess & Yadigaroglu, 2002).

It is also clear, that the remaining mass fraction of unsteady LES approach is less than that of the time-averaged LES. This means that more particles are resuspended when the unsteady approach is used, as a result of the variable wall shear stress profile at every time step that is capable of resuspending particles from the entire body of the deposit, instead of a predominant profile during the whole process.

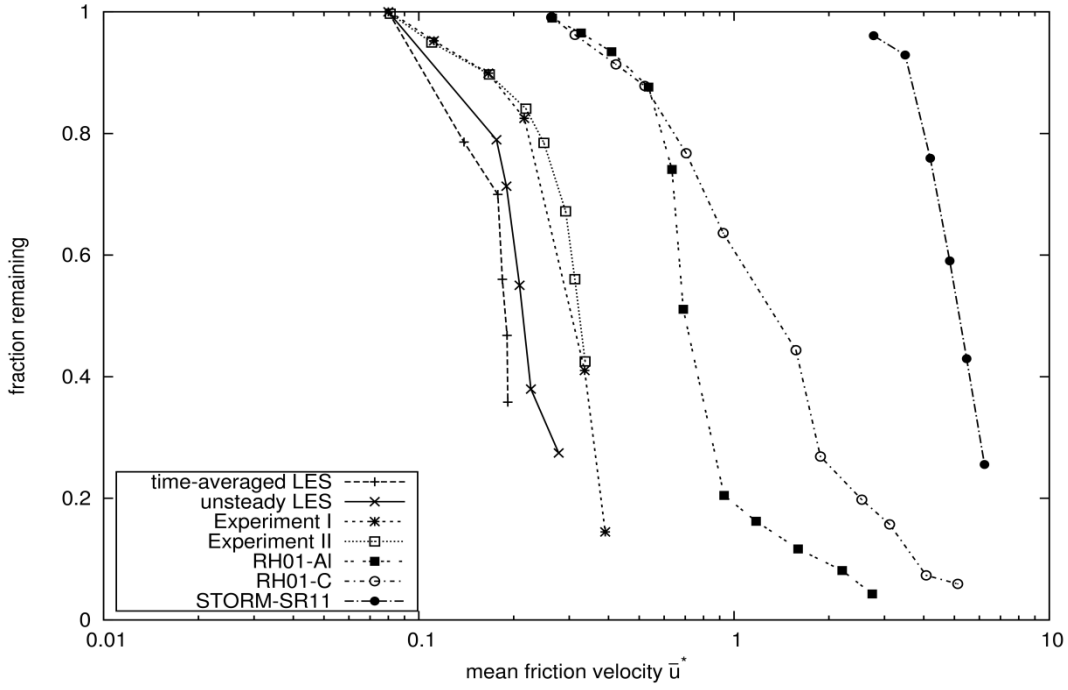

Figure 4.10: Comparison of the remaining mass fraction of the initial multilayer against the mean friction velocity.

Chapter 5

Summary and outlook

5.1 Conclusions

In this work, the multilayer particle build-up and resuspension in a ribbed duct subject to a turbulent flow was studied. Background motivation was the investigation of High-Temperature Reactor related graphite dust transport in turbulent flows.

As far as the multilayer build-up is concerned, a deposition algorithm was developed, capable of re-producing deposits of variable porosity and thickness in complex geometries in short time.

Regarding the multilayer particle resuspension, which was the main case of the research, a novel approach was introduced to confirm:

a) the conjecture if the main resuspension mechanism is based on the friction velocity, and

b) the connection of the inverse time law and resuspension rate, cases observed in many experiments.

Cluster resuspension was taken into account. The friction velocity was computed in two ways; one by the direct time-dependent flow field solutions of the Large Eddy Simulation turbulence model, in the other the mean friction velocity was calculated by time-averaging the solutions of LES. The results of these two methods were validated against experiments carried out at HZDR.

The two test cases examined present common findings. What comes out is the evidence, of the strong relationship between the friction velocity and the resuspension probability. It seems that particles stay immobilized until a critical friction velocity is reached. The greater the friction velocity, the greater the resuspension rate.

Also, it was drawn out from the two test cases that the time-dependent friction velocity provides better predictions in relation to the experimental data.

The inverse time law used to eliminate the resuspension probability after a certain period of time seems to be confirmed by the predictions regarding the remaining mass fraction.

Furthermore, the discrepancy between the experimental measurements and numerical predictions, actually pointed out the limitations of the adopted model, namely the resuspension criterion not based on the size of the particle's diameter, a decisive factor as indicated by other models in the literature. The reason that this factor was not included in the developed model, is that there was no evidence from the experiments of the exact diameter and position of each particle in the deposit. So, this conjecture could not be validated by real data. Another shortcoming of the model was the use of a static initial mesh during the whole process of the resuspension, rather than a dynamic mesh adapting to each time step's particle bed interface. Moreover, there was evidence of re-deposition after particles' detachment from the bed, an issue that was not taken into account in the current model.

5.2 Future work

Starting from the results obtained in this thesis, and taking into account the mentioned limitations of the developed model, several directions for future research could be suggested, ranging from small projects to very challenging tasks:

- A more elaborate resuspension criterion could be implemented, taking into account the particle diameter, a crucial factor for particle's re-entrainment.
- A parametric study regarding the effect of porosity on the remaining mass fraction should be done.
- The model should be extended to cover the effect of relative humidity on resuspension process. There have been observations that the more the relative humidity is, the more unlikely a particle to resuspend.
- Performing the similar study on a three-dimensional artificial deposit, in the whole depth of the plate, thus reducing the discrepancies between the experimental and numerical results.
- The algorithm developed in this work could be implemented by means of parallel computing, thus reducing the computational cost.

- Implementation of a dynamic mesh, able to adjust its boundary lines to the granular interface of each time step.
- Finally, particles re-depositing in the particle bed after their detachment, should be taken into account by augmenting the model with one that tracks the subsequent trajectory of resuspended particles.

References

Agrati G., Parozzi F., Sandrelli G., Valisi M., Carraro G., Markovina A., (1991). STORM: Simplified Tests On Resuspension Mechanisms. Preliminary description of the Project, ENEL/DSR/CRTN Report N6/91/01/MI.

Ahmadi G., Guo S., Zhang X., (2007). Particle adhesion and detachment in turbulent flows including capillary forces. Particulate Science and Technology, 25(1), 59-76.

Atkins P.J., (2005). Dry powder inhalers: an overview. Respir. Care, 50 (10) 1304-1312.

Barth T., Reiche M., Banowski M., Oppermann M., Hampel U., (2013). Experimental investigation of multilayer particle deposition and resuspension between periodic steps in turbulent flows. Journal of Aerosol Science, (forthcoming).

Benson C.G., Bowsher B.R., (1988). Physical resuspension and revaporization phenomena in control rod aerosols. UKAEA-Winfrith, AEEW-R2427.

Berselli L.C., Iliescu T., Layton W.J., (2006). Mathematics of Large Eddy Simulation of Turbulent Flows. New York: Springer Berlin Heidelberg.

Biasi L., de los Reyes A., Reeks M.W., de Santi G.F., (2001). Use of a simple model for the interpretation of experimental data on particle resuspension in turbulent flows. Journal of Aerosol Science, 32(10), 1175-1200.

Boehme G., Krupp H., Rabenhorst H., Sandstede G., (1962). Adhesion measurements involving small particles. Chemical Engineering Research and Design, vol.40a, 252-259.

Braaten D.A., Paw U K.T., Shaw R.H., (1990). Particle resuspension in a turbulent boundary layer-observed and modelled. Journal of Aerosol Science, 21(5), 613–628.

Braaten D.A. (1994). Wind tunnel experiments of large particle reentrainment-deposition and development of large particle scaling parameters. Aerosol Science and Technology, 21(2), 157-169.

Cherukat P., McLaughlin J.B., (1994). The inertial lift on a rigid sphere in a linear shear flow field near a flat wall. Journal of Fluid Mechanics, vol.263, 1-18.

Cleaver J.W., Yates B., (1973). Mechanism of detachment of colloidal particles from a flat substrate in a turbulent flow. Journal of Colloid and Interface Science. 44(3), 464-474.

Cleaver J.W., Yates B., (1976). The effect of re-entrainment on particle deposition. Chemical Engineering Science, 31(2), 147-151.

Corn M., Stein F., (1965). Re-entrainment of particles from a plane surface. American Industrial Hygiene Association Journal, 26(4), 325–336.

Deardorff J.W., (1970). A numerical study of three-dimensional turbulent channel flow at large Reynolds numbers. Journal of Fluid Mechanics, 41(2), 453-480.

Fauske and Associates, (1984). Resuspension of Deposited Aerosols following primary system or containment failure. IDCOR technical report, vol.11(6). Bethesda, Md.: Atomic Industrial Forum.

Friess H., Yadigaroglu G., (1998). Inclusion of structural parameters in the modelling of aerosol resuspension. Proceedings of the third OECD specialist meeting on nuclear aerosols in reactor safety, Cologne, Germany.

Friess H., Yadigaroglu G., (2001). A generic model of the resuspension of multilayer aerosol deposits by turbulent flow. Journal of Nuclear Science and Engineering, 138(2), 161-176.

Friess H., Yadigaroglu G., (2002). Modelling of the resuspension of particle clusters from multilayer aerosol deposits with variable porosity. Journal of Aerosol Science, 33(6), 883-906.

Fromentin A. (1989). Particle resuspension from a multi-layer deposit by turbulent flow. Ph.D. thesis, ETH University: Zurich, Switzerland.

Gomes C., Freihaut J., Bahnfleth W., (2007). Resuspension of allergen-containing particles under mechanical and aerodynamic disturbances from human walking. Atmospheric Environment, 41 (25), 5257-5270.

Gradón L., (2009). Resuspension of particles from surfaces: Technological, environmental and pharmaceutical aspects. Advanced Powder Technology, 20(1), 17-28.

Guingo M., Minier J.P., (2008). A new model for the simulation of particle resuspension by turbulent flows based on a stochastic description of wall roughness and adhesion forces. Journal of Aerosol Science, 39(11), 957-973.

Hontañón E., de los Reyes A., Capitão J.A., (2000). The CÆSAR code for aerosol resuspension in turbulent pipe flows. Assessment against the storm experiments. Journal of Aerosol Science, 31(9), 1061-1076.

Ibrahim A.H., Dunn P.F., Brach R.M., (2003). Microparticle detachment from surfaces exposed to turbulent air flow: controlled experiments and modelling. Journal of Aerosol Science, 34(6), 765-782.

Iimura K., Watanabe S., Suzuki M., Hirota M., Higashitani K., (2009). Simulation of entrainment of agglomerates from plate surfaces by shear flows. Chemical Engineering Science, 64(7), 1455-1461.

Johnson K.L., Kendall K., Roberts A.D., (1971). Surface energy and the contact of elastic solids. Proceedings of the Royal Society, 324(1558), 301-313.

Jurcik B., Wang H.C., (1991). Modelling of particle resuspension in turbulent flow. Journal of Aerosol Science, 22(1), 149-152.

Kern W. (Ed.), (1993). Handbook of semiconductor wafer cleaning technology - Science, Technology, and Applications. New Jersey: Noyes Publications.

Kissane M.P., Zhang F., Reeks M.W., (2012). Dust in HTRs: Its nature and improving prediction of its resuspension. Nuclear Engineering and Design, vol.251, 301-305.

Lazaridis M., Drossinos Y., (1998). Multilayer resuspension of small identical particles by turbulent flow. Aerosol Science and Technology, 28(6), 548-560.

Lecrivain G., Sevan D.M., Barth T., Hampel U., (2013). Numerical simulation of multilayer deposition in an obstructed channel flow. Advanced Powder Technology, (forthcoming).

Lennard-Jones J.E., (1931). Cohesion. Proceedings of the Physical Society, 43(5), 461-482.

Mantz P.A., (1978). Bedforms produced by fine, cohesionless, granular and flakey sediments under subcritical water flows. Sedimentology, 25(1), 83-103.

Matsusaka S., Masuda H., (1996). Particle reentrainment from a fine powder layer in a turbulent air-flow. Aerosol Science and Technology, vol.24, 69-84.

Moormann R., (2008). Fission product transport and source terms in HTRs : Experience from AVR Pebble Bed Reactor. Science and Technology of Nuclear Installations, vol.2008, Article ID 597491, 1-14.

Ould-Dada Z., Baghini N.M., (2001). Resuspension of small particles from tree surfaces. Atmospheric Environment, vol.35, 3799-3809.

Parozzi F., Alonso A., Bolado R., Hontañón E., Capitão J.A., Drossinos Y., (1995). Nuclear science and technology: Aerosol physical resuspension under LWR severe accident conditions. State of the Art Review, Final Report, EUR 16505, Brussels.

Paw U K.T., (1983). The rebound of particles from natural surfaces. Journal of Colloid and Interface Science, 93(2), 442-452.

Pope S.B. (200), Turbulent flows. United Kingdom: Cambridge University Press.

Pöschel T., Schwager T., (2005). Computational granular dynamics, models and algorithms. New York: Springer Berlin Heidelberg.

Rahn F.J., (1988). The LWR Aerosol Containment Experiments (LACE). Project summary report, LACE TR-012.

Raunio T., (2008). Experimental study on fine particle resuspension in nuclear reactor safety. PhD thesis, Helsinki University of Technology: Finland.

Reed J.R., Rochowiak P., (1988). The adhesion of small particles to a surface. Proceedings of the second conference of the aerosol society (p229), Oxford: Pergamon.

Reeks M.W., Reed J., Hall D., (1988). On the resuspension of small particles by a turbulent flow. Journal of Physics D: Applied Physics, 21(4), 574-589.

Reeks M.W., Hall D., (2001). Kinetic models for particle resuspension in turbulent flows: theory and measurement. Journal of Aerosol Science, 32(1), 1-31.

Reiche M., (2012). Experimentelle Untersuchung des Multilayer-Staubablagerungsverhaltens in turbulenten Strömungen mittels Lasertriangulation und Röntgenmessungen. Diploma thesis. Dresden University of Technology: Germany.

Rostamian M., Potirniche G.P., Cogliati J.J., Ougouag A., and Tokuhiro A., (2012). Computational prediction of dust production in pebble bed reactors. Nuclear Engineering and Design, vol.243, 33-40.

Rott, Wahsweiler, (1991). Auswertung von Inbetriebnahmeergebnissen am THTR-300 für HTR-Nachfolgeanlagen: Nachuntersuchungen von THTR-Betriebselementen(BTE). Hochtemperatur-Reaktorbau GmbH.

Schmidt E., Löffler F., (1991). The analysis of dust cake structures. Particle and Particle Systems Characterization, vol.8, 105-109.

Sehmel G.A., (1980). Particle resuspension: a review. Environment International, 4(2), 107-127.

Shafiqul I.M., Haga K., Kaminaga M., Hino R., Monde M., (2002). Experimental analysis of turbulent flow structure in a fully developed rib-roughened rectangular channel with PIV. Experiments in Fluids, vol.33, 296-306.

Smagorinsky J., (1963). General circulation experiments with the primitive equations. Monthly Weather Review, 91(3), p.99.

Stempniewicz M.M., Komen E.M.J., de With A., (2008). Model of particle resuspension in turbulent flows. Nuclear Engineering and Design, 238(11), 2943-2959.

Stempniewicz M.M., Komen E.M.J., (2010). Comparison of several resuspension models against measured data. Nuclear Engineering and Design, 240(6), 1657-1670.

Stempniewicz M.M., Winters L., Caspersson S.A., (2012). Analysis of dust and fission products in a pebble bed NGNP. Nuclear Engineering and Design, vol.251, 433–442.

Ström L., (1986). Resuspension of dust deposits in pipes. Studsvik - The Marviken Project, Report, MXIP-11.

Telko M.J., Hickey A.J., (2005). Dry powder inhaler formulation. Respir. Care, 50 (9), 1209-1227.

Vainshtein P., Ziskind G., Fichman M., Gutfinger C., (1997). Kinetic model of particle resuspension by drag force. Physical Review Letters, 78(3), 551-554.

Viswanathan A.K., Tafti D.K., (2005). Detached Eddy Simulation of Turbulent Flow and Heat Transfer in a Ribbed Duct. Journal of Fluids Engineering, 127(5), 888-896.

Wang S., Zhao B., Zhou B., Tan Z., (2012). An experimental study on short-time particle resuspension from inner surfaces of straight ventilation ducts. Building and Environment, vol.53, 119-127.

Weber A.P., Friedlander S.K., (1997). Relation between coordination number and fractal dimension of aerosol agglomerates. Journal of Aerosol Science, 28(1), 765-766.

Wen H.Y., Kasper G., (1989). On the kinetics of particle reentrainment from surfaces. Journal of Aerosol Science, 20(4), 483-498.

Wright A.L., Pattison W.L., King J.Y., (1992). Series-2 Aerosol Resuspension Tests results. Report presented at the LACE TAC Meeting, Richland (USA).

Wu Y.L., Davidson C.I., Lindberg S.E., Russell A.G., (1992). Resuspension of particulate chemical species at forested sites. Environmental Science and Technology, 26(12), 2428-2435.

Yuan Y., Wei H., Zhao L., Cao Y., (2009). Implications of intermittent turbulent bursts for sediment resuspension in a coastal bottom boundary layer: a field study in the western Yellow Sea, China. Marine Geology, vol.263, 87-96.

Zhang F., (2011). The modelling of particle resuspension in a turbulent boundary layer. Ph.D. thesis, Newcastle University: United Kingdom.

Zhang F., Reeks M.W., Kissane M., (2013). Particle resuspension in turbulent boundary layers and the influence of non-Gaussian removal forces. Journal of Aerosol Science, vol.58, 103-128.

Zimon A.D., (1964). Adhesion of Dust and Powders. New York: Plenum Press.

Ziskind G., Fichman M., Gutfinger C., (1997). Adhesion moment model for estimating particle detachment from a surface. Journal of Aerosol Science, 28(4), 623-634.